Synthesis of cubic boron nitride by low pressure ICP-CVD

（和訳 低圧ＩＣＰ－ＣＶＤ法による c－ＢＮ合成）

Takanori Ichiki

一 木 隆 範

Synthesis of cubic boron nitride by low pressure ICP-CVD Takanori Ichiki

Synthesis of cubic boron nitride by low pressure ICP-CVD

Department of Metallurgy,
Faculty of Engineering,
The University of Tokyo

Takanori Ichiki

Synthesis of cubic boron nitride by low pressure ICP–CVD

Department of Metallurgy,
Faculty of Engineering,
The University of Tokyo

Takanori Ichiki

Contents

List of Figures

List of Tables

Chapter 1

Introduction

1.1 Background and purpose of this research

Over the past two decades, synthesis of diamond and cubic boron nitride (*c*-BN) from gas phase has been intensively studied. Their excellent properties as well as the academic interest in the crystal growth mechanisms have involved many researchers around the world in the low pressure synthesis of these thermodynamically unstable materials. Consequently remarkable progress has been seen in the diamond synthesis in the last 10 years, and currently some applications are available. In contrast, *c*-BN synthesis at low pressures was still in its infant stage in 1990. The synthesis of *c*-BN may be essentially more difficult than that of diamond due to the fact that *c*-BN is a binary compound material unlikely to diamond. The significant problem in the study of *c*-BN synthesis was a lack of the definitive identification of cubic phase for a long time. As a result, not a few misleading informations have confused the researchers in the field. The situation is very similar to that of diamond synthesis at low pressures in early '80s. It is well-known that the early reports of diamond synthesis from gas phase were viewed with great skepticism until the dramatic increase in diamond growth rate and the definitive identification by Raman spectroscopy were reported by the researchers at NIRIM. Generally speaking, synthesis of the metastable phase materials usually requires intensive control of the growth process. Use of plasma is one of the most promissing techniques to provide various reaction circumstances. On these background, this thesis tries to develop a novel plasma CVD process for the *c*-BN film. The special feature of this study is *an application of low-pressure inducitvely coupled plasma (ICP), a new-type high-density plasma source, to the materials processing.* Some characteristic features of this novel film deposition technique are revealed by plasma diagnostics **in chapter 2** and are proved to be advantageous for the *c*-BN film deposition in the later chapters.

Researches of *c*-BN synthesis have been undertaken by using almost every kind of film deposition techniques. The terms chemical vapor deposition (CVD) and physical vapor deposition (PVD) are often used to characterize different vapor-phase

deposition, depending on whether chemical reactions or the physical phenomena such as ion bombardment play a key role for the deposition process. In many cases, differentiation can also be made on the basis of whether or not local equilibrium exists, with those methods, where it does exist being CVD and where it does not being PVD [1]. For instance, well-crystalized diamond has been achieved by numerous CVD methods. It is believed the stabilization of the growing surface by the chemisorption of hydrogen plays an important role in diamond growth. In contrast, PVD methods usually fail to synthesize diamond, but result in the deposition of so-called diamond-like-carbon (DLC: dominantly sp^3-bonded, but non-crystalline carbon) and so on. By the end of 1980s, a number of researchers have stated the successful *c*-BN synthesis mainly by PVD methods and some have also by CVD methods. Methodology and conditions applied in these CVD experiments were often very similar to those of diamond; for example, plasma CVD and hot filament CVD in hydrogen gas have been reported. As mentioned above, however, not a few of them have uncertainty in identificaiton of structure and/or composition of the deposits. These have raised the doubts and the question, *whether or not c-BN can be prepared with a certain kind of chemistry similarly to diamond.* **In the first half of chapter 3**, an explorative attempt has been made to synthesize *c*-BN in high density hydrogen radicals. High density plasma utilized in this experiment can actually provide a plenty of hydrogen radicals. Indeed, diamond has been successfully synthesized by this technique from the methane and hydrogen system at relatively lower pressure of 0.2 Torr (See Appendix A). The results of this attempt have shown difficulties with using methods successful for diamond to the synthesis of *c*-BN. Favorable chemistry of hydrogen would not be expected for the *c*-BN growth. **In the last half of chapter 3**, *c*-BN synthesis under ion bombardment has been achieved by developing low pressure ICP-CVD process with a substrate bias control technique. Identification and characterization of high content *c*-BN films have been carried out by using various techniques.

Fundamental understanding of the growth mechanisms of *c*-BN is considered to be of major importance to control the film properties and to utilize the substantial promise of *c*-BN. At present, major problems commonly reported in *c*-BN films are as follows. (1) Limited crystalline size (no more than 10^2 nm) and imperfect crystallinity, which are too poor for the applications in electronics and cutting tools coating. (2) Very high compressive stress in the films and resulting poor adhesion to the substrate. These problems are usually attributed to the ion bombardment during film growth, while ion bombardment is considered to be essential for *c*-BN synthesis. Therefore, there arises a crucial question *whether or not it is possible to form c-BN and to depress such unfavorable effects simultaneously.* In the last part of the thesis, roles and mechanisms of ion bombardment in film modification have been examined. **In chapter 4**, roles of the energetic ion bombardment of growing surface have been parametrically studied and quantitatively discussed for better understanding of the *c*-BN growth. **In chapter 5**, we have addressed the growth mechanisms

by the detailed film characterization of *c*-BN films at the different growth stage, especially focusing on the initial stage of the *c*-BN growth on Si substrate. For this purpose, thin *c*-BN films with thickness gradients were prepared by a plasma diffusion technique. It has been revealed the initial thin sp^2-bonded BN layer on Si is required to form *c*-BN. Detailed analysis around the interface between sp^2-bonded BN and *c*-BN has revealed some important knowledge to give a insight into the *c*-BN formation mechanisms. In chapter 6, the summary of this thesis has been given.

1.2 Inductively coupled plasma (ICP)

1.2.1 Historical review

Inductively coupled plasma uses an inductive circuit element to couple energy from the rf power source to the gas. The inductive element is usually a helical coil. Although this electrodeless discharge was discovered by Hittorf as early as in 1884 [2], there had been conflicting views regarding its origin for almost 50 years. A number of experimental evidences have been given that the discharge is the result of the large alternating potential differences which exist between the ends of a coil carrying rf-currents, while according to Hittorf and to J.J.Thomson the discharge is due to electromagnetic induction. Thus the early works were mainly undertaken on the origin of the inductively coupled rf discharge [3,4]. These works led to the conclusions that at low excitation the discharge is of electrostatic origin and at high excitation it is of electromagnetic origin [5]. Babat classified so called "inductively coupled discharge" into two different types [6]. (1)Glow–like discharge in which the elementary conductance currents are continued by dielectric currents is called "E–discharge". (2)Arc–like discharge with elementary conductance currents in the form of closed roop is called "H–discharge". At the constant pressure, first, while rf voltage is increasing, a weak E–discharge generates. Then, further increasing rf voltage, it abruptly becomes the strongly luminent H–discharge. Here, we name the H-discharge generated at a low pressure "low pressure inductively coupled plasma (ICP)".

High-pressure (~1atm) induction plasmas have been extensively studied and used in various applicational fields, which include spectral chemical analysis, plasma-assisted chemical synthesis, film growth and destruction of toxic materials [7]. On the other hand, the applications of low-pressure ICP to the materials processing have been rarely seen for a long time. However, today's plasma processing, such as manufacturing of DRAM, has come to require high–density plasma sources such as ECR plasmas and helicon whistler plasmas [8] and an increasing focus on low pressure ICP has been seen quite recently, in '90s [9]. Inductively coupled plasma generated at low pressures (~1mTorr) is revealed to satisfy the requiremets for the modern plasma processing, which include high density ions, electrons and radicals, excellent uniformity over diameter of at least 20cm, low and controllable ion energies and negligible contamination from reactor sputtering or particulate generation. In

addition, it is of great advantage that ICP uses a readily available rf generator and relatively simple source designs. Therefore, the researches of the ICP source for subhalf micron etching process have been rapidly increasing for the last 2~3 years. Besides etching process, however, there have been still few reports of the applications of low pressure ICP to the materials synthesis. Yamashita introduced inductively coupled discharge in a dc diode sputtering system and reported a dense plasma of the order of 10^{12}cm^{-3} [10]. The high deposition rates are reported for Al (4400Å/min), Ti (2200Å/min), Fe (4400Å/min) and Cu (11200Å/min) in 10mTorr argon with 700W rf power and 800 W dc sputter target power. A group of ANELVA corporation in Japan has utilized inductively coupled plasma generated at ~1 Torr for the plasma assisted CVD of silicon nitride [11] and oxidation of superconducting YBCO films [12]. It should be noted that the ICPs generated at 1 Torr show quite different behavior than those at 1 mTorr.

In Yoshida's laboratory and Akashi's laboratory in the university of Tokyo, applications of the ICP at 0.1~1 Torr for materials processing have been attempted from the early 80's. Direct nitridation of silicon and chemical vapor transportation of boron and boron nitride were investigated. On the basis of these studies, in this thesis, chemical vapor deposition using ICP at the pressures from 100mTorr to 1mTorr has been investigated. Especially the highlight of this work is the synthesis of *c*-BN by using highly-ionized low-pressure ICP at 1mTorr; substantially a development of a novel vapor deposition technique. This thesis has experimentally revealed some superior features of low pressure ICP-CVD to the conventional plasma CVD, such as higher reactivity, independent controllability of ion energy and flux to the substrate etc.

1.2.2 Characteristics of ICP

Recent focuses on ICP as a tool for the plasma etching have stimulated both experimental and theoretical studies [13,14,15], but unfortunately even the fundamental property of low pressure ICP is still not clear. Needless to say, comprehension of the plasma characteristics is indispensable for the process design and control, and further progress in the basic research of ICP is expected.

Preliminary discription of ICP over the wide pressure range has been given by Babat [6]. Figure 1.1 and 1.2 show the schematic diagram of the plasma structure. Low pressure ICP has unique characteristics such as 10^1 ~10^3 times higher electron, ion and radical densities than glow plasmas utilized in conventional plasma-aided materials processing application, as graphically illustrated in Fig. 1.3.
Amorim *et al.* measured the electron temperature and the plasma density of low pressure ICP in argon by using Langmuir probe and double probe [17]. Figure 1.4 shows the variation of the plasma density with rf power and the transition from E to H mode of discharge. High density of 10^{12}cm^{-3} was observed for the argon plasma

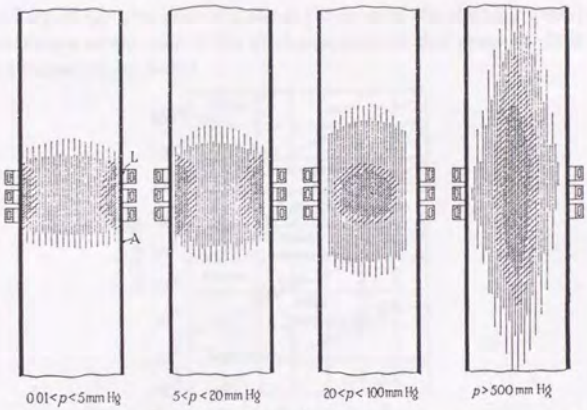

Figure 1.1: The electrodeless discharge at various gas pressures (after [6]).

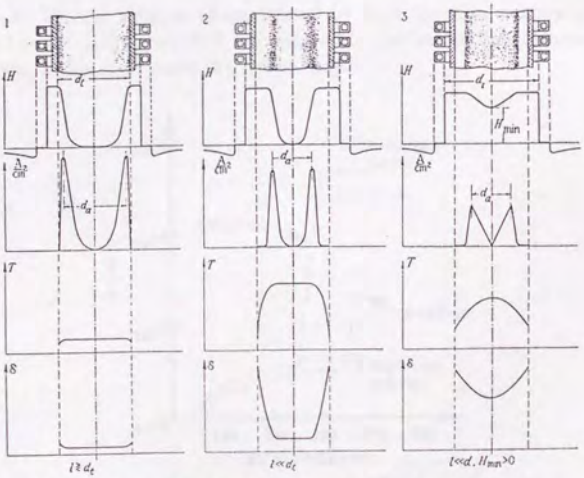

Figure 1.2: Distribution of the electromagnetic field density H, the current density, the gas temperature T, and the gas density δ in the H-discharge with different correlation between the diameter of the discharge (d_t) and the free run of electrons (l) (after [6]).

at ~100mTorr. They also observed the slight drop of the electron density and electron temperature at the axis of the discharge tube at this pressure. It is consistent with the observation by Babat.

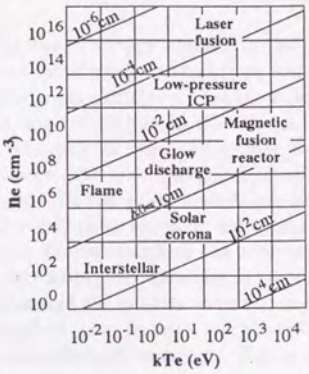

Figure 1.3: Typical plasmas characterized by their electron density and energy. Figure 1.1 in ref. [16] is modified to indicate the position of low-pressure ICP. The lines drawn in this chart show the Debye length.

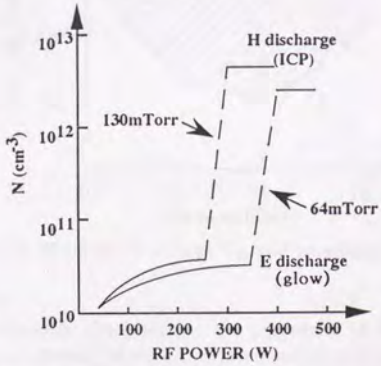

Figure 1.4: Abrupt change of plasma density as the coupling mode changes from capacitive to inductive is shown. Amorim *et al.* reported that at a pressure of 30mTorr or lower the transition from E to H discharge occurs smoothly (after [17]).

From as early as the '70s Takamoto *et al.* have reported a series of study of the transition mechanisms from capacitive to inductive coupling discharge. Unfortunately

their works are less well appreciated since they were written in Japanese [18]~[21]. In the following, some of their results would be cited, especially those about the transition mechanism and the property of ICP.

[Transition to ICP]
By gradually increasing the rf voltage applied to the coil surrounding a tube, the gas breakdown occurs at the *starting* or *breakdown voltage* V_B. As shown in Fig. 1.5 [22], V_B versus pressure graph exhibits a U-shaped curve. Further increase of the input power generates large oscillation in the plasma, afterwards electron density, emission intensity etc. abruptly increase and discharge mode changes into luminous and high-density discharge. At lower pressures, breakdown and transition occur almost at the same time. The transition mechanism is explained as follows. In the plasma generated with rf coil there exists dc ambipolar diffusion due to the density gradient of electron from the tube axis to the tube wall. Interaction between the rf magnetic field and this ambipolar diffusion in the radial direction results in the unstability of the plasma and the plasma comes to show negative conductance. It leads to the non-linear effect, that is, an rf electric field is amplified in the plasma and the further ionization abruptly increases. This is the transition from so-called capacitive to inductive coupling.

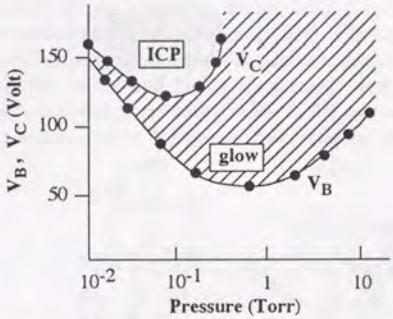

Figure 1.5: Breakdown voltage V_B and transition voltage V_C.

[Properties of ICP]
They have experimentally characterized the properties of ICP by electrical probe technique. Hydrogen discharges were generated in the tube of 3cmϕ-inner diameter at 10~100 mTorr using rf coil, and some features of low pressure ICP and glow discharge were compared as follows [19].

1. The electron density of low pressure ICP measured at the center axis of the discharge tube was about 100 times higher than that of glow discharge.

2. In contrast to the glow discharge, the electron density was almost constant along the radial direction in the case of low pressure ICP.

3. Ion saturation current was 30~300 times larger for low pressure ICP than for glow discharge.

4. Electron temperature was not so different between the two discharge modes. The electron temperature distribution along the radial direction was small for the both discharge modes.

1.3 Boron Nitride (BN)

1.3.1 The crystalline structure of boron nitride

Crystalline Structure

Boron compounds are characterized by a variety of compositions and structures. Above all, boron nitride, which does not exist in nature, has been recently noted in various fields. The compounds, such as BN, formed by the atoms from the first row of the Periodic Table behave differently than the counterparts in the later rows. The unusual properties are generally attributed to the small core size and the absence of p electrons in the cores. BN exhibits polymorphism similarly to carbon. Stoichiometric BN exists in four crystalline forms; cubic (zincblend, c-BN), wurtzite (w-BN), hexagonal (h-BN) and rhombohedral (r-BN). They are the structural analog of cubic diamond, hexagonal diamond (lonsdalite), graphite and rhombohedral β graphite, respectively. c-BN and w-BN are formed from tetrahedrally bonded boron and nitrogen hybridized in sp^3 state, while h-BN and r-BN have trigonal sp^2 hybridized covalent bonds. Figure 1.6 shows the crystalline structures of BN.

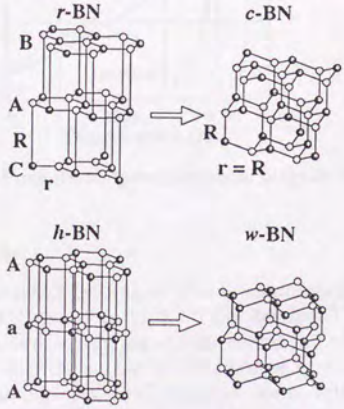

Figure 1.6: The crystalline structures of boron nitride (after [23]).

Hexagonal BN has a two-layered stacking sequence (*Aa Aa*...) which is structurally different from hexagonal graphite which has an *AB AB*... stacking sequence [24]. Rhombohedral BN has a three-layered stacking sequence (*ABC ABC*...). Rhombohedral BN has been identified in the BN whiskers grown from the gas phase [25,26]. As shown in a pressure-temperature phase diagram (Fig. 1.7) [27], at ordinary temperatures and pressures hexagonal phase (*h*-BN) is stable, and *c*-BN is stable at high temperatures and pressures. The denser zinc-blende(*c*-BN) and wurtzite structure (*w*-BN) are produced directly without catalysis from the so-called low-pressure phase, hexagonal and rhombohedral BN, under static or dynamic compression. From the comparison of theoretical density with *c*-BN [28] and numerous experiments by shock compression etc [27][29]~[32], it is considered that *w*-BN is a meta-stable phase. Other crystalline forms such as turbostratic BN (*t*-BN) and amorphous BN (*a*-BN) have also been observed. Turbostratic BN has a similar structure to *h*-BN. Its B_3N_3 hexagon layers are stacked roughly parallel to each other but show random rotation and transition about the layer normal [33]. Amorphous BN has been reported to be observed in thin films prepared by CVD and sputtering etc [34]~[37].

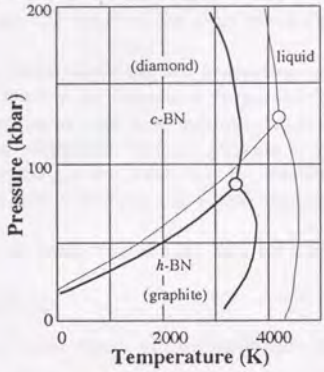

Figure 1.7: Pressure-temperature phase diagram for BN.

High pressure synthesis

At the General Electric research laboratory Bundy and coworkers succeeded in the reproducible synthesis of diamond in 1955. They developed the necessary high-pressure and high-temperature equipment and discovered and elucidated the solvent-catalytic processes. Just after the success in the diamond synthesis, in 1957, Robert H. Wentorf JR., who was one of the GE-diamond team, achieved the first high-pressure growth of *c*-BN crystals [38,39]. Wentorf found that alkali and alkali earth metals and their nitrides are effective catalysts for converting hexagonal BN into cubic at 45~80 kbar and 1500~2000 °C. There are two main types of HP-HT technique

for preparing high-pressure phases of *c*-BN and *w*-BN: those using static pressure and those using dynamic pressures. Wurtzite-type BN is mainly obtained by using the latter technique. The formation of the wurtzite phase under static compression has been shown to requier lower temperatures than the formation of *c*-BN [28].

1.3.2 Properties and Potential applications

Properties of boron nitride

(1) *c*-BN

Cubic BN has unique characteristics comparable to those of diamond. It shows extreme hardness, high melting point, low dielectric constant, interesting thermal characteristics, large band gap and so on. Electronic property of *c*-BN has been the subject of numerous theoretical studies. The calculated indirect band gap for *c*-BN is uncertain with values in the range of 3.0 to 10.5 eV [40]~[44]. This variation in theoretical gap values is attributed to the difficulties in the treatment of the valence states in the absence of *p* core states. Studies using UV absorption [45] and X-ray emission spectroscopy [46] reported the value of ~6 eV.

(2) *h*-BN

Since *h*-BN has similar structure and properties to graphite, it is well-known as "white graphite". Some of its important properties are good thermal and electrical insulating properties at high temperature, chemical and thermal stability and excellent tribological properties. Though graphite is a semimetal, *h*-BN , ordinally regarded as a wide-band-gap insulator, may be considered as one of the wide-band-gap semiconductors and it displays multiband luminescence in the violet and UV regions [47].

Some characteristic properties of *c*-BN and *h*-BN are listed in Table 1.1.

Potential Applications

Both hexagonal and cubic boron nitride films have been found useful for lots of applications [52].

(1) *c*-BN

Since *c*-BN is stable at high temperatures and does not react with ferrous metals, it is excellent for the cutting tools material. Superior chemical inertness is favorable as corrosion resistive coating. Moreover, BN has emerged as a very strong competitor with diamond and SiC as far as high-temperature applications are concerned. Possibility as a wide-band-gap semiconductor is quite attractive because *c*-BN has both *p*- and *n*-type electrically active, moderately shallow dopants, while only the *p*-type was made for diamond. Beryllium is doped to form the *p*-type; and S, Si, and KCN are doped to form the *n*-type [53]. High thermal conductivity, high charge carrier mobility, strongly non-ohmic high field conductivity of *c*-BN is promissing for the high-power microwave and millimeter wave devices. In 1988, Mishima *et*

al. prepared the *pn* junction diode by HTHP method, and demonstrated rectifying diode characteristics at 530 °C and the ultraviolet photo-emission [54,55]. Thus *c*-BN has potential for deep UV detectors and UV light-emitting devices. Together with the environmental stability and superior wear resistance, wide-ranging transparency from ultraviolet to infrared is also preferable for optical applications, such as windows, lens coatings and X-ray lithography masks.

Table 1.1: Properties of boron nitride

properties	*c*-BN	*h*-BN
density	3.45 g/cm^3 [38]	2.27 g/cm^3
lattice constant	3.6155 ±0.0005 Å[48]	a=2.504 Å, c=6.66 Å
heat conductivity	13 W/cm·K [49]	0.6 W/cm·K (a direction)
	(single crystal, theoretical)	0.015 W/cm·K (c direction)
micro Vickers hardness	4695 – 8600 kg/mm^2	—
melting point	more than 2700°C [38]	3000°C (in N_2)
	(in vacuum)	
coefficient of linear expansion	$\sim 3.5 \times 10^{-6}$/K	-2.9×10^{-6}/K (‖ a-axis)
	(0 – 400°C) [50]	40.5×10^{-6}/K (‖ c-axis)[24]
refractive index	2.117(Sodium light) [50]	2.20±0.05($\lambda = 0.5\mu$m)
resistivity	$10^{14} - 10^{16}\Omega$cm	$10^{9} - 10^{14}\Omega$cm
band gap	~6 eV(indirect transition)	5.6 eV(direct transition) [51]

(2) *h*-BN

Bulk BN is widely used as a heat-resistive insulator. It can also be used for thermal insulation as a die-wash material and as a lubricant and pressure transmission medium. An interesting application of the BN film is as an insulator in a metal-insulator-semiconductor (MIS) memory diode [56] and as high quality gate insulating films [57] and passivation layers for MIS structure. Shono *et al.* also found the BN film is useful as a restricted-area boron diffusion source in the fabrication of planar diode using only one photomask [56]. Since BN is a poor absorber of soft X-ray and visible light, an important application of BN films is as transparent substrates for X-ray lithography masks [58,59].

1.3.3 Reviews of the c-BN synthesis from gas phase

A number of researches have been carried out over the past 20 years to synthesize BN from vapor phase by using various deposition techniques. A review of the early works of the BN film coating until 1986 was written by Arya and D'Amico [52]. A book titled "Synthesis and Properties of Boron Nitride", including some detailed

reports of synthesis, properties and applications, was published in 1990, when the remarkable progress in the BN preparation technique made *c*-BN films more available [60]. This section presents a thorough review on the deposition techniques applied to boron nitride synthesis from the early 1980s to the present time. The papers on the preparation of boron nitride have been increasing year by year [61]. More than 100 papers were published in 1990. Unfortunately many of the results in the early 1980s, and moreover, even a few recent reports have met with skepticism for the lack of the sufficient characterization of structure and composition. Special care is required to prevent the misidentification of *c*-BN as discussed later in chapter 3.

Vapor synthesis methods can be generally classified as either physical vapor deposition (PVD) or chemical vapor deposition (CVD). Most of the techniques successful in *c*-BN synthesis are categorized in PVD, whereas CVD techniques generally lead to *h*-BN film. This is attributed to the fact that ion bombardment of the film surface during deposition plays an important role in the *c*-BN growth. In recent years plasma assisted CVD with substrate biasing has been successfully applied to the deposition of *c*-BN films.

c-BN deposition by PVD process

The first attempt to obtain the high-pressure phase BN coating is found in the report of reactive pulse plasma crystallization by Sokolowski from Poland in 1979 [62]. It is reported that *w*-BN and E-BN, which has been reported to be obtained with the use of "shock compression" by Batsanov [63], were crystallized. In 1981 they presented the continuation of the work with some film characterizations [64]. It is reported that thin *c*-BN layer with 40~100Åcrystalline size were deposited, but the film showed an IR absorption at 1020cm^{-1} and 2400cm^{-1}, not corresponding to the *c*-BN absorption peak. In 1980 and the later years, Weissmantel *et al.* reported the deposition of hard BN films by (1) ion plating using a mixture of electron-beam-evaporated boron and nitrogen, (2) ion plating starting from borazine ($B_3N_3H_6$) and other volatile compounds and (3) the dual-beam technique operated with a boron or boron nitride target and nitrogen ion beams [65]~[67]. They called this hard BN film "i-BN" from analogy with "i-carbon" to designate the critical role of ion bombardment during film growth. Structural analysis using TEM indicated a predominantly amorphous matrix in which 5~20nm crystallites were randomly embedded. From EELS spectra, the major component was concluded to be a metastable i-BN phase. However the films contained significant amounts of oxygen contamination. Therefore they "hesitated to designate the films as boron nitride". Later this group deposited BN films of low oxygen contamination, but their results of IR absorption analysis did not show any features of *c*-BN [68,69] . Afterwards, however, lots of researchers have prepared *c*-BN films by the similar ion beam processes [70,71,72]. Satou and Fujimoto prepared BN films by the electron beam evaporation of boron and the simultaneous bombardment of 30keV N_2^+ ion beam and firstly provided the electron diffraction of *c*-BN. However the reported crystalline size seems to be exceptionally large (more than 1μm) in comparison with any other reports of *c*-BN

synthesis with ion bombardment. Afterwards their coworkers reported the preparation of *c*-BN at lower ion energy [73]~[76]. Activated reactive evaporation was originally developed by Bunsha *et al.* The group of Chopra and Bunsha applied this method for the preparation of BN film using evaporated H_3BO_3 and ammonia plasma [77]. In this work, faint electron diffraction lines corresponding to *c*-BN were reported, but IR absorption due to *c*-BN was not observed. In the mid-1980s, Inagawa *et al.* firstly prepared BN films of high-content cubic phase by modified activated reactive evaporation with a gas activation nozzle by using the electron beam evaporation source of the HCD gun and the conventional EB gun [78]~[80]. An rf bias was applied to the substrate in order to accelerate the ionized speices in the incident gas on the substrate. Their works should be appreciated for at least two reasons. They firstly presented the detailed characterization of structure and composition enough to identify the *c*-BN film. Second, Inagawa found that Ar ion bombardment during film growth promote the *c*-BN growth. Following their work, many researchers have reported the deposition of high-content *c*-BN films by mainly using the ion beam deposition or ion plating method (including ARE). Ikeda *et al.* have synthesized *c*-BN on various substrates by arc-like plasma-enhanced reactive ion plating method and have reported the reduce of compressive stress by inserting buffer layer of i-BN [81]. Tanabe *et al.* used ion beam enhanced deposition method (IBED) with boron and *h*-BN target, and have investigated the effect of various experimental parameters on the *c*-BN growth [82]~[85]. Recently Murakawa *et al.* have reported several works on the *c*-BN coating by activated reactive evaporation. A special feature of their process is that a hot cathode plasma discharge in a parallel magnetic field is used [86,87]. Bias sputtering technique has been also applied to the synthesis of *c*-BN. First anounce of *c*-BN synthesis by bias sputtering was given by Seidel *et al.* [88]. They have found the strong variation of TED patterns from the film with increasing substrate bias. However no IR absorption due to *c*-BN was observed. Detailed reports of the preparation of *c*-BN film by bias sputtering and film characterizations have been presented by Mieno *et al.* [89,90]. After these works, several reports using sputtering have been presented by other researchers [91,92]. Other PVD methods such as excimer laser and CO_2 laser PVD have been applied to BN film deposition [93]~[97], but they are not discussed in detail here, since so far it is not clear whether or not *c*-BN has been really achieved by these methods. Doll *et al.* have reported the epitaxial growth of thin *c*-BN film on silicon substrate. Friedmann *et al.* previously claimed the synthesis of *c*-BN on silicon using similar conditions as reported by Doll *et al.*. Afterwards, however, they have noticed the misidentification due to the contamination of copper. Ion-assisted laser PVD has been successfully applied to the *c*-BN preparation, but it is considered to be a variation of ion plating [98]~[103]. Representative PVD techniques and their deposition conditions are listed in Table 1.2.

Table 1.2: PVD methods and conditions for *c*-BN films

Preparation technique	Gas, source	Accerelation or substrate bias (V)	Pressure	Reference
ARE with HCD/EB gun	B, N_2, Ar	200~400	1mTorr	[80]
Arc-like plasma enhanced ion plating	B, N_2, Ar	–	1~10mTorr	[81]
Bias-sputtering	BN target, Ar	200	1~50mTorr	[89]
Bias-sputtering	BN target, N_2, Ar	400	10~30mTorr	[91]
Magnetron sputtering	BN target, N_2, Ar	105~120	1mTorr	[92]
IBAD	B, N_2, Ar	500	–	[189]
IBAD	B, N_2, Ar	300~700	0.1mTorr	[72]
IBAD	B target, N_2, Ar	500	0.3mTorr	[82]
ARE in a magnetic field	B, N_2, Ar	–	0.2~1mTorr	[86]
Ion-assisted pulsed laser deposition	BN target, N_2, Ar	800~1200	0.01~0.05mTorr	[103]

c-BN deposition by Plasma CVD with ion bombardment

Chayahara *et al.* deposited *c*-BN films on silicon substrate from diborane and nitrogen. They initially used 13.56MHz rf discharge in a magnetic field and afterwards electron cyclotron resonance (ECR) plasma [104,105]. The deposited films were characterized by IR absorption spectroscopy, TEM and optical reflectance measurements in the photon range 5~25 eV. The substrate bias required for *c*-BN growth was $-200 \sim -300$ V and $-50 \sim -100$ V in Ar rf-discharge and ECR plasma, respectively. Okamoto *et al.* from the same group have deposited *c*-BN films on boron buffer layer [106], diamond [107] and WC [108] substrates. It is reported that BN films directly deposited on WC were a mixture of cubic and hexagonal phases and that the predominant films in the cubic phase were only formed with use of a thin buffer layer of boron. They also observed that the *c*-BN film on diamond shows better adhesion than that on Si. Following their works, some researchers have reported the *c*-BN film deposition using ECR plasma and substrate biasing technique. Weber *et al.* have deposited *c*-BN films from N-trimethylborazine in a downstream ECR plasma. N-trimethylborazine is a less toxic, non-explosive source, but the deposits contained 4~6% carbon impurity originating from the methyl groups of the precursor. The RF (13.56MHz) or LF (100~400kHz) was applied to the substrate in order to control the self-bias [109,110]. From diborane and nitrogen, Ichiki *et al.* have deposited *c*-BN films by low pressure ICP-CVD with substrate bias technique [111]~[116]. Synthesis of *c*-BN by ICP-CVD has been also reported by Reinke *et al.* from Germany [117]. Recently *c*-BN deposition by rf plasma CVD with magnetic field has been investigated in terms of various experimental conditions [118].

Common features of these successful CVD techniques are apparently a use of low-pressure high-density plasma and substrate bias technique. Representative plasma CVD techniques for *c*-BN film deposition and their deposition conditions are listed in Table 1.3.

Table 1.3: Plasma CVD methods and their deposition conditions for *c*-BN films.

Preparation technique	Gas	Pressure [Pa]	V_{sub} [V]	T_{sub} [°C]	Comment	References
rf plasma CVD	B_2H_6 (diluted with Ar), N_2	0.04	-200~-300	room temp.~600	magnetic field	[104]
	B_2H_6 (diluted with Ar), N_2, (He, H_2)	2	-650	370~450	magnetic field	[118]
ECR plasma CVD	B_2H_6 (diluted with Ar or He), N_2	0.04	-50	room temp.~400		[105,106]
	N-trimethylborazine, Ar, N_2	0.1~0.6	-200	600~870	LF(250kHz)	[110]
ICP-CVD	B_2H_6 (diluted with He), N_2, Ar	0.1~0.2	V_{sheath}=-80	900		[112,113]

Chapter 2

Characterization of low pressure ICP*

2.1 Introduction

Plasmas utilized in plasma enhanced CVD are generated by several types of gas discharge, such as dc, radio-frequency, microwave discharge and so on. Above all, rf glow discharge has been most commonly used in materials processing so far. In this thesis, a low-pressure ICP, which has been scarcely utilized in materials processing, is used to develop a novel deposition method. The largest problem in the use of a new-type plasma is always a lack of basic researches on its fundamental properties, discharge mechanisms and so on. To exploit the full capabilities of the plasma sources and to improve the existing processes, a detailed understanding of the fundamental chemical and physical phenomena in the systems is required. Furthermore, also from the standpoint of film growth study, plasma diagnostics are indispensable. Plasma process is actually controlled by external process parameters such as rf power, gas pressure, gas flow rate, substrate temperature, and bias potential. However, these variables strongly depend on each apparatus and are not universal parameters to characterize the film deposition. For the comparison of experimental results of different researchers and for the speculation upon the microscopic film growth mechanisms, it is indispensable to reveal the quantitative physical parameters in the system. In this section, plasma diagnostics have been carried out to comprehend the fundamental property of the ICP source and to clarify the quantitative parameters of the incident species to the growing surface of *c*-BN films.

*Partly in: J.Appl.Phys. **75** 1330 (1994) and Jpn.J.Appl.Phys. **33**, 4385 (1994).

2.2 Experimental

Description of the plasma reactor

The reactor system consists of a vacuum chamber with low pressure ICP source and vacuum pumps (ultimate pressure 10^{-6} Torr). The 13.56MHz rf power was coupled into the plasma with a 3-turn coil around a water-cooled quartz tube. Plasma was generated inside a 38mm diameter pyrolytic boron nitride tube placed inside the quartz tube of 50mm in diameter to avoid contaminations from the quartz tube. The gas-feed rates were controlled by needle valves and mass flow controllers. A schematic view of the experimental system is shown in Fig. 2.1.

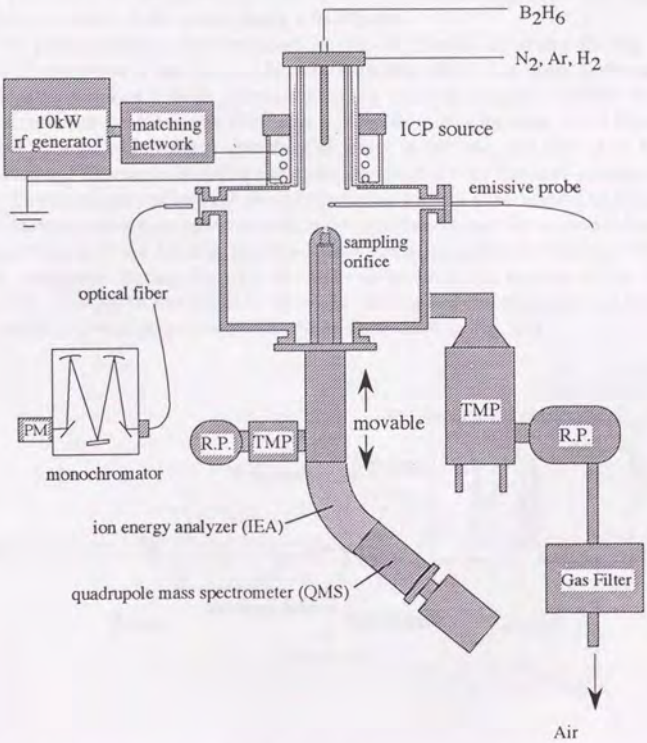

Figure 2.1: Schematic view of the ICP-CVD apparatus with some diagnostics.

Emissive probe

Plasma potential is an important parameter which affects the ion energy impinging on the substrate and was measured by the emissive probe method. Emissive probe method [119, 120] is a convenient and effective diagnostic technique for measuring plasma potential over a wide range of plasma density (from 10^5 to 10^{13} cm^{-3}) and for ion and electron temperatures as high as Ti=1keV and Te=20eV [121]. Moreover, this method has the advantage of reduced surface contamination due to the use of hot wire. Therefore emissive probe method was adopted to measure the plasma potential in this study. The floating potential of a sufficiently heated probe in strong thermionic emission of electrons can be close to the plasma potential [120, 122, 123]. So the plasma potential can be obtained only by measuring the dc floating potential of the probe using a voltmeter.

The probe construction employed in this experiment is shown in Fig. 2.2. A probe filament was of tantalum, 0.3mm in diameter, about 1cm long, and was welded to tungsten wires of 0.5mm diameter running through ceramic insulator tubes. A typical emissive probe circuit [124] was utilized for probe heating. A 50-Hz signal is applied to a variable-voltage transformer which is fed into one side of an isolation transformer. The variable-voltage transformer controls the filament current and the isolation transformer allows the rest of the circuit to float with respect to the ground. The filament heating current was half-wave-rectified by the diode inserted in series. Measurements of the floating potential were made using the oscilloscope with high input impedance during the part of the cycle in which no heating of the filament occurred. The probe was inserted from the side wall of the chamber and located at the position 11mm above the substrate as illustrated in Fig. 2.3.

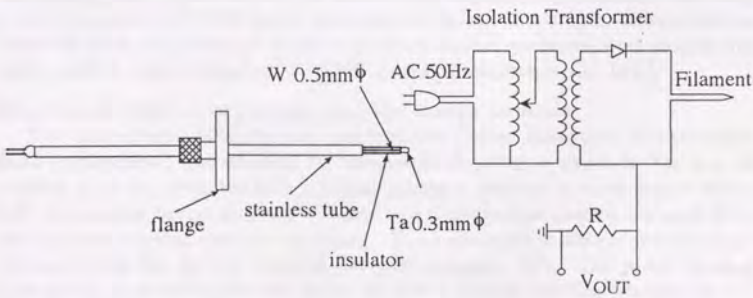

Figure 2.2: Construction details of the emissive probe used for the plasma potential measurement.

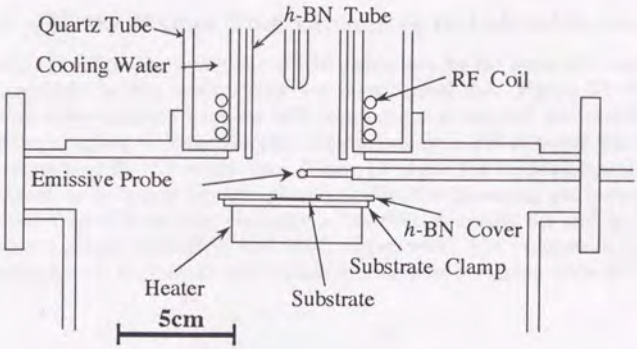

Figure 2.3: The experimental configuration showing relative positions of the plasma source, the diagnostic probe and the substrate.

Optical emission spectroscopy

In order to obtain informations on the species in the plasma used for *c*-BN film deposition, plasma emission at about 5mm above the substrate was observed through the viewport to a monochromator through an optical fiber for optical emission spectroscopy. Wavelength scans from the 240–600nm range were obtained using a monochromator (JY38PII Seiko) with high resolution. In addition, series measurements of some representative emission lines at various pressures were carried out using another monochromator (CT 250C Japan Spectroscopic Co. Ltd.).

Quadrupole mass spectroscopy and ion energy analysis

The differentially pumped mass spectrometer (Hiden Analytical Limited EQP mass spectrometer) was mounted on the plasma chamber as shown in Fig. 2.1. It consists of an ion extractor with a 100μm aperture followed by a 45 degree sector field electrostatic energy analyzer matched to a triple section quadrupole mass filter and a pulse counting electron multiplier. The spectrometer design provides high dynamic range for plasma ions and neutrals (typically 10^6). The probe housing is pumped by a turbomolecular pump to give a typical working pressure in the manifold of the order 10^{-6} Torr.

2.3 Results and discussion

2.3.1 Mode change from capacitive to inductive coupling

In order to confirm the conditions of ICP generation for the apparatus used in this work, optical emission spectroscopy has been carried out. Figure 2.4 shows the variation of the emission intensity with increasing rf power and the transition from capacitive coupling to inductive one. Approximately 5-kW rf power was required to generate pure H_2 ICP at 0.1 Torr. Figure 2.5 shows the emission intensity of H_β normalized by hydrogen pressure plotted against the increasing gas pressure. The transition from ICP to glow discharge is observed at around 0.2 and 0.5 Torr for the plasma generated at 5kW and 7kW, respectively. The pressure range of ICP operation for our ICP source with 10-kW rf generator is ranging from 10^{-1} to 10^{-4} Torr.

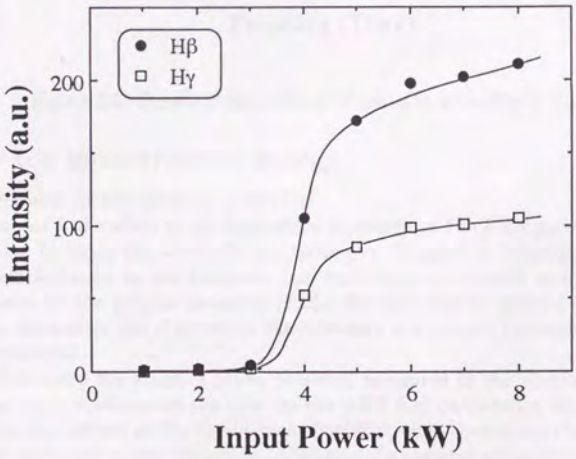

Figure 2.4: Emission intensity of H_β and H_γ *versus* rf input power.

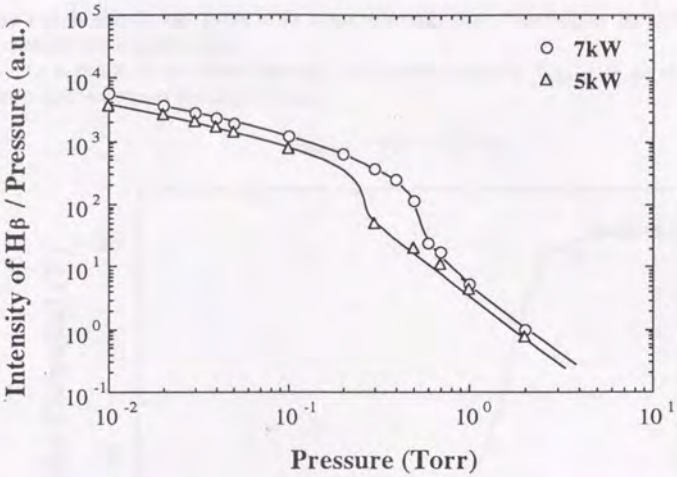

Figure 2.5: Pressure dependence of emission intensity of H_β

2.3.2 Ion bombardment energy

Measurement of the plasma potential

In chapter 4, the effect of ion bombardment energy on the *c*-BN growth has been investigated by using the substrate bias technique. In order to investigate the roles of ion bombardment by the substrate bias technique, one should at first examine its influence to the plasma potential [125]. For the case of pallarel electrode rf discharge apparatus, the rf power to the substrate often cause the evolution of the plasma potential.

Fig. 2.6 shows the emissive probe potential measured in the plasma generated under the same condition as the case for the *c*-BN film preparation in section 3.2. At the heating current of 6A, the filament begins to emit thermionic electrons, and the probe potential rapidly increases. Increasing the filament current further causes the floating potential to roll over and finally to saturate at 92V. The saturated probe potential can be assigned as the plasma potential. Maximum uncertainty including noises were within ±1V. The plasma potential was quite constant irrespective of the applied rf power to the substrate. This is due to the fact that the substrate power input was relatively low by no more than 10W, while RF power for generating ICP was 7kW. Therefore the power to the substrate has little influence to the bulk plasma. The relatively high plasma potential could be attributed to the fact that helium occupied more than 80% of the total gas flow. Since helium–electron collisions

are mainly elastic and make little electron energy loss, the electron temperature is expected to be rather high.

As a result of the measurement, the sheath potential V_{sheath} is given for the measured substrate potential V_S as

$$V_{\text{sheath}} = 92 - V_S(\text{Volt}). \tag{2.1}$$

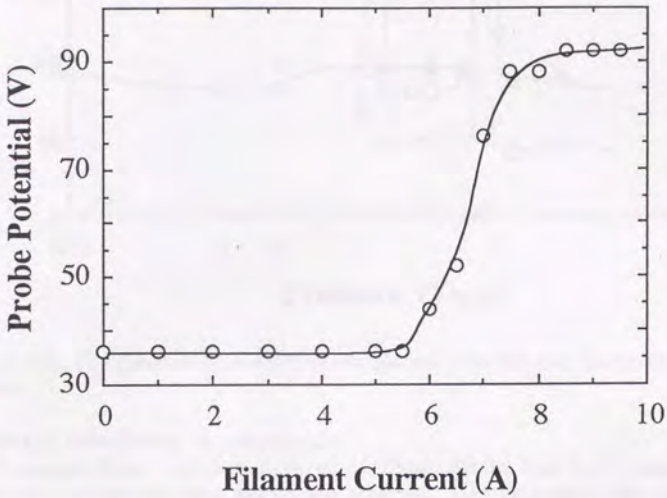

Figure 2.6: An example of the measured floating potential as a function of the filament current. ICP was generated by 7kW rf power at 1×10^{-3}torr. Flow rates of 10% diborane diluted with helium, nitrogen and argon were 20 sccm, 1.2 sccm and 2 sccm, respectively.

Pressure dependence of the plasma potential

Figure 2.7 shows the pressure dependence of the plasma potential and floating potential. Upon increasing the pressure from 1 mTorr, the plasma potential decreases gradually from about 90V to 60V and it suddenly drops to 35V at around 80 mTorr. The sudden change of the plasma potential is attributed to the fact that the plasma is restricted to the source volume at pressures above 10^2 mTorr. The plasma potential shows an apparent hysteresis curve toward the pressure. From the viewpoint of the processing, the plasma diffusion toward the substrate at the lower pressure is advantageous for *c*-BN synthesis and generally for ion-assisted material processing.

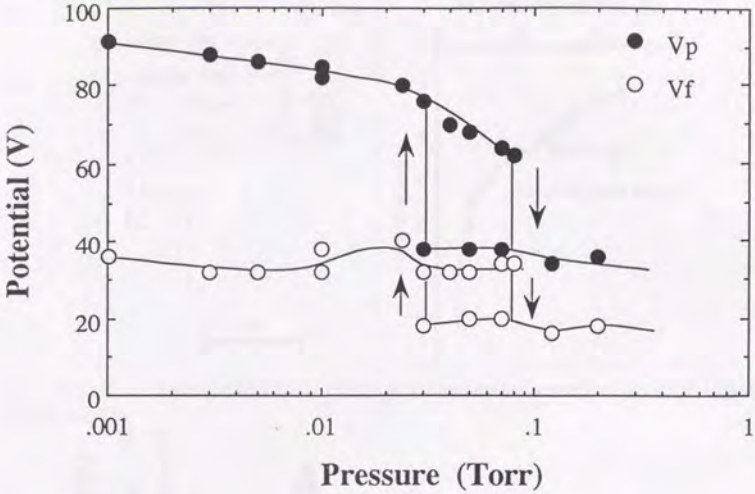

Figure 2.7: The pressure dependence of the plasma potential and the floating potential.

Potential distribution in the plasma

It was also found that there exists an additional electric field in the plasma to accelerate the ion impinging toward the substrate. The decrease of the charged particle density along the plasma stream causes the gradual decrease of the plasma potential [126,127]. For example, Fig. 2.8 shows the plasma potential distribution along the center axis of the plasma source for pure argon plasma generated at 7kW, 2×10^{-3}Torr. In order to examine the influence of this plasma potential distribution on the ion energy in the plasma, energy distribution of Ar^+ was measured by an energy analyzer at the plasma downstream. Figure 2.9 shows the ion energy distribution function (IEDF) for Ar^+ ions (mass number = 40). The IEDF shows a peak at around 5 eV with a weak tail extending to about 40 eV, which is almost corresponding to the plasma potential. The fact that most ions do not acquire the full potential drop in the plasma is due to charge exchange. It has been reported by the group of Boswell that, even at the low pressure of 10^{-3} Torr or less, charge exchange has a dramatic effect on the IEDF [126]. Accordingly the average energy of ions impinging to the substrate is expected to be almost the same as the sheath potential or higher than the sheath potential by only several eV.

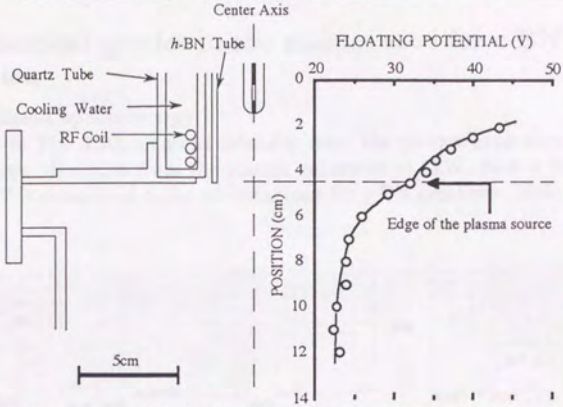

Figure 2.8: The plasma potential distribution along the center axis of the pure argon plasma stream.

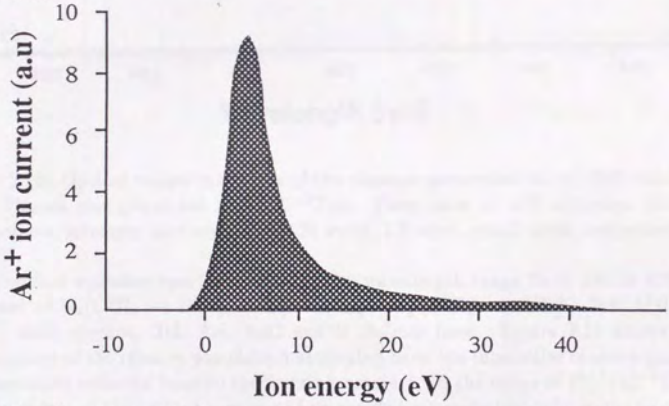

Figure 2.9: The energy distribution of Ar^+ ions. Ar plasma was generated at 7kW.

2.3.3 Chemical species in the plasma used for c-BN deposition

Optical emission spectroscopy

As shown in Fig. 2.10, emission intensity from the plasma generated at 7kW is much stronger than that from the plasma generated at 1kW. Such a higher ion density of ICP is considered to be advantageous for *c*-BN synthesis. Main features

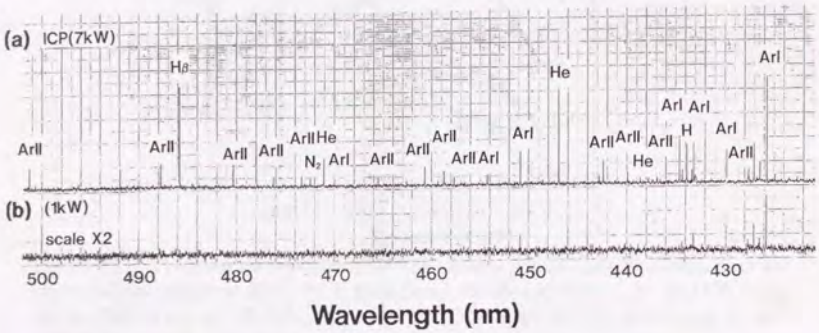

Figure 2.10: Optical emission spectra of the plasmas gernerated at (a) 7kW and (b) 1kW. Plasma was generated at 1×10^{-3}Torr. Flow rates of 10% diborane diluted with helium, nitrogen, and argon were 20 sccm, 1.2 sccm, and 2 sccm, respectively.

of the optical emission spectra of ICP in the wavelength range from 240 to 600nm consisted of $N_2(C^3\Pi_u \rightarrow B^3\Pi_g$, $B^3\Pi_g \rightarrow A^3\Sigma_u^+)$, $N_2^+(B^2\Sigma_u^+ \rightarrow X^2\Sigma_g^+)$, $NH(A^3\Pi_i \rightarrow X^3\Sigma^-)$ band spectra, HeI, ArI, ArII and H Balmer lines. Figure 2.11 shows the dependences of the relative population estimated from the intensities of some typical representative emission lines on the working pressure. In the range of 10^{-3}–10^{-1}Torr, the population of the excited species at low energy level monotonically increases with the pressure, while that of the species at high energy level shows a maximum. This is interpreted by a lowering of the electron temperature with increasing pressure.

Quadrupole mass spectroscopy

Figure 2.12 shows the raw mass spectrum data for positive ions for 7-kW ICP used for *c*-BN films deposition. Mass spectral data are presented in Table 2.1. It has been revealed that Ar^+ comprises approximately 50% of the total ion current, and besides, H^+, H_2^+ and N_2^+ occupy approximately 10% each, and N^+ occupies approximately 5%.

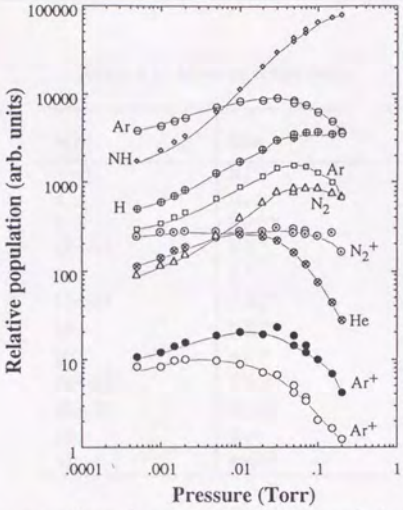

Figure 2.11: The pressure dependence of the relative populations estimated from the representative emission lines. ⊕: H (434.1nm), ⊗: He (587.6nm), ⊖: Ar (420.1nm), □: Ar (763.5nm), △: N_2 (311.7nm), ⊙: N_2^+ (391.4nm), ◇: NH (336.0nm), •: Ar^+ (434.8nm), ○: Ar^+ (476.5nm).

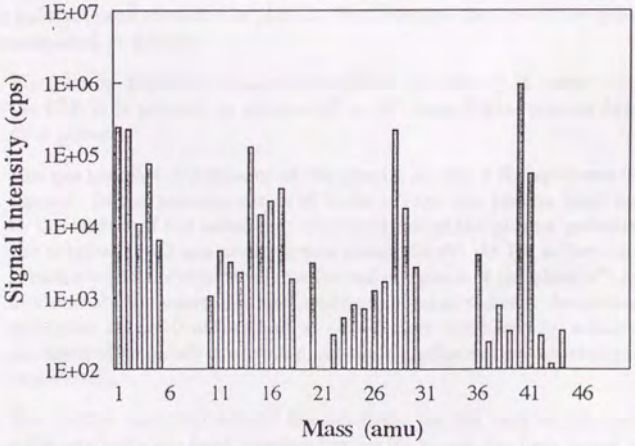

Figure 2.12: Mass spectrum intensities in counts per second for positive ions at plasma downstream.

Table 2.1: Mass spectral data.

m/e	Ions
1~3	H_x^+
4	He^+
5	HeH^+
10~13	BH_x^+
14	N^+
15~17	NH_x^+
18	NH_4^+
20	Ar^{2+}
24~27	BNH_x^+
28~30	$N_2H_x^+$
40	Ar^+
41	ArH^+

2.4 Conclusion

Plasma diagnostics have been carried out to comprehend the fundamental property of the ICP source and to clarify the quantitative parameters of the species impinging to the substrate and those in the plasma. Fundamental features of low-pressure ICP are summarized as follows.

1. The plasma density is widely controllable by altering rf power coupled into the ICP. It is possible to achieve $10^2 \sim 10^3$ times higher plasma density than glow plasma.

2. The gas pressure dependence of the plasma for the *c*-BN synthesis was investigated. In the pressure range of 1~10 mTorr, the plasma itself can diffuse to the surface of the substrate. The variation of the plasma potential nearby the substrate with gas pressure was within 10 eV. At 10^2 mTorr, the plasma is restricted to the source volume (so-called "pinch of the plasma") and serves to dissociate the source gas and produce activated radicals. Accordingly, ICPs generated at 1~10 mTorr and at 0.1~1 Torr are basically suitable for the ion-assisted materials processing and the high-flux radical-assisted processing, respectively.

3. The plasma potential nearby the substrate for the case of the condition of *c*-BN synthesis has been measured to be 92 V and has been found not to be affected by the rf power to the substrate required to control the substrate bias. Accordingly, independent control of energy and flux of the ions impinging to the substrate is possible.

4. Existence of the plasma potential distribution along the plasma axis due to the change of the charged particle density by diffusion has been observed at about 1 mTorr. Accordingly the ions impinging to the substrate are accelerated by the electric field in the plasma and by the sheath potential. However, acceleration of ions in the plasma is expected to be within several eV, since collisions between particles significantly occur even at $\sim 1 \times 10^{-3}$ Torr.

5. Emission species and ionic species in the plasma generated under the same condition as that for the *c*-BN synthesis were assigned by OES and QMS. The pressure dependence of the relative density of emission species was also examined.

Chapter 3

Preparation and Characterization of BN films

3.1 BN synthesis under hydrogen plasma*

3.1.1 Introduction

Hexagonal BN is a material of high chemical inertness and thermal stability. Many applications have been found such as a membrane for X-ray masks, a protective coating and a wide band gap insulator. Studies of BN film deposition have been carried out by using various CVD techniques, such as thermal CVD, low pressure CVD (LPCVD) and plasma enhanced CVD (PCVD). A great variety of gases have been used as a source, such as (a)diborane and ammonia (CVD :[56,128,129], LPCVD: [58,130], PCVD:[35][131]~[133]) ,(b)trichloroborazole (BCl_3) and ammonia [36][134]~[137], (c)borantriethylamin ($BH_3{\cdot}N(C_2H_5)_3$) and ammonia [138]~[140], (d)borazine [141], (e)decaborane ($B_{10}H_6$) and ammonia [37], (f)hexachloroborazine ($B_3N_3Cl_6$) [142] and so on. In these works, *h*-BN, *t*-BN, *a*-BN and boron-rich BN have been usually obtained. Although *h*-BN is well-known as a stable phase at low pressures, it is commonly observed that well crystallized *h*-BN can be obtained only at high substrate temperatures above ~1100 °C. Matsuda and co-workers reported the effects of pressure and temperature on the crystal structure and microstructure of the CVD-BN. They have investigated the structure evolution with the increase of the substrate temperature by XRD; the structure varies from *a*-BN to *t*-BN and at last to *c*-axis oriented *h*-BN [143].

In order to clarify the viewpoint of the study in this section, our attention is focused only on the CVD from the hydrogen/boron-nitrogen system. Early studies of CVD were intended to use the films in silicon device fabrication as an insulator. Rand *et al.* [128] and Murarka *et al.* [129] prepared amorphous BN films at the high ratio of NH_3 to B_2H_6 $\geq$10 by atmospheric pressure CVD. Hirayama and Shono prepared BN films on silicon substrates as a boron diffusion source in the fabrica-

*Adapted from: Proc.4th Jpn. Symp. Plasma Chem. Kyoto, 227 (1991).

tion of a planar diode. They obtained polycrystalline hexagonal BN at 1000 °C [56]. Deposition of BN at lower temperatures was attempted by using LPCVD. Adams *et al.* prepared amorphous films at temperatures ranging from 250~600°C. They estimated the activation energy to be 20~26 kcal/mol [141]. Dana and Maldonado also studied the films deposited by LPCVD at temperatures lower than 440 °C for use in X-ray lithography [58]. They found that the films deposited at such low temperatures contained a large amount of hydrogen. Studies of PCVD have been carried out with a view to obtaining stoichiometric BN at lower substrate temperatures. Hyder and Yep studied the growth of stoichiometric crystalline BN films by plasma-enhanced CVD at 1000 °C for the case: NH_3/B_2H_6 =7.1 [131]. Yuzuriha and Wess prepared amorphous BN by PCVD with a parallel plate reactor incorporating an electromagnet. The ratio of B to N in the film was approximately 1.7 when NH_3/B_2H_6=4 [133]. Miyamoto *et al.* prepared amorphous BN using capacitively coupled rf discharge at substrate temperatures below 300 °C. They referred to the etching effect by the hydrogen radical. Stoichiometric BN was obtained in the range $NH_3/B_2H_6 \geq 2.7$ [132]. Due to the excitation of reactant gas in the plasma, the film with B/N=1 can be prepared at lower NH_3/B_2H_6 ratio and lower substrate temperature than by thermal CVD. On the other hand, there have been some reports that suggest the possibility of *c*-BN synthesis under hydrogen plasma. The used approaches were very similar to those found successful with diamond sysnthesis [144]~[154]. From analogy with diamond synthesis, well crystallized *c*-BN may be achieved if there exists a special chemistry in the hydrogen/boron-nitrogen system to promote the *c*-BN growth. Unfortunately, however, all of these reports seem to be lacking in sufficient characterization for the definitive statements on the crystalline structure. Therefore, it was considered to be of great significance to examine these possibility and to resolve the caos state in this field.

In the section 3.1, BN films have been deposited by CVD under ICP at 0.1Torr from the H_2+B_2H_6+NH_3 system [155]. The main purposes of this experiment are (1) to examine the possibility of *c*-BN synthesis under high density hydrogen radicals and (2) to characterize CVD under ICP in comparison with that under glow plasma. Experiments have been carried out especially in terms of the substrate temperature.

3.1.2 Experimental

The schematic diagram of the experimental apparatus is shown in Fig. 3.1. The 13.56-MHz rf excitation is coupled into the plasma with a 3-turn coil around a water-cooled quartz tube. Plasma was generated inside a 38mm diameter pyrolytic boron nitride tube placed inside the quartz tube of 50mm in diameter to avoid contaminations from the quartz tube. Diborane, which is easy to decompose, was introduced through a water-cooled probe into the plasma, while all other gases were fed into the reactor from the top of the plasma source.

The reactor was pre-evacuated to $\sim 10^{-5}$ torr by a diffusion pump and backfilled with desired gases. ICP was generated at 5 kW and glow discharge was generated

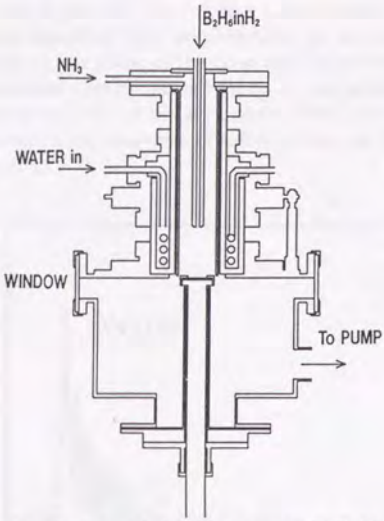

Figure 3.1: Schematic diagram of the low pressure ICP–CVD apparatus using the B_2H_6+H_2+NH_3 system.

at 3 kW for comparison. Flow rates of 5% diborane diluted with hydrogen and ammonia, both electronic grade, were 10 sccm and 1 sccm, respectively. The total gas pressure was kept at 0.1 torr throughout the experiments. A mirror-polished Si wafer (100) substrate was mechanically fastened to an electrically floated substrate holder. Substrate temperatures were measured using a chromel alumel thermocouple and regulated to the desired temperature ranging from 300 to 600 °C with a heater in a substrate holder. The film depositions were carried out for 2 hours. After the deposition, films were cooled down to the ambient temperature in hydrogen flow.

Structure and composition of deposited films were characterized by X-ray diffraction, IR absorption spectroscopy and X-ray photoelectron spectroscopy. Substrate temperature effects on the optical property and deposition rate were investigated by using ellipsometry and scanning electron microscopy.

3.1.3 Results and discussion

Structure and composition of the films

No clear difference could be found in the structure or the composition of the films prepared under ICP and under the high power glow plasma. Figure 3.2 shows a typical X-ray diffraction pattern of the deposited films. The fact that no (101)

reflection is observed in the (10) band means a structure lacking three dimensional ordering. Hence the deposited films were identified as the so-called turbostratic BN. The layer dimension in the plane of the layer can be calculated from the theory of the random layer lattice powder pattern [157]. It was estimated from the breadth at half the maximum intensity of the asymmetric (10) band to be $L_a = 8$ to 17 nm. No systematic change in the structure of the films was recognized for the substrate temperature variation.

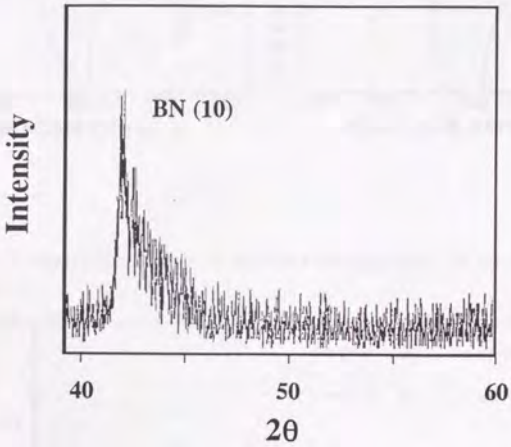

Figure 3.2: X-ray diffraction pattern from the film deposited at 588°C.

Figure 3.3 shows infrared absorption spectra of the films deposited at 600 °C. The absorption peaks at 1380 and 800 cm^{-1} are due to the B–N stretching bond and the B–N–B bending bond respectively [156]. Though N–H and B–H absorption peaks (at 2000~4000cm^{-1}) were not observed in the spectrum for the films deposited for 40 minutes [Fig. 3.3(a)], they appeared for the 5μm-thick film deposited for 120 minutes [Fig. 3.3(b)].

Figure 3.4 shows a typical example of the compositional depth profile determined by XPS using Ar ion beam etching, which revealed that relatively pure stoichiometric films with low oxygen content (~4%) could be deposited above 400°C. The increase of B concentration inside the film may be caused by selective sputtering effects. It is noteworthy that the oxygen and carbon content at the surface of the films are at the same level as that inside the film. The films deposited above 400°C in this work were stable in the ambient atmosphere. Surface reactivity of BN films is believed to result from bond breaking [158]. Therefore, the inertness of the surface is considered to be due to hydrogen termination of the dangling bonds.

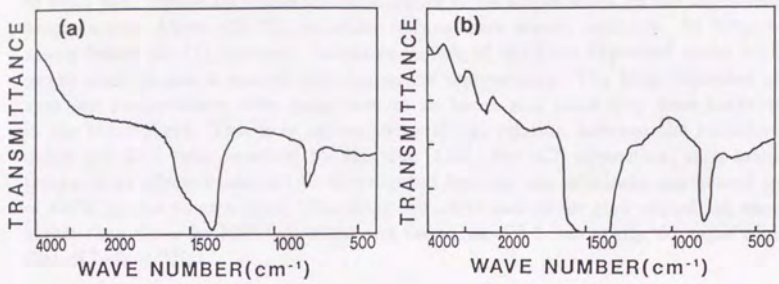

Figure 3.3: IR absorption spectra of the films deposited (a) for 40 minutes and (b) for 120 minutes .

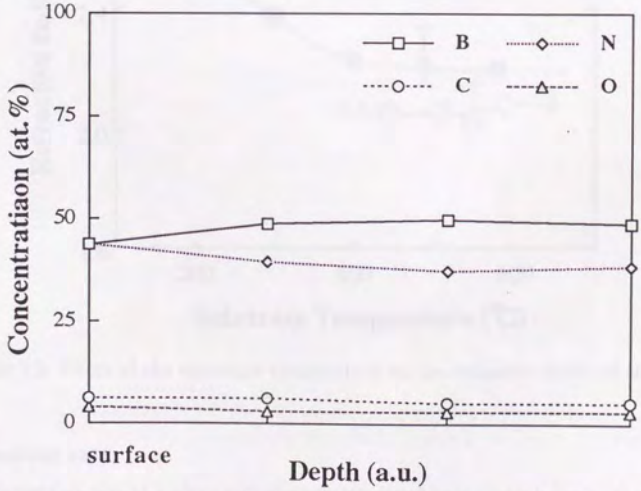

Figure 3.4: ESCA depth profile of the film deposited at 500 °C under ICP.

Optical property

Refractive indices of the films were measured using an ellipsometer at a wavelength of 546.1 nm. Figure 3.5 shows the dependence of refractive index on the deposition temperature. Above 400 °C, refractive indices were almost constant. At temperatures below 400 °C, however, refractive indices of the films deposited under high power glow plasma increased with decreasing temperature. The films deposited at such low temperatures were considered to be boron rich since they were unstable in the atmosphere. This is in agreement with the relation between the refractive index and B/N ratio reported by Murarka [129]. For ICP deposition, such lower temperature effects could not be investigated because the substrate was heated to ~ 400°C by the plasma alone. Saturated refractive indices for glow deposition were higher than those for ICP deposition and the value of 2.2 was nearly the same with that of bulk h-BN.

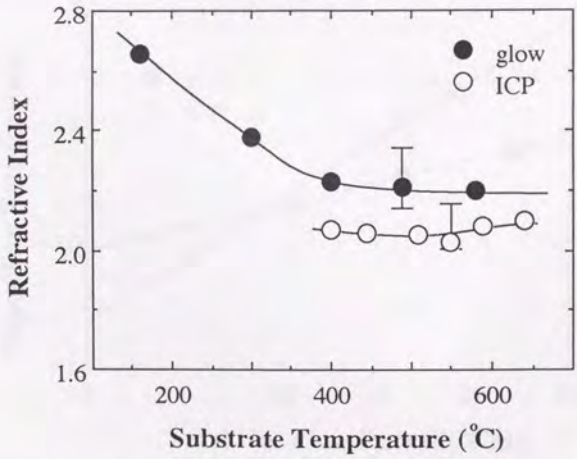

Figure 3.5: Effect of the substrate temperature on the refractive index of the film.

Deposition rate

The deposition rate at a given temperature increased linearly with the total gas flow rate as shown in Fig. 3.6. The yield was approximately 5% at a flow rate of 10 sccm. By extrapolating the deposition rate to a flow rate of zero, the apparent etching rate under ICP was estimated to be around 42nm/min. If the etching rate could be

inhibited, the deposition rate under ICP would be more than twice as high as that under high power glow plasma. The effect of the substrate temperature on the deposition rate is shown in Fig. 3.7. The deposition rate under high power glow plasma approximately followed the Arrhenius equation. The apparent activation energy was estimated to be about 4.2kcal/mol. On the other hand, the deposition rate under ICP exhibits a minimum at approximately 550 °C. This may be explained by the change of chemical reactivity of hydrogen in analogy with the etching of graphite (see Fig. 3.8) as follows. At temperatures below 550°C etching by atomic hydrogen causes a monotonic decrease of deposition rate with increasing temperature, while above 550 °C recombination of hydrogen on the surface predominantly occurs. The hydrogen molecule is less reactive than atomic hydrogen. The much higher hydrogen radical density in ICP than that in glow plasma has been demonstrated by optical emission spectroscopy in Fig. 2.4 in section 2.1 (p. 20).

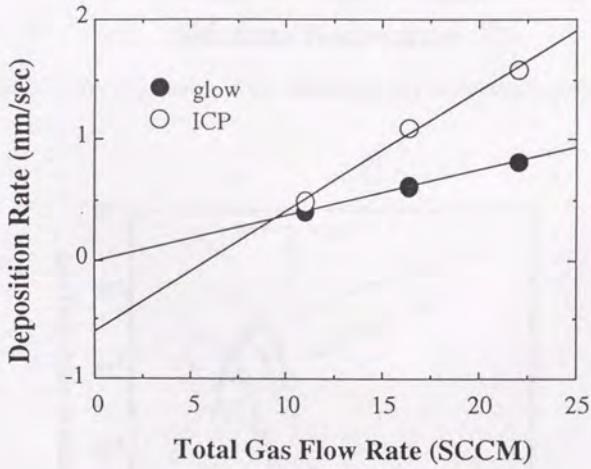

Figure 3.6: The dependence of the deposition rate at 500°C on total gas flow rate. The B_2H_6/NH_3 ratio and the pressure were kept constant throughout the series of experiments.

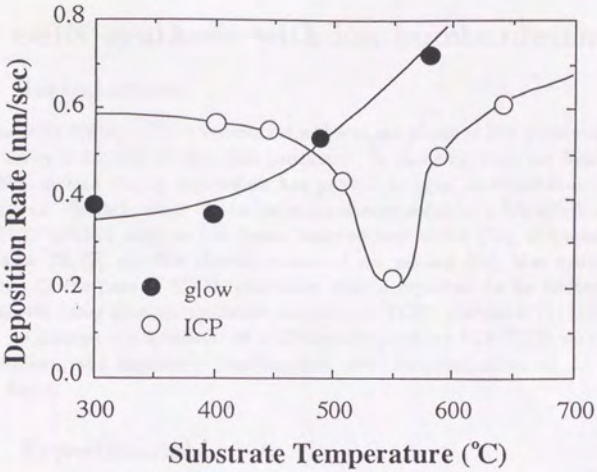

Figure 3.7: The dependence of the deposition rate on substrate temperature.

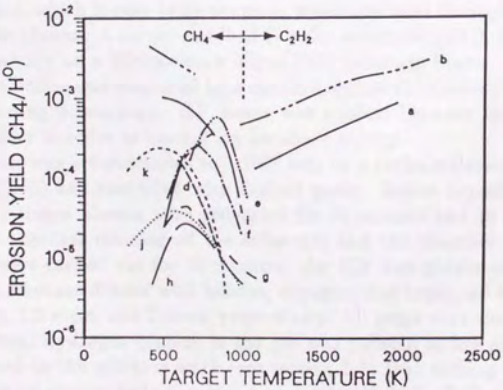

Figure 3.8: The dependence of the erosion yield on substrate temperature (after [159]).

3.2 c-BN synthesis with ion bombardment*

3.2.1 Introduction

From the early 1980s, *c*-BN synthesis from the vapor phase at low pressures has been studied using a number of thin film processes. In these studies, ion bombardment of the film surface during deposition has proved to play an important role in the *c*-BN growth. In fact, most of the techniques successful in *c*-BN synthesis are so-called PVD method such as ion beam assisted deposition [70], activated reactive evaporation [78,79], arc-like plasma enhanced ion plating [81], bias sputtering [89] etc. Also, in the case of CVD, substrate bias is reported to be necessary for *c*-BN synthesis using electron cyclotron resonance (ECR) plasma CVD [106]. In this section, we present the synthesis of *c*-BN by low pressure ICP-CVD with substrate bias technique, and especially identification and characterization of the deposited films in detail.

3.2.2 Experimental

The experimental apparatus is shown in Fig. 3.9. The 13.56-MHz rf excitation is coupled into the plasma with a 3-turn coil around a water-cooled quartz tube. Plasma was generated inside a 38mm diameter pyrorytic boron nitride tube placed inside the quartz tube of 50mm in diameter to avoid contaminations from the quartz tube. Nitrogen and argon were fed into the reactor from the top of the plasma source, while diborane, which is easy to decompose, was introduced through a water-cooled probe into the plasma. A mirror-polished Si wafer substrate [(100), 20×20 mm^2] was fixed mechanically on a Microscience Micro 1000 substrate heater. Temperature of the substrate heater was measured by a chromel alumel thermocouple and regulated to 900 °C during depositions. RF power was applied between the ground and a substrate holder in order to control ion bombard energy.

The reactor was pre-evacuated to $\sim 10^{-6}$ torr by a turbo molecular pump (Osaka Vacuum, TG550) and backfilled with desired gases. Before depositions, hydrogen plasma and nitrogen plasma were generated for 30 minutes and 10 minutes respectively for the sputter cleaning of the substrate and the chamber wall. The film depositions were carried out for 10 minutes. An ICP was generated at 7kW. Flow rates of 10% diborane diluted with helium, nitrogen, and argon, all electronic grade, were 20 sccm, 1.2 sccm, and 2 sccm, respectively. All gases were controlled by mass flow controllers. Hydrogen content in the gas was reduced as low as possible, since it was revealed in the previous work (see section 3.1) that etching rate of growing boron nitride by atomic hydrogen is not negligible in ICP–CVD and that the deposition of films with substrate bias is quite difficult under hydrogen plasma. The working gas pressure was monitored by a Shulz gauge calibrated for N_2 and was kept

*Partly in: Proc.11h Int.Symp.Plasma Chem. Loughborough U.K., 1022 (1993) and Appl.Phys.Lett. 64, 851 (1994).

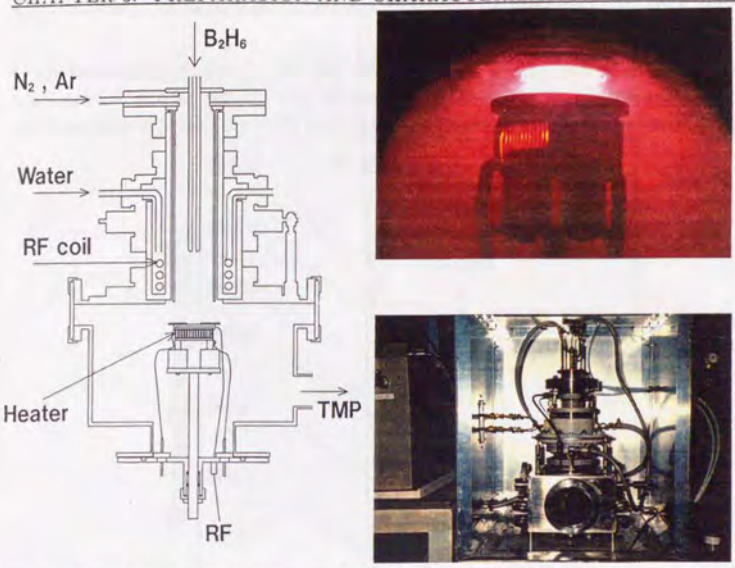

Figure 3.9: Schematic diagram and photographs of the low pressure ICP–CVD apparatus using the B_2H_6+N_2+He+Ar system.

at 1×10^{-3} torr throughout the experiment. After the depositions, films were cooled down to the ambient temperature in nitrogen flow. Deposited films were analyzed by IR absorption spectroscopy, X-ray photoelectron spectroscopy, Auger electron spectroscopy and transmission electron microscopy.

3.2.3 Results and discussion

IR absorption spectroscopy

The structure of the as-deposited films was studied using an infrared spectrometry in transmittance mode, using a bare silicon wafer as a reference. Figure 3.10 shows the IR absorption spectra of BN films deposited at various bias potential defined as a difference between the substrate potential and plasma potential which was measured 11mm above the substrate by emissive probe method as previously described in section 2.2.

The film prepared at the bias potential lower than 65 eV exhibits a strong absorption peak near 1370 and a weak one near 800cm^{-1}, due to the *h*-BN phase, assigned to B–N bond stretching and B–N–B bond bending respectively [156]. As the bias potential increases, the deposition rate drcreases by the sputter-etching effect. The film prepared at 68~91V exhibits a broad absorption band near 1060cm^{-1} attributed

to the reststrahlen band of c-BN [50]. Moreover, the higher bias potential depresses c-BN growth and at last the film deposition is prevented by sputter-etching. The optimum bias potential for c-BN growth in this experimental condition was 80~86V.

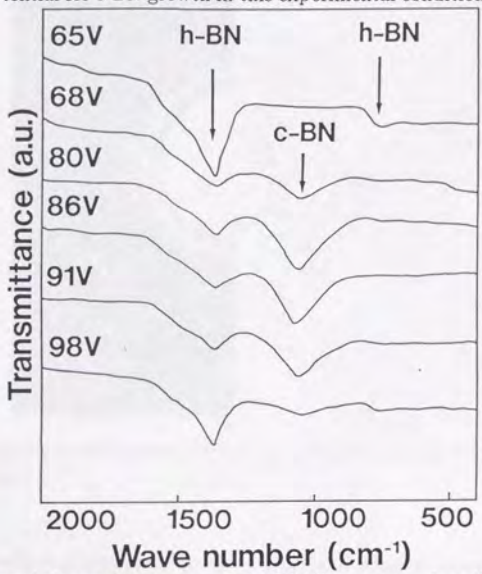

Figure 3.10: Infrared absorption spectra of the BN films prepared at different sheath potentials.

Transmission electron microscopy

Microstructure of BN was observed by Hitachi H-800 transmission electron microscope (TEM) operating at 200kV. Figure 3.11 shows a transmission electron diffraction (TED) pattern from the film prepared at 86V of bias potential. The TED pattern shows sharp rings indexable as c-BN, and the interplanar spacings agree well with the reported value as shown in Table 3.1. Relative intensities of the observed diffraction rings are also in good agreement with those calculated using the kinematical theory of electron diffraction and data of atomic scattering amplitudes for electrons [160]. A broad hollow diffraction ring of h-BN(002) observed inside the ring of the c-BN(111) suggests that c-BN is mixed with the turbostratic BN and it is in consistent with the result of IR absorption spectroscopy. Figure 3.12 (a) and (b) are bright- and dark-field images of TEM respectively. The size of the c-BN crystallites was estimated from the sizes of bright spots in the dark-field images to be 50 nm or less.

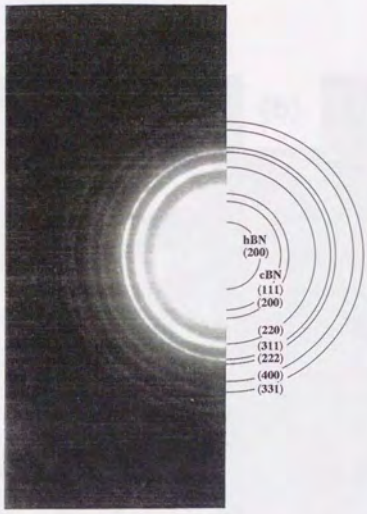

Figure 3.11: A transmission electron diffraction pattern from the film deposited at the sheath potential 86V.

Table 3.1: Comparison of observed lattice spacings and relative intensities with the reported and calculated values.

Observed value		ASTM 25-1033 (c-BN)			Calculated relative intensity
d(Å)	I	d(Å)	I/I_0	hkl	
3.36	M	...			
2.10	VS	2.088	100	111	100
...	...	1.808	2	200	0.65
1.28	S	1.2785	6	220	31
1.09	S	1.0901	3	311	14
1.04	W	1.0433	1	222	0.22
0.90	M	0.9041	1	400	2.4
0.83	M	0.8297	3	331	3.0

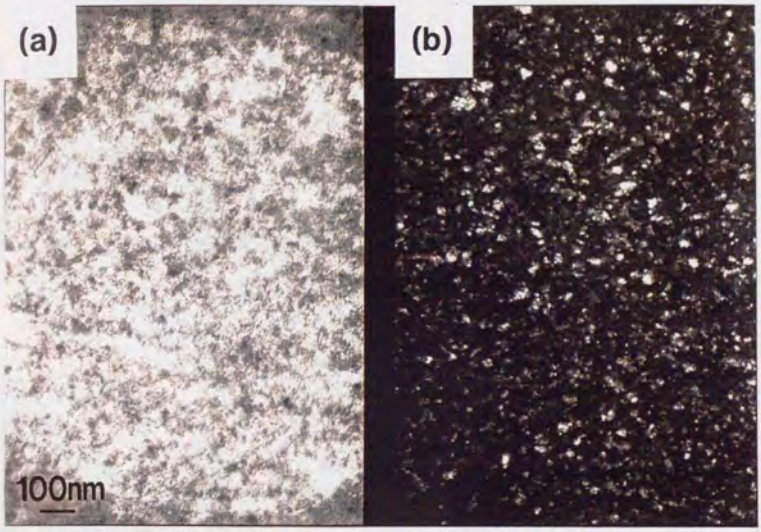

BRIGHT FIELD IMAGE DARK FIELD IMAGE

Figure 3.12: (a) and (b) are bright and dark field images of TEM respectively. The dark field image was observed using (111) orientation.

Figure 3.13 shows a high resolution TEM (HRTEM) image of *c*-BN obtained by using JEM-3010F (JEOL) operated at 300 kV. In ⟨110⟩ textured films, {111} cross-fringes of 2.09Åspacings are visible. The observed twin boundaries are of $\Sigma 3$ type (rotation angle of about 71°) using the coincidence site lattice notation [161], and besides, stacking faults are also observed. The heavily faulted microstructures and highly twinned crystallites in *c*-BN films have been reported also in the *c*-BN films deposited by bias-sputtering [90] and by ion-assisted pulsed laser deposition [162]. Figure 3.14 is the first HRTEM observation showing the multiply-twinned particles (MTP) in the *c*-BN film. As far as I know, MTP in *c*-BN has been previously observed only in the small *c*-BN particles grown as a by-product of an electron induced collapse of *h*-BN which had been treated by a hydrostatic compression with a solution of ethanol, methanol and water [163]. The samples of *h*-BN examined in the work were compressed in a diamond cell under a pressure of 13 GPa at room temperature. It has been reported that this kind of phenomenon was never observed in the original (non-treated) powders of *h*-BN illuminated under similar conditions.

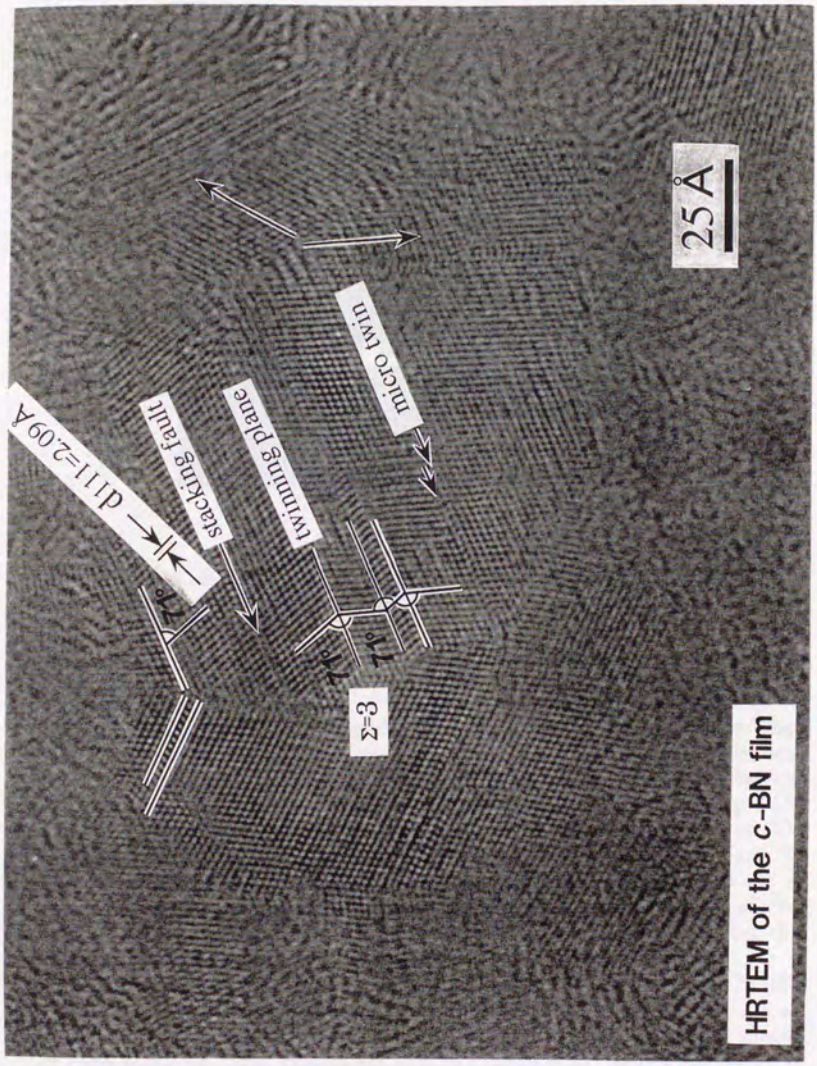

Figure 3.13: High resolution TEM image of c-BN. Numerous twin bondaries of $\Sigma 3$ type are observed.

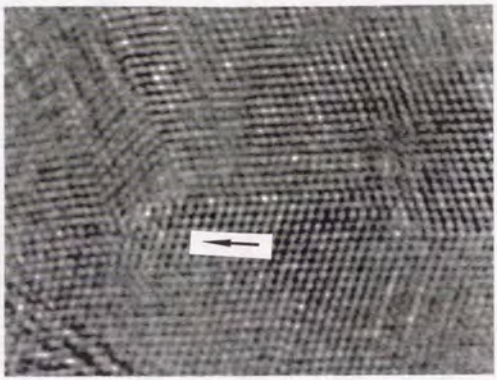

Figure 3.14: HRTEM of the multiply-twinned particles in *c*-BN film.

XPS and AES measurement

X-ray photoelectron spectroscopy (XPS) measurement was carried out in Shimadzu ESCA 850. Compositional depth profiles were obtained using neon ion beam etching, so that argon content in the film also could be investigated. Ion-sputter etching was performed with a beam energy of 2keV at 14mA beam current with a neon pressure of 3×10^{-4}Torr. Typical XPS spectrum of the deposited film is shown in Fig. 3.15. Figure 3.16 presents the compositional depth profile of the film prepared at 86V of bias potential. The B/N ratio calculated from the area ratio of B-$1s^{1/2}$ and N-$1s^{1/2}$ spectra indicates a stoichiometric value of 1.0 at the surface. The increase of B concentration inside the film is probably caused by selective sputtering effects. XPS analysis also revealed the film contained 5~6% carbon and oxygen, but the spectrum of argon could not be detected.

Auger electron spectroscopy measurement was carried out in JEOL JAMP-7100E. The Auger transitions were excited by an electron beam of I_p= 1 μm at 10 kV. In the literature, it has been reported that the Auger boron *KVV* line shapes of *c*-BN and *h*-BN differ significantly [164,165]. Figure 3.17 shows the measured Auger boron *KVV* spectra of *c*-BN film and *h*-BN film, together with the standard spectra in the literature [164]. The standard B-*KVV* spectrum of *h*-BN has six peaks, A_2(160.5 eV), A_3(151 eV), and A_4(143.5 eV) on the lower kinetic energy side

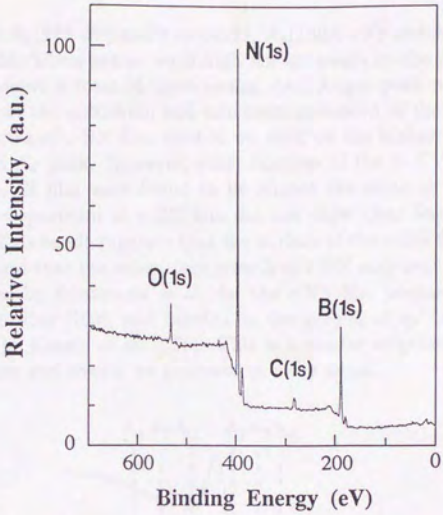

Figure 3.15: XPS spectrum of the *c*-BN film.

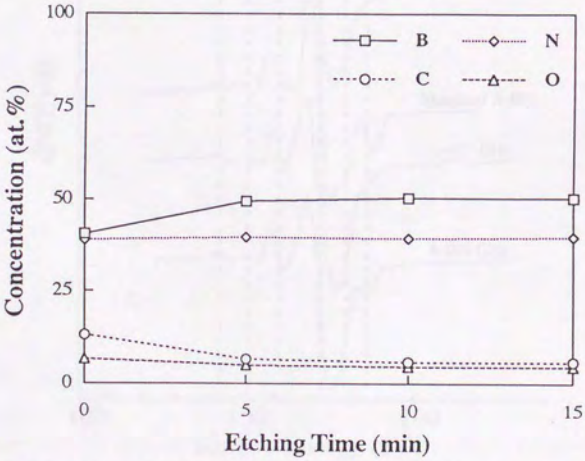

Figure 3.16: Compositional depth profile of the BN film prepared at the sheath potential of 86V.

of the main peak A_1(173 eV) and two peaks, A_5(180.5 eV) and A_6(187 eV), on the higher energy side. There are no such high energy peaks in the B Auger spectrum of *c*-BN, which shows a total of three peaks. (All Auger peak positions are taken as the mid-point of the maximum and minimum excursion of the derivative curve.) The B-*KVV* spectra of *c*-BN film showed no peak on the higher energy side, while that of *h*-BN had A_6 peak. However, other features of the B-*KVV* spectra of both *c*-BN film and *h*-BN film were found to be almost the same as those of standard *h*-BN. The Auger spectrum of *c*-BN film did not show clear features observed for standard *c*-BN. This result suggests that the surface of the *c*-BN film may consist of sp^2-bonded BN and that the subsurface growth of *c*-BN may occur. A similar result has been reported by Friedmann *et al.* for the *c*-BN film prepared by ion-assisted pulsed laser deposition [103], and besides, in the growth of sp^3-bonded amorphous carbon films by McKenzie *et al.* [166]. This is a matter of great concern with the growth mechanism and should be analyzed in more detail.

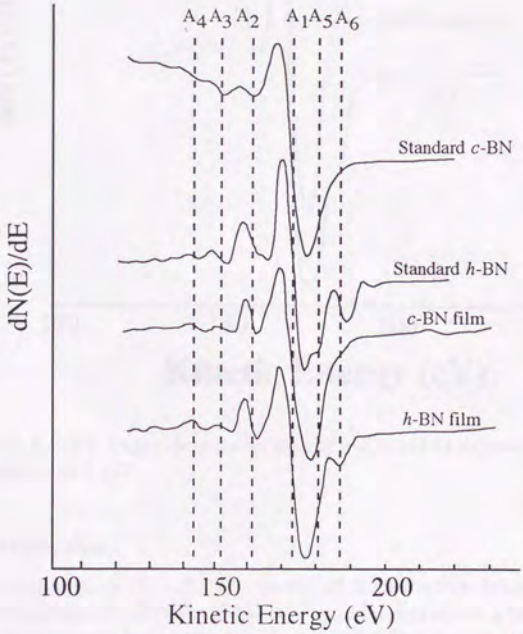

Figure 3.17: B-*KVV* Auger spectra from *c*-BN film and *h*-BN film.

Figure 3.18 shows the changes of B-*KVV* Auger electron spectra of the *c*-BN film upon Ar^+ irradiation at 1keV. It is clearly observed that the B Auger line shape developed hexagonal features, i.e., the peak on the higher energy side appeared. Trehan *et al.* also have reported that ion irradiation on *c*-BN changes the bonding characteristics sp^2-type.

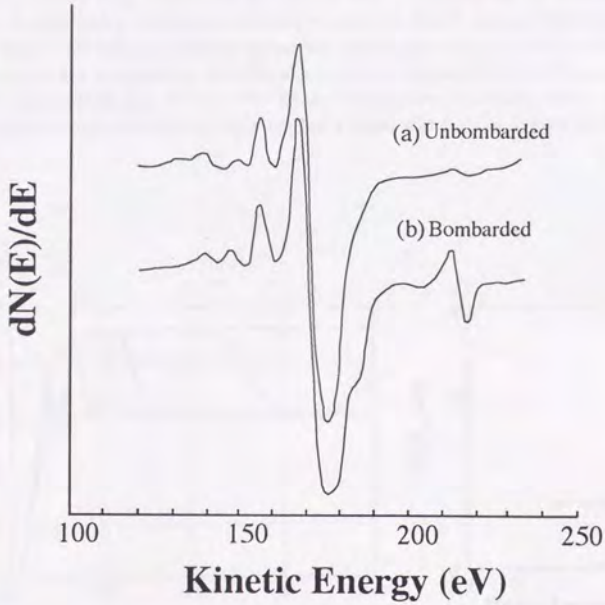

Figure 3.18: B-*KVV* Auger electron spectra of *c*-BN; (a) as deposited and (b) after Ar^+ irradiation at 1 keV.

Optical absorption

UV-visible spectrum of the *c*-BN film peeled off from the Si substrate was recorded on a spectrophotometer (Hitachi U-3410). Figure 3.19(a) shows a typical UV-visible transmission spectrum in the wavelength range of 0.2~1 μm for the thin *c*-BN film peeled away from the substrate. The *c*-BN film was found to be nondispersive and nonabsorbing in the visible light region and showed only the interference fringe pattern. However, as a matter of fact, the film consists of the double layers of *t*-BN

and c-BN, as will be clarified later in chapter 5. Hence it is difficult to determine the valid optical constants from the spectrum. In Fig. 3.19(b), the same data is plotted as the square of optical densities d multiplied by photon energy $h\omega$, $(dh\omega)^2$, versus incident photon energy to test for a relation of the form

$$(dh\omega)^2 = B(E_{opt} - h\omega). \tag{3.1}$$

The figure shows that, except for the lowest tail, the values lie on a straight line. This is characteristic to a semiconductor having a direct energy band gap. It is known that c-BN has an indirect transition band-gap, while h-BN has direct one. Therefore, on the assumption that the absorption at about 0.2μm is dominantly due to h-BN, the optical gap of the h-BN phase was crudely estimated to be about 5.4 eV, which is in agreement with the reported values, which lie in the range from 5~6 eV [52].

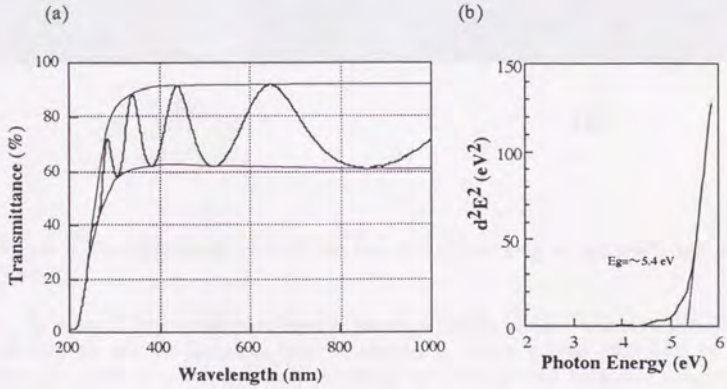

Figure 3.19: (a)UV-visible transmission spectrum of c-BN film. (b)Absorption edge fitted to direct allowed transition.

Compressive stress and adhesion

Films with high c-BN content have large compressive stress and store strain energies. Hence, thick film often results in buckling, cracking and peeling off from the substrate. It is well-known that when the stress is compressive, the peeling forms

specially shaped wrinkles in the film. Figure 3.20 shows the various stress relief patterns observed in *c*-BN films. Many researchers have reported the similar phenomena obeserved in diamond-like carbon films [167]~[173]. In addition, compressive stress in the film has been confirmed by the evidence of the shift of the IR absorption peak assigned to the reststrahlen band of *c*-BN to the higher wavenumber.

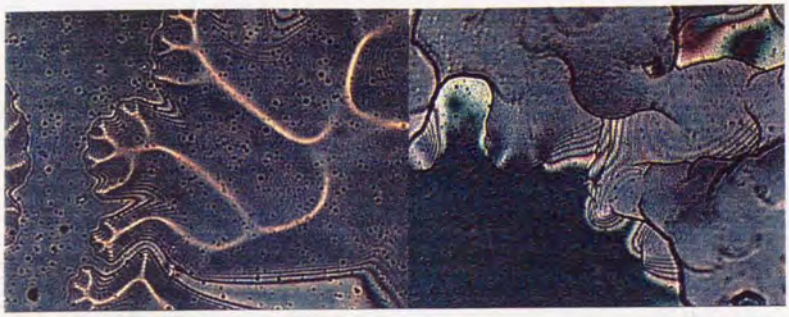

(a) (b)

Figure 3.20: (a)Buckling front of the film and (b)cracking of the *c*-BN film after buckling.

It is most likely that compressive stress is closely related with the formation of *c*-BN as will be discussed later in chapter 5, hence a breif discussion of the intrinsic stress is presented here. Virtually all metallic and inorganic compound films are in a state of stress. The total stress is composed of a thermal stress and so-called intrinsic stress. The thermal stress is due to the differences in the thermal expansion coefficients of the film and substrate materials. The intrinsic stress is due to the accumulating effect of the crystallographic flows that are built into the film during deposition, and is a process sensitive property [174]. The stress induced within the film may be large enough to either break the substrate or cause the film peel away from the substrate. Therefore special attentions have been paid to the relation among the stresses and the process parameters in various kinds of deposition processes. Though the exact origin of the intrinsic stress has not been known so far, the cause of stress in polycrystalline film has been generally explained in terms of several phenomelogical models. The grain growth and grain-boundary

relaxation model are fairly successfully applied to explain the intrinsic tensile stress. On the other hand, the compressive stress observed in the film deposited with ion bombardment has been attributed to so-called atomic peening, i.e., lattice distortion produced by energetic particles striking the condensing film [175]. The question has been raised in the literatures whether the ion peening mechanism is energy or momentum controlled. However, the dicision of the issue is not easy, since the stress data presented is not always presented in terms of a fundamental quantity. From the investigations of the relations between compressive stress and deposition conditions, some researchers have suggested that the momentum-per-atom may be the appropriate stress scaling factor [176,177], that is, the processes dominated by momentum transfer, as opposed to energy transfer, control the cause of intrinsic stress. Such processes include forward recoil implantation of film material atoms, which could change the amount of defects such as interstitials and dislocations, as well as the average density. However, since neither reliable measurement of the exact lattice positions nor the density of the stressed films have been made, an atomistic model to explain all the experimental results has not been established yet. Recently Müller has used a molecular dynamics (MD) model to study the intrinsic stresses in sputter-deposited thin films and has shown that interatomic attractive forces across atom scale pores provide a mechanism for the generation of tensile stresses in the film [178,179]. However his results predicted only tensile stresses in the range of governing parameter considered by him. Following his work, Fang *et al.* have studied the intrinsic stress in thin Ni films deposited in the presence of a background of argon and energetic ions by using 2-dimensional MD model over a wide range of parameters and have derived an interesting results [180,181]. They have concluded that argon impurities trapped into the deposited film are primary cause of the state of compressive stress and the magnitude of the compressive stress depends more strongly on the film structure than on the total quantity of the argon gas trapped in the film. A tight packing of film atoms around argon atoms is supposed to lead to higher compressive stress. However, in this simulation expected self-interstitial which is expected to be observed when the film is dense, was not obtained probably due to a smaller space provided by the 2D model or the symmetric character of the pair potential function.

Comments on the identification of c-BN films

The characterization of microcrystalline materials is often difficult. It seems to be substantially imposssible to convince oneself whether or not very small amount of cubic phase is contained in the sp^2-bonded BN matrix. Hence, it is meaningful to derive certain guidelines for the c-BN identification.

Once a working definition of "crystalline diamond material" was suggested by Messier *et al.* in a paper discussing the differences between crystalline diamond and DLC coatings [182]. "Crystalline diamond" produced by vapor deposition technique were defined by the following properties:

1. a crystalline morphology visually discernible by microscopy
2. a single-phase crystalline structure identifiable by X-ray and/or electron diffraction
3. a Raman spectrum typical for crystalline diamond

In the same way, guidelines for the identification of "vapor synthesized *c*-BN film" can be given by the following properties:

1. stoichiometry
2. crystalline structure identifiable by electron diffraction
3. IR absorption due to reststrahlen band at 1050~1100 cm^{-1}

In addition, there are a number of techniques that are potentially useful in studying the microstructure of *c*-BN films. Among them, X-ray [46] or UV spectroscopy [183,184], EPMA [185,186] and electron spectroscopy such as EELS [187,188], AES and XPS [165,164] have been reported to be useful techniques to distiguish *c*-BN from *h*-BN. It should be emphasized that total characterization is indispensable for the strict identification of *c*-BN. Silicon substrate is often used as a substrate for the *c*-BN deposition since it is suitable for IR absorption spectroscopy. However, it is indeed impossible to distinguish Si–O absorption peak at 1080cm^{-1} from that of *c*-BN. Therefore it is too dangerous to indentify *c*-BN by using only IR absorption spectroscopy. Similarly, identification by using only TED often results in the misidentification. A TED pattern from *c*-BN is very similar to the *t*-BN, which is readily prepared by vapor deposition. In addition, incorporation of f.c.c. metal impurity often leads to misidentification. It should be noted that the lattice spacing of cupper is almost the same as that of *c*-BN. It is also the case for XRD, though XRD analysis is unsuitable for thin BN films. XRD patterns from the BN film usually show only a few broad peaks due to the small crystalline size and small X-ray scattering factor of boron and nitrogen.

3.3 Conclusion

In chapter 3, *c*-BN synthesis has been attempted by two different approaches. In section 3.1, preparation of BN films under hydrogen plasma has been investigated. Stoichiometric BN was obtained by low pressure plasma CVD from gas mixtures of NH_3/B_2H_6=2. Microcrystalline turbostratic BN was obtained at substrate temperatures $\geq$400 °C. In ICP deposition, the etching reaction rate due to the atomic hydrogen was found not to be negligible comparing with the deposition rate. No evidence for the existence of cubic phase was found. In section 3.2, *c*-BN films have been successfully prepared by ICP–CVD with substrate bias technique. Characterization of *c*-BN films has been carried out by various techniques. Stoichiometric films

consisted of microcrystalline *c*-BN are obtainable with adequate ion bombardment during film growth. In conclusion, it is very unlikely to exist some particular chemistry in hydrogen/boron-nitrogen system to promote *c*-BN growth, while physical effects of ion bombardment of the growing surface make *c*-BN synthesis possible.

Chapter 4

Phase Control of BN films

4.1 Introduction

From the late 1980s several reports have clearly shown the evidence of *c*-BN formation from gas phase. These studies have shown that *c*-BN can be synthesized with proper ion bombardment of the film surface during deposition. As described in section 3.2 we have also succeeded to prepare *c*-BN by ICP–CVD with applying a proper bias to the substrate [112]. Low-energy ion bombardment is extensively used in today's film deposition technology to modify film microstructure and hence film properties. Numerous effects of ion bombardment on the film structures include reduction of grain size, differences in preferred cyrstalline orientation, densification, lattice expansion, modificaiton of crystal structure and film morphology. Physical properties that are sensitive to microstructure have been found to reflect these effects, including stress, adhesion, resistivity, refractive index and so on. In recent years, there have been increasing interests in elucidating the mechanisms of film modification by ion bombardment. However, role of energetic ions are often masked and complexly modified by differences in other deposition parameters. It is also the case in the field of *c*-BN film growth study. In spite of the numerous reports of the *c*-BN synthesis, quantitative experimental data available for the quantitative analysis of the growth mechanisms are still in short. On the other hand, so far, it has been commonly reported that ion bombardment also results in the poor adhesion to the substrate due to their strong compressive stress and the very small crystalline size of no more than 10^2nm. Therefore, there arises a crucial question whether or not it is possible to form *c*-BN and to depress such unfavorable effects simultaneously. Fundamental understanding of the growth mechanisms of *c*-BN by vapor deposition is indispensable for the improvement of deposition techniques to resolve these problems and to utilize the substantial promise of *c*-BN. Accordingly it is essential to clarify the fundamental parameters of the deposition system such as ion energy, flux of the incident accelerated-ions and flux of the deposited atoms and to reveal their quantitative correlations among structures and properties of the deposits. In section 4.2 and 4.3, the effects of sheath potential and gas pressures on

the formation of *c*-BN have been parametrically investigated respectively in order to examine the role of ion bombardment of the growing surface.

4.2 Experimental

Details of a low pressure ICP–CVD system and deposition procedures have been described previously in section 3.2.2 (p. 37), so a brief discussion is presented here. The plasma source and deposition chamber were pre-evacuated to $\sim 10^{-6}$ torr by a turbo molecular pump and backfilled with desired gases. Before depositions, hydrogen plasma and nitrogen plasma were generated for cleaning the substrate and the reactor wall for about 40 minutes. Subsequently the film deposition under low pressure ICP generated at 7kW was carried out for 10 minutes. After the depositions, films were cooled down to the ambient temperature in nitrogen flow. Flow rates of 10% diborane diluted with helium, nitrogen and argon were 20 sccm, 1.2 sccm and 2 sccm, respectively. A Si wafer substrate [(100), $2\times 2\text{cm}^2$] was fixed mechanically on a substrate heater. A substrate temperature was regulated to 900 °C. Sheah potential and working gas pressure were systematically changed as experimental parameters. Sheath potential was controlled by varying externally applied rf power to the substrate. In the experiment discussed in section 4.3.1, effects of ion bombardment energy on the *c*-BN formation have been dominantly investigated at the constant gas pressure of 1 mTorr. In section 4.3.2, gas pressure, as well as sheath potential, was also varied from 0.5∼2 mTorr. The crystallite phases of the as-deposited films were examined by using infrared (IR) spectrometer (Shimadzu IR 435) in transmittance mode. Film thicknesses were measured from the cross-sectional scanning electron micrographs (SEM) of the deposited films.

4.3 Results and Discussion

4.3.1 Effect of substrate bias on the c-BN synthesis*

IR absorption spectroscopy

Figure 4.1 shows the evolution of the IR transmission spectra of the BN films deposited at the various sheath potentials.

For the quantitative analysis the dependence of the IR absorbance at 1060cm^{-1} (*c*-BN) and 1370cm^{-1} (*h*-BN) on V_{sheath} is presented in Fig. 4.2. Strictly speaking, the absorption at 1370cm^{-1} is mainly due to so-called turbostratic BN with disordered layer structures. Substrate bias condition can be divided into four regions relating to the polymorphism of the deposited films. At V_{sheath} =27∼65V only the absorption peaks due to *h*-BN are observed, and they decrease as the substrate bias increases (region I). At V_{sheath} =68V an additional peak due to *c*-BN appears. At

*Adapted from: J.Appl.Phys. **75** 1330 (1994).

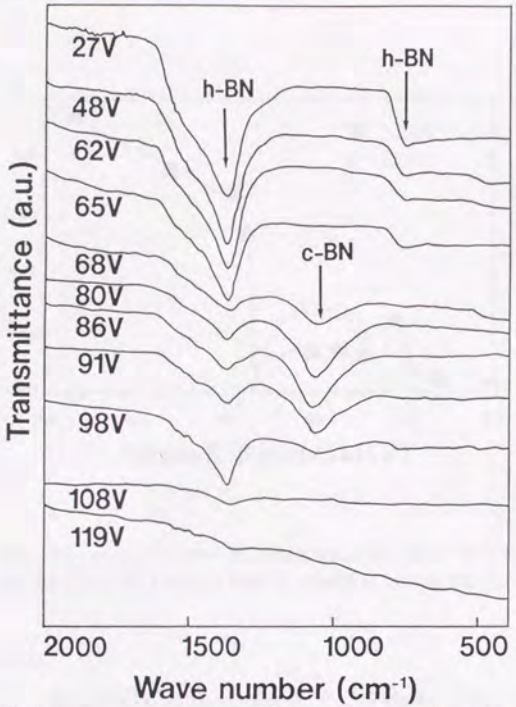

Figure 4.1: IR absorption spectra of the BN films deposited at the various sheath potentials.

V_{sheath} =68~91V absorptions due to *h*-BN are nearly constant, but those due to *c*-BN vary with the sheath potential with a maximum at 80~86V (region II). At V_{sheath} =98V absorption due to *h*-BN increases again (region III); too high energy ion irradiation prevents the *c*-BN growth. At V_{sheath} above 108V, almost no absorption is observed (region IV). Such tendency is qualitatively in agreement with some other reports [89,189,190]. In this study, the lower threshold sheath potential for the formation of *c*-BN and the upper one are about 65eV and 100eV respectively. The threshold self-bias voltage reported in ECR plasma CVD is also as low as several tens volt [105]. (The plasma potential is not clear in their work.) It is noteworthy that the actual average energy of ions impinging towards the substrate is expected to be higher than the sheath potential by several eV, as discussed in section 2.2. On the other hand, the threshold ion bombardment energies reported for PVD methods often exceed around several hundreds eV (See Table 1.2 p. 14).

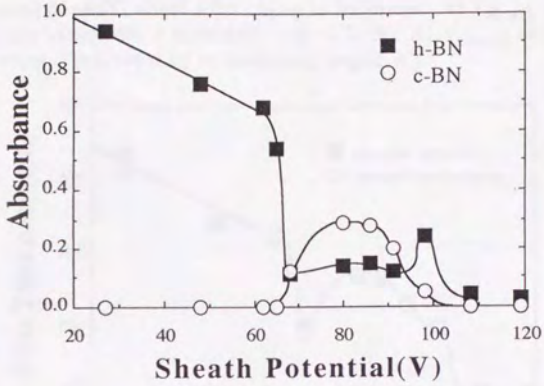

Figure 4.2: The dependence of the IR absorbance of boron nitride at 1060cm^{-1} (c-BN) and 1370cm^{-1} (h-BN) on the sheath potential during the film deposition.

Deposition rate

A typical cross-sectional SEM of the deposited film is shown in Fig. 4.3.

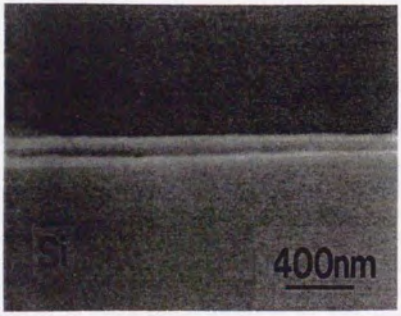

Figure 4.3: A cross-sectional scanning electron micrograph of the BN film deposited at the sheath potential of 86V.

The measured film thickness is plotted against the sheath voltage in Fig. 4.4. With increasing the sheath potential, the film thickness decreases (region I) and drastic drop occurs at 65~68V, where *c*-BN begins to be formed. At V_{sheath} =68~98V the film thickness varies with a maximum (region II, III). At V_{sheath} above 108V, the film deposition is prevented by re-sputtering (region IV).

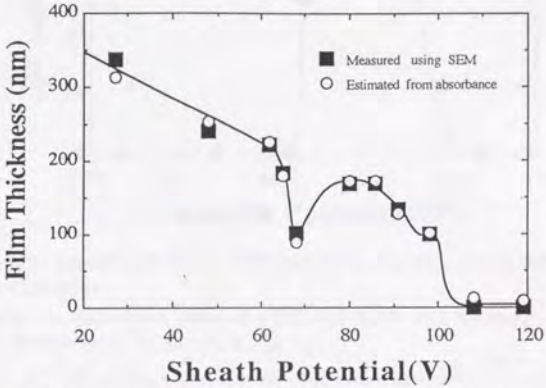

Figure 4.4: The dependence of the BN film thickness on the sheath potential during the deposition. Film thicknesses measured by SEM are fitted using measured IR absorptions assuming the absorption coefficient of each BN phase is constant.

The absorption coefficients of *c*-BN and *h*-BN in the film (k_{c-BN}, k_{h-BN}) have been estimated by fitting the IR absorbance of *c*-BN and *h*-BN (A_{c-BN}, A_{h-BN}) to the film thickness d from the following formula:

$$d = A_{c-BN}/k_{c-BN} + A_{h-BN}/k_{h-BN}. \tag{4.1}$$

As shown in Fig. 4.4, the measured film thicknesses are well fitted by evaluating the absorption coefficients of cubic BN (at 1060cm^{-1}) and hexagonal BN (at 1370cm^{-1}) to be 23000cm^{-1} and 30000cm^{-1} respectively. In general, optical constants of the thin film are apt to depend on the deposition condition. In the present case, however, the absorption coefficients were evaluated to be almost constant irrespective of the bias voltage and are about 1/3 of the values estimated from the data of bulk BN [156, 50]. Using these values, the *c*-BN contents in the films are estimated as presented in Fig. 4.5, which demonstrates the strong dependence of *c*-BN formation on the sheath potential. The maximum *c*-BN content of the film deposited in the series of the experiment seems to be saturated at about 75%. This has been revealed to be due to the existence of the interface layer of sp^2-bonded BN deposited at the initial stage of the film deposition, as will be shown in chapter 5.

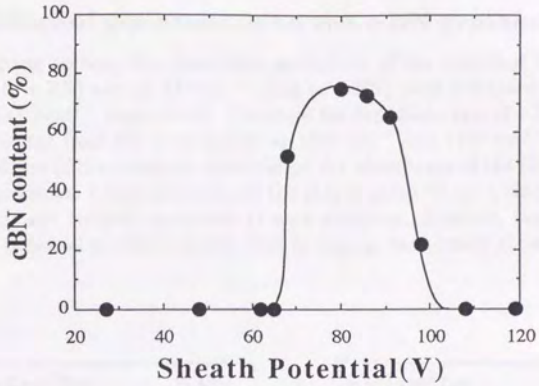

Figure 4.5: The dependence of the *c*-BN content in the film on the sheath potential during the deposition.

Consequently the deposition rates of *c*-BN and *h*-BN as a function of the sheath voltage can be evaluated as shown in Fig. 4.6.

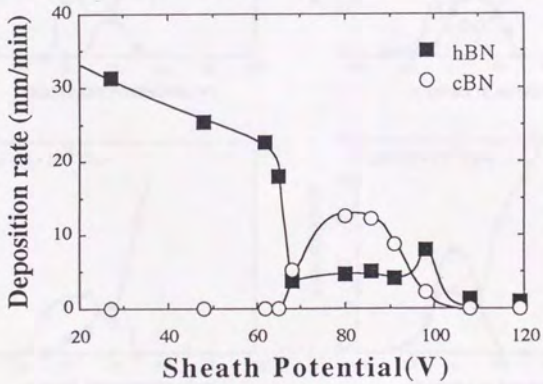

Figure 4.6: The growth rates of *h*-BN and *c*-BN as a function of the sheath potential during the film deposition.

4.3.2 Effect of gas pressure on the c-BN synthesis*

In the foregoing section, the absorption coefficients of the deposited films at 1060 cm^{-1} (due to *c*-BN) and at 1370cm^{-1} (due to *h*-BN) were evaluated to be 23000 cm^{-1} and 30000 cm^{-1}, respectively. Therefore the deposition rate of *c*-BN and *h*-BN can be estimated from the absorbances at 1060 cm^{-1} and 1370 cm^{-1}. Figure 4.7 shows the effects of the substrate potential on the absorbance of the films deposited at various pressures. I dare not estimate the sheath potential here, since the plasma potential was not precisely measured at each pressures. However, the variation of the plasma potential is within several Volt or less, as has already shown in Fig. 2.7 (p. 23).

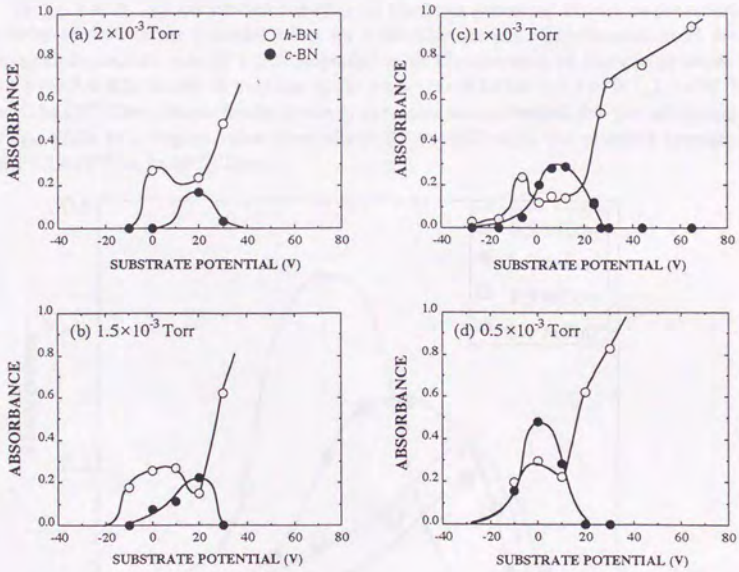

Figure 4.7: Dependence of the the absorbance at 1060cm^{-1} (•) and 1370cm^{-1} (∘) on the substrate potential. BN films were deposited at (a) 2×10^{-3}Torr, (b) 1.5×10^{-3}Torr, (c) 1×10^{-3}Torr and (d) 5×10^{-4}Torr.

*Adapted from: Jpn.J.Appl.Phys. **33**, 4385 (1994).

At any given constant pressure, the substrate bias condition can be divided into four regions relating to the polymorphism of the deposited films. At higher substrate potentials, that is, at lower sheath potentials; only the absorption peaks due to *h*-BN are observed, and A_{h-BN} decreases as the substrate bias increases (region I). At a certain threshold bias potential, the absorption due to *c*-BN appears. As the sheath potential increases, the *c*-BN content in the film increases.At the substrate bias at which the absorbance of *c*-BN reaches its maximum,that of *h*-BN remains almost constant at 0.15–0.2. As will be presented in chapter 5, under optimal conditions single *c*-BN phase can be grown over the 50–70-nm-thick sp^2-bonded BN initial layer (region II). Further increase of the bias voltage causes the decrease of A_{c-BN}, and then A_{h-BN} increases again (region III); the excess ion bombardment lowers the *c*-BN content in the film. At lower pressures this region tends to disappear. Finally, film deposition is prevented by re-sputtering (region IV).

In Fig. 4.8, A_{c-BN} are plotted together for the films deposited at various pressures in order to discuss the pressure effect on *c*-BN film growth. The maximum of the averaged deposition rate of *c*-BN increased with the decrease of the gas pressure: they were 7.4, 9.6, 13 and 21 nm/min at the pressures of 2×10^{-3}, 1.5×10^{-3}, 1.0×10^{-3} and 0.5×10^{-3} Torr, respectively. Second, the substrate potential for the maximum A_{c-BN} shifts to a higher value from about 0V to 20V with the pressure increase from 0.5×10^{-3} to 2×10^{-3} Torr.

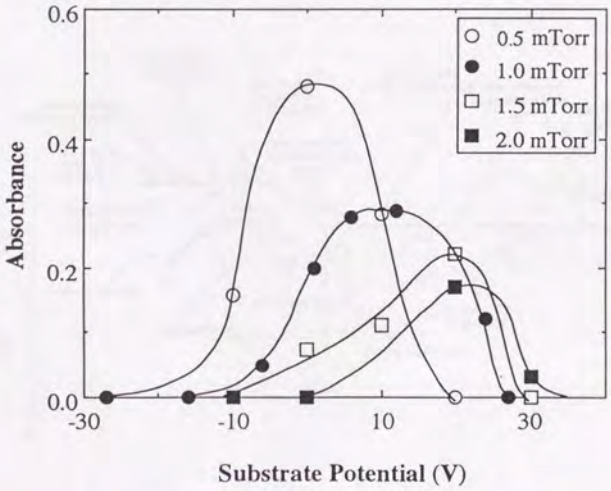

Figure 4.8: Pressure effect on the cubic phase growth.

As shown in the previous sections, in the pressure range of this series of deposition

As shown in the previous sections, in the pressure range of this series of deposition experiments the plasma potential slightly decreases with increasing pressure, while the densities of the ions and radicals tend to increase. Generally the sensitivity to ambient pressures is often linked to the particle transport processes from plasma to substrate. However, in the pressure range of this experiment collision frequency would not be so affected. Therefore higher plasma density may result in lowering of the ion bombardment energy necessary for *c*-BN growth. In other words, *c*-BN growth can not be described only by the ion bombardment energy. This result is interesting in relation with the recent suggestion by Kester and Messier that the momentum per atom transferred into the film by ion bombardment is the controlling factor for *c*-BN growth [189].

4.3.3 Role of ion bombardment

Ion bombardment is the most important factor in the *c*-BN growth mechanism. In this section, the roles of the ion bombardment are discussed in connection with the cubic phase BN formation.

Ion bombardment is extensively used in the film deposition technology. Figure 4.9 depicts the numerous effects on the surface and the subsurface region by bombardment by energetic species.

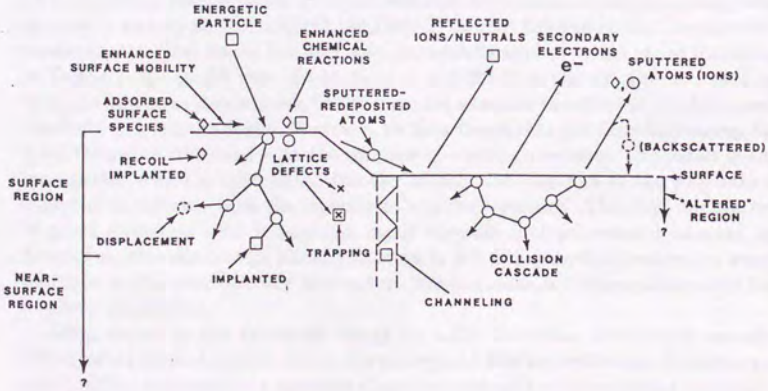

Figure 4.9: Schematic depiction of the energetic particle bombardment effects on surfaces and growing films (after [191]).

Some models of *c*-BN formation have been proposed so far. Weissmantel [65] has attempted to interpret the *c*-BN forming process by a first approximation model based on the concept of rapidly collapsing thermal spikes and displacement spikes as introduced by Seitz and Koehler [192]. In so-called thermal spike model, energy of a bombarding ion is shared with the atoms it collided with, i.e., dissipated as lattice vibrations or "heat" in the microscopically localized region. It is suggested that a thermal spike region is similar to the high pressure high temperature conditions which are used for *c*-BN synthesis. This model has been cited by many researchers, however, thermal spike model can give only a qualitative explanation to the experimental results.

Recently Kester and Messier have experimentally studied the effect of preparation conditions on the resulting phase using the ion beam assisted evaporation with various kinds of ion species (Ar, Xe and Kr) [189]. They have revealed that at 300–400 °C a sharp threshold value of momentum-per-atom exists below which films are hexagonal and above which they are cubic. For 400 °C the threshold was reported to be 200 $(\mathrm{eV}\times\mathrm{amu})^{1/2}$/atom. They have concluded that the momentum per atom transferred into the film by ion bombardment is the controlling factor for *c*-BN growth by ion-beam-assisted evaporation. It is noted that the thermal spike model is essentially an energy driven process, while the momentum transfer model is momentum driven. In general, the parameter of momentum-per-atom may be the most important parameter to characterize the film property modification in the ion assisted deposition process. Momentum-per-atom has been recognized to be a important scaling factor by some researchers in terms of film properties such as density and stress [171,176,193,194,195]. It is very interesting that recently the momentum transfer model has been also successfully applied to the phase transition of Ta film [196]. In the case of our study, it is difficult to discern whether the data favor the energy or momentum, for we have not examine the effect of ion flux quantitatively and systematically. However, we have found that the threshold energy for *c*-BN formation decreases with the increase of working pressure. This result is not inconsistent with the momentum transfer model, since ion flux to the substrate is expected to increase with the increase of working pressure. The close correlation of phase formation with momentum input suggests that processes dominated by momentum transfer control phase formation in BN film growth. However, an exact atomistic mechanism whereby momentum transfer leads to phase stabilization has not been established.

With regard to the threshold energy for *c*-BN formation, momentum transfer model indicates that, within limits, the energy and flux are equivalent, interchangeable entities. However, it is apparent that one hundred 1 eV ions are not equivalent to one 100 eV ion. (This case is out of limit). Thus there should exist a lower limit of the ion energy for *c*-BN growth. Recently Kidner et.al. have reported to have found a sharp bias voltage threshold above which *c*-BN is formed by using the magnetron sputtering [92]. They suggested that *c*-BN formation requires the arrival of energetic species with about 100 eV kinetic energy to facilitate bond breakage

of surface atoms during growth, which causes a hybridization change from sp^2 to sp^3. It is ambiguous whether their interpretation is proper or not. However, it is noteworthy that their low threshold energy is almost the same with that of our result.

The processes dominated by momentum transfer include forward recoil implantation of film material atoms, which could change the amount of defects such as interstitials and dislocations. Therefore it is most probable that approximately 100 eV is the lower threshold energy for *c*-BN formation, as approximately estimated below by using the theoretical and empirical equations for the sputtering and ion plating. For the threshold energy for the displacement of the target materials E^*

$$E^* = \frac{(M_1 + M_2)^2}{4M_1M_2} E_{th}, \tag{4.2}$$

where M_1, M_2 and E_{th} are mass of incident ion, mass of target atom and the threshold energy for sputtering of target, respectively. E_{th} is given with the sublimation energy U_s by the relation [197]

$$\frac{E_{th}}{U_s} = 1.9 + 3.8(M_2/M_1)^{-1} + 0.134(M_2/M_1)^{1.24}. \tag{4.3}$$

The sublimation energy can be estimated from the published value 13.43 eV of the enthalpy of the following reaction: BN(s) $\longrightarrow$ B(g)+N(g) [198]. The average value of the sublimation energy for either a boron or a nitrogen atom is therefore U_s=13.4/2=6.7 eV. Using the mass of incident ion M_1=39.948 (Ar) and M_2=12.4085 (average mass of B and N), E_{th} and E^* are estimated to be around 95 eV and 130 eV, respectively. When an incident ion is N_2^+, the values becomes smaller by tens V. The experimental estimates of the threshold energy for displacing an atom in diamond, derived from high-energy electron scattering, vary from 35~80 eV [199,200]. Recent theoretical investigations have shown that the displacement energy for diamond is approximately 50 eV [201]. Wu *et al.* attributed this high threshold energy to a rapid dissipation of kinetic energy from the bombarded atom into incoherent vibrational energy of its neighboring atoms, i.e., large speed of sound in diamond.

Furthermore, in order to speculate the atomistic behavior of Ar^+ ions impinging to BN surface with energy of 100 eV, simulation has been undertaken by using TRIM code [202,203,204]. Monte Carlo TRIM program for the *tr*ansport of *i*ons in *m*atter follows a large number of individual ion histories in a target. The essential assumption of this code are the followings:

1) The target is amorphous. Thus, for instance, channeling effects are neglected.

2) The program is based on the binary collision approximation (BCA).

The ions follow through a sequence of collisions with target atoms, assuming a straight free-flight path between collisions. The particle's energy is reduced after each free-flight path by the amount of electronic energy loss and then (after the collision) by the so-called nuclear energy loss. If the target atom has received a amount of energy which exceeds the dislplacement energy, it would be called primary

knockon atom (PKA), and its history will be followed in the same way as that of incident ion. The same would hold true with any higher generation recoil atoms created in the course of further collisions. The history of an ion or recoil atom is terminated either when the energy drops below a prespecified value , or when the particle has moved out of the surface of the target. At low ion energy below 10 eV, the BCA breaks down and molecular dynamics (MD) techniques have to be used, so that multiple collisions can be accounted for. Fortunately the practical experiences of the binary encounter model yield quite satisfactory agreement with available experimental data, even in following recoils to extremely low energies. The BCA is believed to remain valid at energies above 50 eV or so.

Figure 4.10 shows the results of 100 eV Ar^+ ions penetrating into BN target. The approximated simulation predicts the displacements of surface atoms and narrow range within a few atomic layers. Thus, ion bombardment is expected to cause frequent atomic displacement at the surface of the *c*-BN film during film growth. This may be the cause of the unanticipated Auger electron spectrum from the *c*-BN film surface obtained in section 3.2.

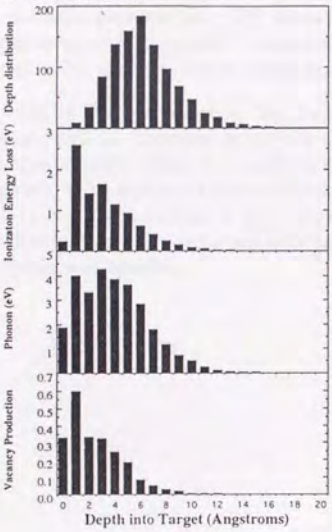

Figure 4.10: Range and damage distribution of 100 eV Ar^+ entering into BN, calculated by TRIM.

4.4 Conclusion

Effects of the (1) sheath potential and (2) gas pressure on the phase formation of BN film have been studied by using low pressure ICP–CVD.

1. A narrow ion energy "window" for the *c*-BN formation has been observed. From IR absorption analysis and the thickness measurement of the deposited films, deposition rates of cubic and hexagonal BN were estimated as a function of the sheath potential. Ion energy condition can be divided into the four different regions, as follows. At V_{sheath} below 65V (region I) only *h*-BN deposits. The linear decrease of the deposition rate from 32nm/min to 18nm/min with increasing the sheath potential is most likely due to the re-sputtering effect. Cubic BN deposition occurs at V_{sheath}=68~98V (region II), at which the deposition rate of *h*-BN is estimated to be rather low and nearly constant. It may be due to the *h*-BN interface layer less than 50nm. The deposition rate of *c*-BN varies with a maximum value of 13nm/min at 80~86V. Further increase of the sheath potential prevents the *c*-BN formation and the deposition rate of *h*-BN increase again at V_{sheath} =98V (region III) and ultimately at V_{sheath} above 108V (region IV) complete resputtering of the film takes place.

2. With the decrease of the gas pressure, the increase of deposition rate was observed. The required ion bombard energy for the *c*-BN formation becomes lower at higher gas pressure. From the results of the plasma diagnostics, these results are supposed to be due to the increase of ion flux with the gas pressure. It is concluded that *c*-BN formation is not controlled only by the ion energy but also by the flux. Our result is cosistent with the momentum transfer model suggested by Kester and Messier.

Chapter 5

Initial stage of the c-BN growth on Si substrate*

5.1 Introduction

At present, as commonly reported, the *c*-BN film synthesized from vapor phase with concurrent ion bombardment suffers from the extremely high compressive stress, which often leads to adhesion failure. Moreover, the *c*-BN crystalline size is no more than several tens nm. It is considered that ion bombardment during film growth is essential for the *c*-BN growth, but that it may also result in the undesirable film quality. Therefore, clarifying the growth mechanism of *c*-BN is of great importance not only as a subject of basic science but also as a guide for the design of favorable deposition process. Recently it has been suggested that the processes dominated by momentum transfer control the growth of cubic phase. However, exact microscopic mechanism whereby momentum transfer leads to *c*-BN formation has not been known yet.

In this chapter, for better understanding of the growth mechanisms, the different growth stages of *c*-BN films have been investigated. For this purpose, it is desirable to prepare the films with different film thickness under similar deposition condition. In the case of laser deposition, for example, a half-shadow technique, whereby the substrate is partially shaded by a shutter located between the target and the substrate, has been reported to permit the preparation of thickness gradient film [205]. However, this technique can not be applied to the ion-assisted depositions, since a shutter has different influence on ions than neutrals. We have used a plasma diffusion technique for film preparation by plasma CVD and have successfully prepared thin *c*-BN films with thickness gradients under identical deposition conditions on a single substrate. Films were analyzed at various lateral positions on the substrate by using several techniques. Results are mainly discussed with regard to the initial stage of the *c*-BN growth.

*Partly in: Proc.7th Symp.Plasma Sci.Mater., Tokyo, 119 (1994).

5.2 Experimental

Details of the ICP–CVD apparatus were described in section 3.2. ICP was generated inside a 38-mm-diam BN tube by 13.56-MHz 7-kW input at 1×10^{-3} Torr. Flow rates of 10 % B_2H_6 diluted with He, N_2, and Ar were 20sccm, 1.2sccm and 2sccm, respectively. The temperature of the silicon (100) substrate was maintained at 900 °C and the substrate potential V_S was controlled by an auxiliary rf power supply from -30V to +54V. At the substrate power = 0W, the floating potential of the substrate was +54V. By using a *plasma diffusion technique* for film preparation, the thin *c*-BN film with thickness gradients was prepared under indentical deposition conditions on a single substrate. A $20\times20mm^2$ substrate was set at an angle of 45° to the axis of the plasma source so that the film can be deposited on the substrate at different rates, depending on the lateral position. The distance from the top of the substrate L is illustrated in Fig. 5.1.

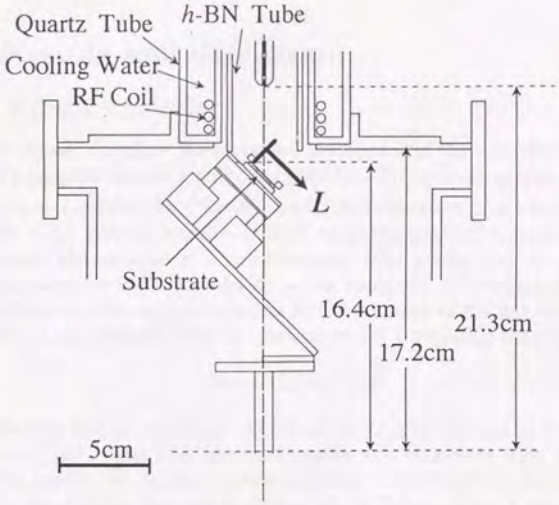

Figure 5.1: The experimental configuration showing relative positions of the plasma source and the substrate.L is the distance from the top of the substrate along the surface.

The polymorphism of the deposited film was analyzed by micro FT-IR (JASCO FT/IR-700). The standard sampling area was $100\times100\ \mu m^2$. The absorbances at about $1080cm^{-1}$ and at about $1360cm^{-1}$ were taken as a quantitative measure of *c*-BN and sp^2-bonded BN, respectively. Strictly speaking, since the absorption peak

at about 1360cm^{-1} is observed for both the hexagonal [graphitic and turbostratic] BN (h-BN) and amorphous BN (a-BN), these sp^2-bonded BN phases can not be distinguished only by IR spectroscopy. Position resolved XPS measurements were carried out in Shimadzu/Kratos AXIS-HS to investigate the composition and chemical state of the film surface. Since this model incorporates a magnetic immersion lens, which enables maximum solid angle collection and transport of photoelectrons from the sapmle surface, micro XPS analysis is possible with high sensitivity. XPS spectra were obtained with nonmonochromatized Mg K_α radiation (1242.6 eV) with the analyzer operating at 80 eV pass energy providing 0.1 eV energy resolution. Furthermore, the surface morphology of the deposited film was observed by atomic force microscopy (AFM) to characterize the initial stage of the c-BN growth. AFM used in this study was Nanoscope II (Digital Instruments, Inc.) operated in air. Images were acquired using a single crystal silicon force sensor (half-angle: 18°, the nominal radius of curvature: 5~20nm, and the nominal force constant: 0.18N/m) in "constant force" mode.

5.3 Results and discussion

5.3.1 FT–IR analysis

Figure 5.2 (a) and (b) show the measured absorbance of the deposited films due to c-BN and hexagonal and/or amorphous BN (h+a-BN) plotted against L.

Films were deposited for 10 min. Under low substrate bias conditions (V_S > 20V), only h-BN growth occurs. In this case, the gradual decrease of the film thickness with the increase of L was observed. The profiles can be explained by the transportation of radicals and ions to the substrate by diffusion [115,126,206]. Plasma diffusion to the substrate results in the decreace of the flux density C with the increase of the distance from the plasma source x following the equation:

$$C(x) = C_0/(x + x_0)^2. \tag{5.1}$$

Here we assume flux conservation. The term of x_0 is introduced as imaginary diffusion center [126]. The film thickness profile was consistent with the expected flux density profile. In contrast, under optimum conditions for the c-BN growth (-30 V<V_S <0 V), the absorbance of h+a-BN is limited below a certain value irrespective of L in spite of the difference of the deposition rate of h+a-BN at each location. Figure 5.3 shows the absorbances at each L as a function of the deposition time. Films were deposited at the constant substrate potential of -10V. Absorbance of c-BN increases linearly with the time, while that of h+a-BN remains constant. Furthermore, the existence of the incubation time for c-BN growth is found by the extrapolation of c-BN line. The results shown in Fig. 5.2 and Fig. 5.3 are definitive evidences for the c-BN growth over the initial non-cubic BN layer, whose thickness is estimated to be about 40nm using the absorption coefficient obtained in section 4.2.

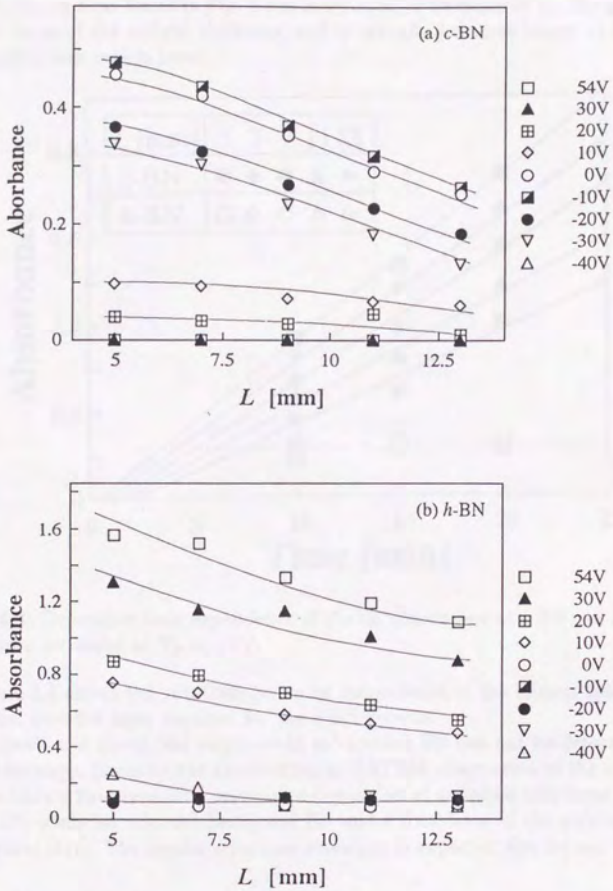

Figure 5.2: The profile of the IR absorbance along L direction. (a) c-BN, and (b) h+a-BN.

The incubation time found in Fig. 5.3 is considered to be required for the growth of h+a-BN layer of the critical thickness, and it actually becomes longer at larger L, where deposition rate is lower.

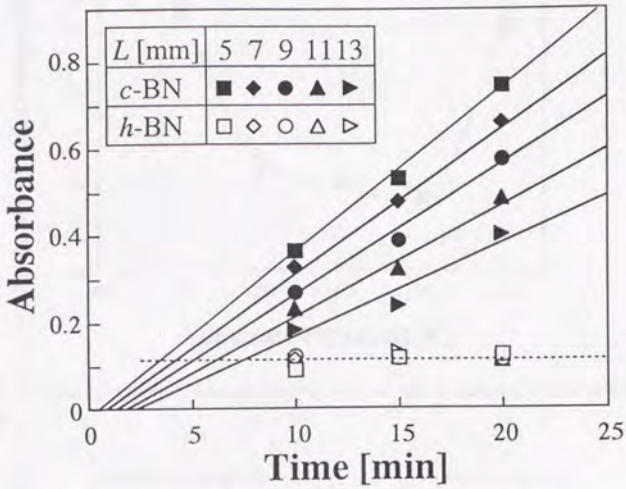

Figure 5.3: Deposition time dependence of the IR absorbance of c-BN and h+a-BN. Films were deposited at V_S = -10V.

Figure 5.4 shows the substrate potential dependence of the critical thickness of the initial h+a-BN layer required for the c-BN growth.

As mentioned above, the structure of sp^2-bonded BN can not be determined by IR spectroscopy. Recently the cross-sectional HRTEM observation of the c-BN film on Si substrate have revealed consecutive deposition of an initial thin layer of amorphous BN, preferred oriented hexagonal BN and a final layer of the polycrystalline cubic phase [211]. The similar structure evolution is expected also for our case.

5.3.2 X-ray photoelectron spectroscopy

Position resolved XPS measurements were carried out to investigate the evolution of composition and chemical state at the different growth stage. The analyzed sample was a film deposited on an oblong Si substrate (40 mm×20 mm), which was confirmed to be suitable for the observation of the different growth stage by FT-IR analysis. The sample is basically distinguished into three different regions as shown in Fig. 5.5. In the large L region (A), a-BN or h-BN is formed. In the middle L region (B), localized nucleation of c-BN occurs on the h-BN. Hence both h-BN and

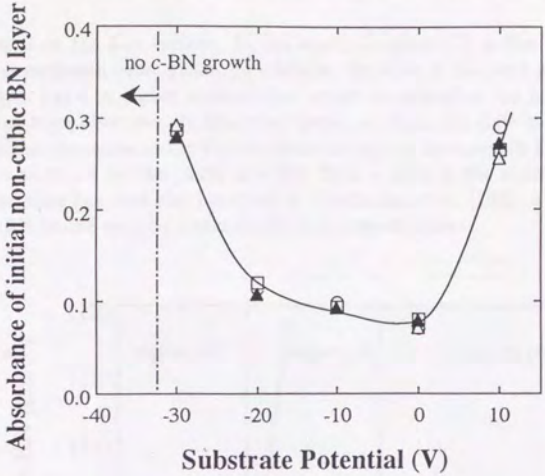

Figure 5.4: The substrate potential dependence of the thickness of the initial h+a-BN layer.

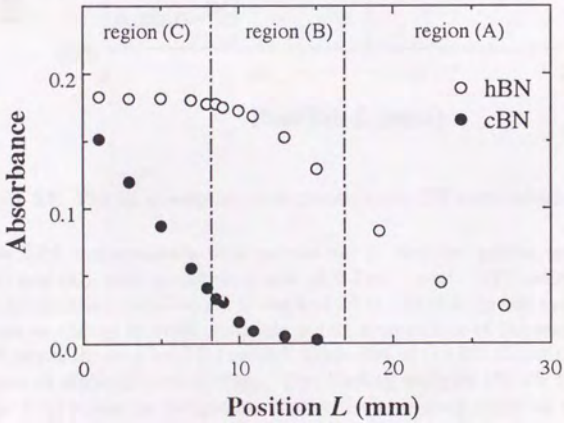

Figure 5.5: IR absorbance – L diagram of the sample for XPS measurement.

c-BN grows on the film surface. In the small L region (C), a film surface is completely covered with cubic phase. In addition, the shift of the peak position of *c*-BN reststrahlen band to higher wavenumber, which is related to the high compressive stress, has been observed. It has been found out that the shift of the absorption peak position decreases as the film thickness increases, as shown in Fig. 5.6, whereas no shift was found for the peaks of *h*-BN. Such a shift in the *c*-BN IR mode with deposition time has been also observed by Friedmann *et al.* [103]. At the nucleation stage, *c*-BN lattice may be under highly compressed state.

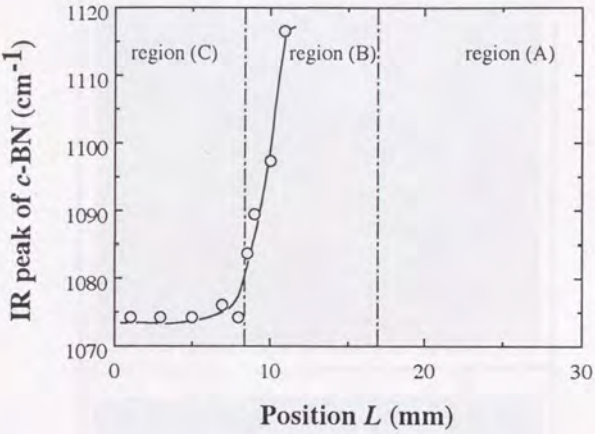

Figure 5.6: The IR absorption peak position of *c*-BN reststrahlen band.

Ex situ XPS measurements were carried out at fourteen points, mainly in the region (B) and (C), with a sampling area of 0.3×0.7 mm^2. XPS estimates of the surface contamination were 7~12% C and 6~10% O. Ion etching was not carried out in order not to change crystalline structure and composition of the sample surface. Figure 5.7 shows the core level B 1*s* and N 1*s* spectra of the BN film with associated loss features at different growth stage. The binding energies 191 eV for B 1*s* and 398 eV for N 1*s* levels are in agreement with the previously reported values [164]. The small peaks at ~10 eV lower binding energy from the main 1 *s* peaks are due to X-ray satellites. All the spectra of B 1*s* and N 1*s* region exihibit a broad bulk plasmon loss peak at ~27 eV higher binding energy from the core level. In the literature, it is reported that the π plasmon loss peak at ~9eV from the main B 1*s* and N 1*s* core level peaks is observed from *h*-BN, but is absent in the spectra

of c-BN [164]. Indeed the π plasmon loss peak is not observed in the spectra from region (C), where the film surface consists of single phase c-BN, while it appears in the spectra from region (A) and (B). The gradual decrease of the intensity of π plasmon loss peak with the increase of film thickness is attributed to an uneven h-BN/c-BN interface. Intensity of the plasmon loss peak can be used to estimate the fraction of sp^2-bonded BN, and thereby, that of c-BN in the surface region of the film. The estimated fraction of it c-BN in the surface region is shown in Fig. 5.8. On the other hand, the quantitative analysis has revealed that the film is stoichiometric irrespective of its thickness as shown in Fig. 5.9, while the drastic increase of Ar incorporation near the h-BN/c-BN interface has been found as shown in Fig. 5.10.

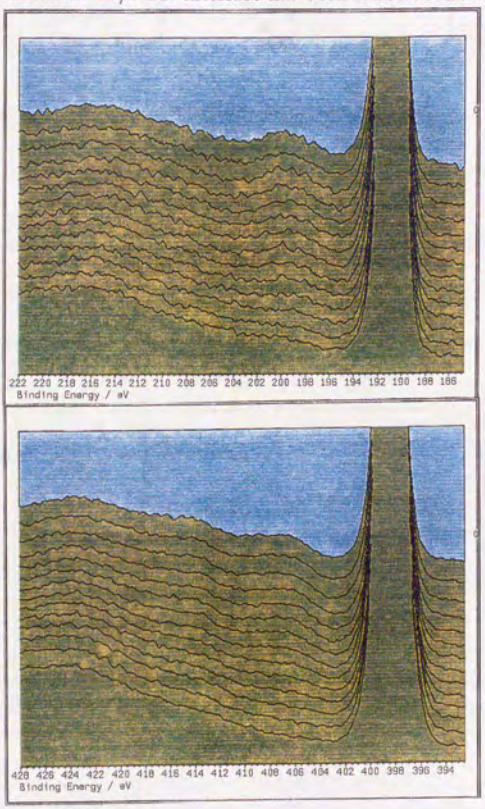

Figure 5.7: B 1s and N 1s core levels of the BN film.

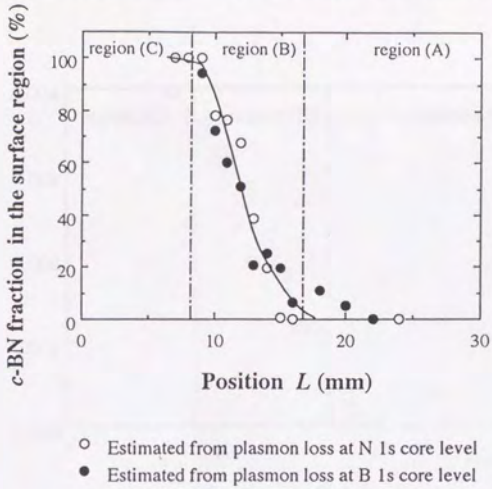

Figure 5.8: Fraction of c-BN in the surface region estimated from the intensity of π plasmon loss peak.

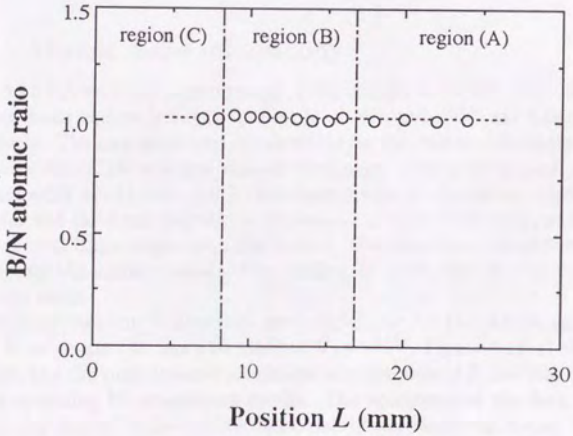

Figure 5.9: Boron to nitrogen ratio plotted against L.

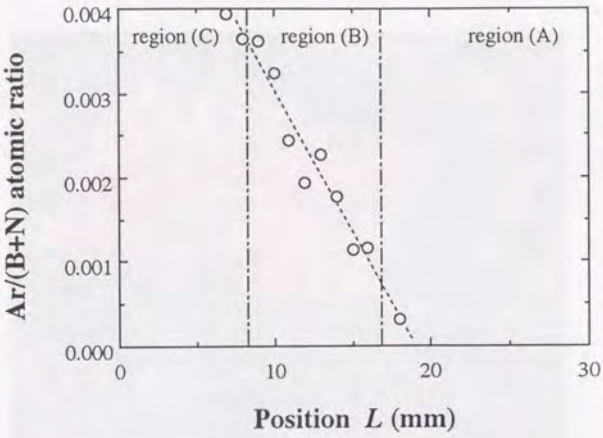

Figure 5.10: Atomic Ar concentration at various positions L.

5.3.3 Atomic force microscopy

Figure 5.11 (a) and (b) show typical AFM images for h-BN film and c-BN film. The root mean square (rms) roughness for h-BN and c-BN are 5.0nm and 1.1nm, respectively. The rms roughness is calculated as the standard deviation of all elevation values within the selected area of the image. The peak-to-peak roughness for h-BN and c-BN are 31.3nm and 7.7nm,respectively. It should be noted that the rms roughness and the peak-to-peak roughness are defined differently, and the latter is usually several times larger than the former. However, these roughness values show qualitatively the similar trend. The surface of c-BN film is very smooth on the nanometer scale.

AFM analysis along L direction were carried out for the sample deposited on an oblong Si substrate (40 mm×20 mm) at V_S= -40V. Figure 5.12(a) shows the rms roughness and the peak-to-peak roughness as a function of L, and Fig. 5.12(b) shows the corresponding IR absorbance profile. The scattering of the data is considered to be mainly due to the inevitable dispersion of the sensor tip shape. It should also be taken into consideration that the lateral resolution of the AFM images is limited for the object which is smaller and sharper than the sensor tip [207] [208]. Here, the position at $L > 30$ mm along L is considered to correspond to the sp^2-bonded BN growth stage (region (A)). The rms roughness and the peak-to-peak roughness are

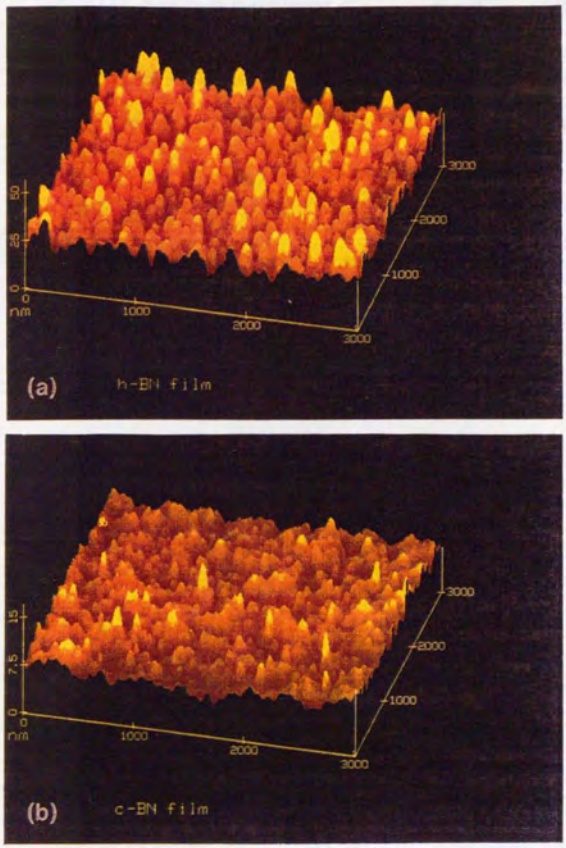

Figure 5.11: AFM images of plasma CVD boron nitride films. (a) *h*-BN film deposited at V_S=+20V, Horizontal scale:3000nm, vertical scale:50nm, perspective view; (b) *c*-BN film deposited at V_S=-40V, Horizontal scale:3000nm, vertical scale:15nm, perspective view.

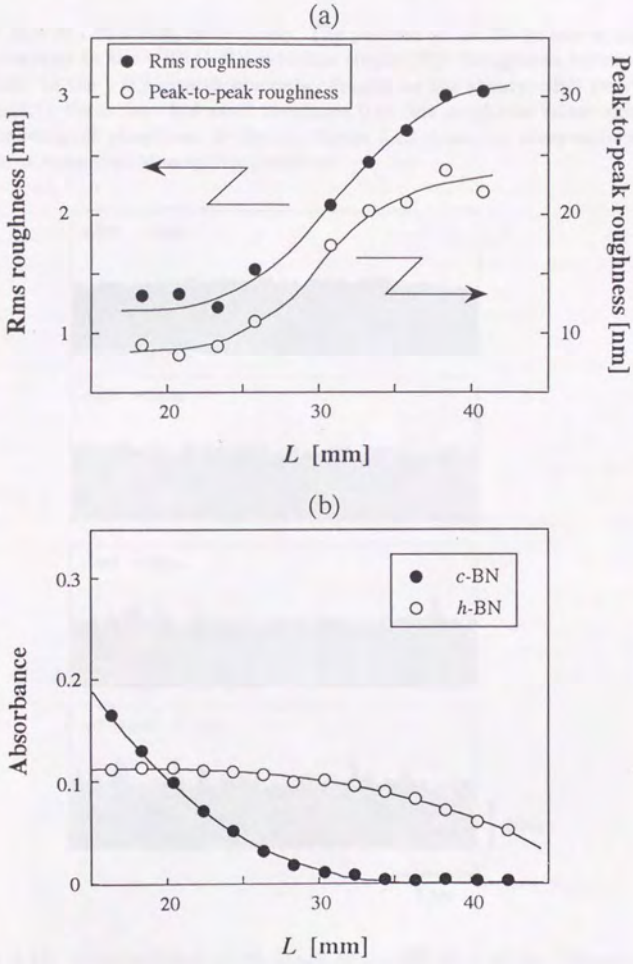

Figure 5.12: (a) The surface roughness plotted against L. The film was deposited at V_s = -40V. (b) IR absorbance profile of the same sample.

about 3nm and 20–25nm, respectively. The position at L= 30–40 mm is considered to correspond to the c-BN/h-BN interface (region(B)). Roughness values decrease gradually as the c-BN growth proceeds. Finally, at the steady c-BN growth stage (region(C)), the surface has small roughness (the rms roughness value: about 1nm, the peak-to-peak roughness: 8–10nm). Figure 5.13 shows the cross-sectional AFM images at some typical sampling positions.

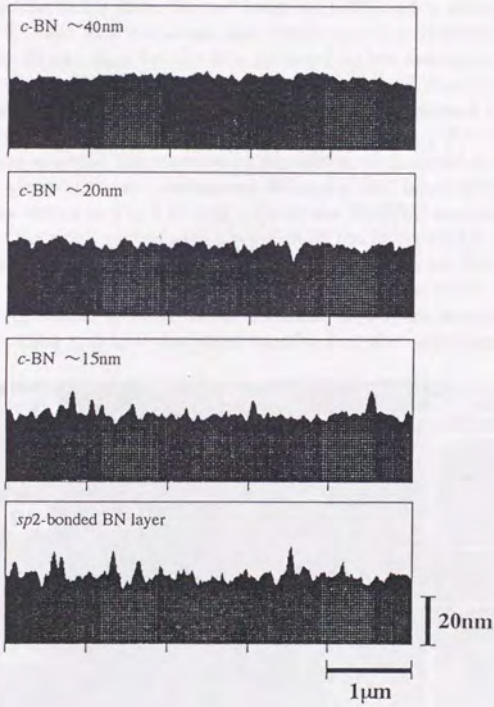

Figure 5.13: Cross-sectional AFM image of the BN film at the different growth stage. The averaged thickness t_c of cubic phase is estimated from IR absorbance. (a) at L=23mm: t_c= 0 nm, (b) L=28mm: $t_c \sim$ 15 nm,(c) L=33mm:$t_c \sim$ 20 nm and (d) L=38mm: $t_c \sim$ 40 nm.

5.3.4 Microstructure evolution and the growth mechanism

Some investigators have previously reported on the interfacial BN layer. In the study of activated reactive evaporation with a gas activation nozzle, Inagawa *et al.* have investigated the evolution of the intensity of IR absorption band with varying deposition time and have found the interfacial hexagonal BN layer of a few ten nm thick [209,210]. Ikeda has presented a cross-sectional HRTEM image of c-BN film prepared on Si substrate by arc-like plasma-enhanced ion plating method and has referred to a thin *a*-BN layer formed between *c*-BN and a silicon substrate [81]. Kohzuki *et al.* have also confirmed the existence of the interfacial *h*-BN layer of approximately 30 nm thick for the film prepared by ion assisted evaporation [214]. Recently Kester *et al.* have reported the results derived from the cross-sectional HRTEM observation of the *c*-BN film deposited on Si substrate by electron beam evaporation with ion bombardment and discussed on the *c*-BN formation. Their observation has revealed the consecutive deposition of an initial thin layer of amorphous BN, preferred oritented hexagonal BN and a final layer of the polycrystalline cubic phase as shown in Fig 5.14 [211]. Using the HRTEM analysis , Medlin *et al.* have reported the similar interfacial layer with 30 nm thickness for the film prepared by ion-assisted pulsed laser deposition [162]. Thus, the initial *h*-BN growth on the substrate is widely observed irrespective of the deposition method. Therefore, there arises crucial questions whether these interfacial layers are essentially required to the *c*-BN formation and how the phase transition to the *c*-BN occurs.

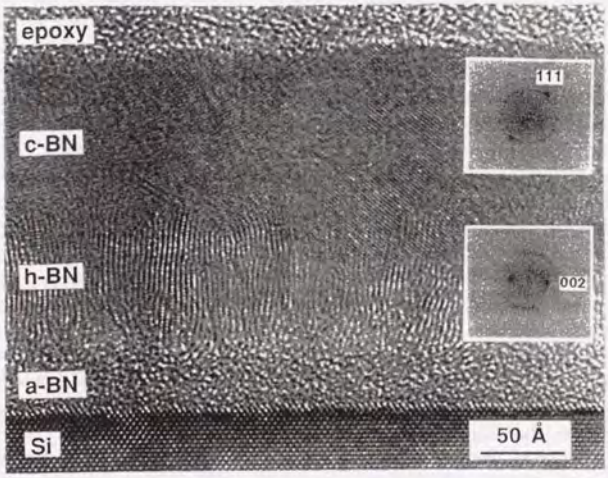

Figure 5.14: Cross-sectional HRTEM image of the BN film (after [211]).

It has been known that an initial *h*-BN layer shows *c*-axis orientation parallel to the substrate surface. As McKenzie *et al.* have suggested, the preferred orientation of *h*-BN is considered to be controlled by the strain energy. Moreover, McKenzie *et al.* have suggested that *c*-BN formation is also the result of the buildup of biaxial film stress [212,213]. They have experimentally shown the initial increase of the compressive stress as a function of the film thickness and the stress dependence of the *c*-BN formation. It was suggested that when the stress reaches a certain level, the internal pressure in the film will be sufficiently high to induce the high pressure phase *c*-BN. Though their explanations seem to be rather crude in some points, the highly compressed state is considered to be the cause of *c*-BN formation.

We have clarified the existence of the critical thickness of initial sp^2-bonded BN in this work. The fact would support their speculation, since it is most probable that the threshold compressive stress for the *c*-BN growth is reached at the critical film thickness. Moreover, we have found the very close correlation of Ar content and *c*-BN fraction at the film surface observed in our work is considered to be consistent with the above model. The simulation by Fang *et al.* has showed that the interstitial Ar incorporation is possibly a primary cause of the compressive stress. However it should be noted that they have pointed out that the total quantity of Ar incorporation is not neccessarily a scale factor for the stress and that the relationship between inert gas incorporation and compressive stress has not been establised. If compressive stress is the driving force for the *c*-BN formation, the growth of *c*-BN would not occur on the film surface. In this regard, the results of Auger electron spectroscopy (see Fig. 3.17 in p. 45) is also consistent with this model. The observed large IR mode shift of *c*-BN at the nucleation stage is also considered to be within reason. Very recently, study of the critical thickess of the interfacial layers has been reported by Kester *et al.* [215]. They have reported that increasing the substrate temperature above 400°C led to the thicker critical thickness, while increased ion flux resulted in the thinner one. They also have attributed the growth sequence to increasing compressive stress with increased film thickness. Temperature effects has been explained by the relaxation of the intrinsic stress in the films at high temperatures due to increased adatom mobility. In addition, the interstitial Ar incorporation in their films was also observzed in Rutherford backscattering spectrometry studies.

Kester *et al.* have also found an uneven *h*-BN/*c*-BN interface and a locally smooth *c*-BN surface by HRTEM observation. The gradual evolution of the *c*-BN fraction at the surface and the surface morphology revealed in our work is explained by the uneven *h*-BN/*c*-BN interface. This indicates that the *c*-BN formation does not initiate simultaneously on the *h*-BN surface. The sites for the onset of *c*-BN nucleation may be highly compressed regions. Nevertheless, not only the compressive stress but also the factors such as interface and/or surface energy may affect the resultant structure of the film. It is probable that the unisotropic nature of BN significantly affects the phase formation. Turbostratic BN consists of a random stacking of the distorted hexagonal planes, which are weakly bonded by van der

Waals force. Hence, the distance between the planes can be easily changed by ion bombardment. Highly compressed *h*-BN may readily transform into the *c*-BN. In concerning with this issue, the fact is interesting that the *h*-BN (or strictly *t*-BN) film deposited under concurrent ion bombardment often shows the very similar TED pattern with *c*-BN. Also interesting is the report that *h*-BN treated by hydrostatic compression can be transformed into *c*-BN by only electron beam irradiation [163].

Finally, at this stage, the mechanism of the cause of compressive stress is not established. Therefore, the causal relationship of ion bombardment with *c*-BN formation is still unclear. Furthermore, detailed study is needed on the microscopic structure and morphology of the *c*-BN film for the realistic explanation of the *c*-BN stabilization.

5.4 Conclusion

The initial growth stage of *c*-BN film has mainly been studied by the film deposition on the tilted silicon substrate using diffusive high-density plasma. It has been clearly shown that the initial sp^2-bonded BN (*a*-BN and *h*-BN) layer of critical thickness is essential for the *c*-BN growth. The thickness of the initial sp^2-bonded BN layer depends on the process parameter such as the substrate bias. XPS measurement revealed the very close correlation between Ar incorporation and *c*-BN formation. FT–IR absorption spectroscopy revealed that at the nucleation stage *c*-BN is under highly compressed state. These results indicate that high compression state in the film is essential for the *c*-BN formation. Furthermore, AFM observation has revealed the surface morphology evolution of the *c*-BN film at different growth stage. The rms surface roughness decreases from 3nm to 1nm at the transition stage from *t*-BN to *c*-BN growth.

Chapter 6

Summary

This thesis concerns the development of a novel plasma enhanced CVD technique using low-pressure inductively coupled plasma (ICP) and the investigations of *c*-BN film deposition process by this technique. Important results of this work are summarized as follows.

(A) We have developed a novel film deposition technique named "low pressure inductively coupled plasma enhanced chemical vapor deposition (ICP–CVD)". Properties of the plasma significantly depend on the working pressure. At the pressure above 0.1 Torr the plasma is restricted within the source volume and serves as a high-density radical source, while in the pressure range of 1∼10 mTorr the plasma itself can diffuse to the substrate. In the latter case, it is a main advantage that the energy of ions impinging to the substrate can be controlled by an rf bias and the flux of ions can be varied by changing the source parameters. Accordingly, ICP–CVD at 0.1∼1 Torr and at 1∼10 mTorr can be characterized as a high-density radical-assisted deposition technique and a controllable ion-assisted deposition technique.

(B) Synthesis of *c*-BN has been attempted from two distinct approaches by using ICP-CVD technique. Following results have been obtained.

1. It has been found difficult to apply the same approach found successful in the synthesis of diamond to that of *c*-BN, that is, there would not exist special chemistry in the hydrogen/boron-nitrogen system.

2. Cubic boron nitride films have been prepared by low pressure ICP-CVD with adequate ion bombardment of the growing surface.

(C) Effects of substrate bias and gas pressure on phase formation of BN have been investigated quantitatively.

At a given constant pressure, the substrate bias condition can be divided into following four regions relating to the polymorphism of the deposited films.
Region I: At lower sheath potentials, only the hexagonal phase grows, and the deposition rate of *h*-BN decreases as the substrate bias increases.

Region II: At a certain threshold bias potential, the *c*-BN appears. As the sheath potential increases, the *c*-BN content in the film increases. Even under optimal conditions, pure *c*-BN can not be grown, that is, several tens-nm-thick *h*-BN always exists as an interfacial layer.
Region III: Further increase of the bias voltage results in lowering *c*-BN content in the film. At lower pressures this region tends to disappear.
Region IV: Finally, film deposition is prevented by re-sputtering.

The required ion bombard energy for the *c*-BN formation becomes lower at higher gas pressure. In view of the results of the plasma diagnostics, these results are attributed to the increase of ion flux with the gas pressure. It is concluded that *c*-BN formation is not controlled only by the ion energy but also by the flux. Our result is cosistent with the momentum transfer model.

(D) Initial stage of *c*-BN film growth on silicon substrate has been investigated by analyzing *c*-BN films prepared by a plasma diffusion technique. The important results are as follows:

1. At the initial stage of the film growth, sp^2-bonded BN growth occurs. The specific thickness of the initial layer depends on the ion bombardment energy.

2. Composition and chemical state at different growth stage was investigated by XPS. Very close correlation of Ar incorporation and *c*-BN formation has been revealed.

3. The surface morphology evolution at the initiation of cubic phase growth has been observed by AFM.

4. Evolution of the IR absorption peak position of *c*-BN with film thickness has been observed. This fact indicates that the initially formed *c*-BN may be under highly compressed state.

These results have showed that the incorporation of compressed state in the film might be a primary cause of the *c*-BN formation.

Appendix A

Diamond synthesis

In this appendix, diamond synthesis by low-pressure ICP–CVD is shortly presented. A number of groups have reported the successful growth of diamond from gas phase by using various techniques. Typically these have been the high-power, high pressure plasma assisted CVD processes at pressures in excess of 10 Torr and H_2 to CH_4 dilution ratio of 100:1. For the deposition of films with uniform thickness over large area, it is preferable to adopt a low pressure plasma CVD technique. However, it usually fails to deposit diamond. An attempt to synthesize diamond under lower pressure (around 10 mTorr) was previously carried out by using a variant of plasma CVD where excited He atoms flowing downstream from an intense plasma region interact with CH_4 molecules [217]. The RHEED characterizaton results indicated the films contained a little diamond, but the matrix was a disordered carbon. In recent years, diamond synthesis at lower pressures (below 0.1 Torr) has been attempted by using ECR plasma CVD. (Strictly speaking, at the pressures where complete electron gyrations could not be expected it is called "magneto-microwave plasma CVD" [218]). Kawarada *et al.* reported that at pressures above 4 Torr, the diamond phase was chiefly observed using the gas sources of methane and hydrogen. The same group has reported that from the C–H–O system diamond can be synthesized at lower pressures [219]. In their paper, a high density plasma is considered to be advantageous for low temperatue and large area deposition. At presesnt, the synthesis at the pressure on the order of 1 mTorr has been achieved by this method. Based on the survey of the literatures and on the results of the characterization of low pressure ICP, it is most likely that low pressure ICP–CVD is a promissing technique for the diamond synthesis at lower pressures. Moreover, it is very attractive to synthesize both diamond and *c*-BN in the same appratus. There are several reports of epitaxial growth of diamond on bulk *c*-BN. Combination of *c*-BN and diamond is expected to extend their possibilities in numerous applications. Here we present the conditions for the successful deposition of diamond from the methane and hydrogen system at low pressure. In the same appratus used for *c*-BN film preparation, diamond deposition was carried out. Si substrate mounted on the heater was electrically floated. 7-kW ICP was generated at about 0.2 Torr. The gas flow rate of hydrogen

and methane was 50sccm and 0.4sccm, respectively. The deposits were analyzed by SEM, TEM and Raman spectroscopy. Figure A.1 shows the SEM images of the samples deposited for 3 hours. Deposits were hardly found at the heater temperature of 600°C. At 700 °C faceted diamond growth was observed. With increasing temperature upto 750 °C, deposits show so-called "cauliflower structure". At temperatures above 800 °C, the substrate was covered with graphitic carbon. Thus the optimum substrate temperature seems to be lower than that for the plasma CVD at high pressure (>10 Torr). The deposition rate of diamond at 0.2 Torr was 0.1μm/min.

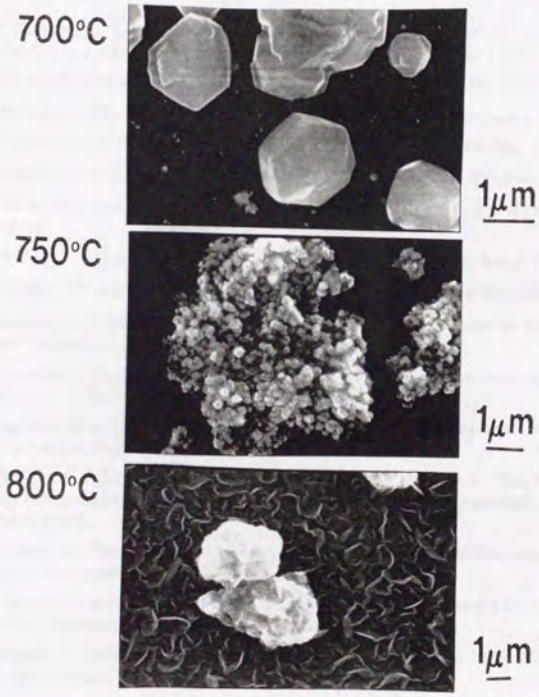

Figure A.1: Scanning electron micrograph of diamond deposited at (a) 700°C, (b) 750°C and (c)800°C.

Bibliography

[1] W.A.Yarbrough, "Current research problems and opportunities in the vapor phase synthesis of diamond and cubic boron nitride", J.Vac.Sci.Technol.A **9**, 1145 (1991).

[2] W.Hittorf,"Über die electricitätsleitung der gase", Ann. Physik **21**, 137 (1884).

[3] J.J.Thomson, "The electrodeless discharge through gases", Phil.Mag.S.7. **4**, 1128 (1927).

[4] J.S.Townsend and R.R.Donaldson,"Electrodeless discharges", Phil.Mag. **5**, 178 (1928).

[5] K.A.Mackinnon, "On the origin of the electrodeless discharge", Phil.Mag. **8**, 605 (1929).

[6] G.I.Babat,"Electrodeless discharge and some allied problems", J.Inst.Electr.Eng. Part3 **94**, 27 (1974).

[7] H.U.Eckert, "The induction arc: a state-of-the-art review", High Temp. Sci. **6**, 99 (1974).

[8] D.L.Flamm, "Trends in plasma sources and etching", Solid State Technol. **34**, 47 (1991).

[9] For example, J.Hopwood, "Review on inductively coupled plasmas for plasma processing", Plasma Sources Sci.Technol. **1**, 109 (1992).

[10] M.Yamashita, "Fundamental characteristics of built-in high-frequency coil-type sputtering apparatus", J.Vac.Sci.Technol.A **7**, 151 (1989).

[11] H.Mito and A.Sekiguchi, "Induction heated plasma assisted chemical vapor deposition of SiN", J.Vac.Sci.Technol.A **4**, 475 (1986).

[12] S.Takagi, A.Sekiguchi, N.Hosokawa, N.Terada, M.Jo and H.Ihara, "$Ba_2Y_1Cu_3O_{7-y}$ oxidation by thermodynamic nonequilibrium high-temperature (TNH) plasma", Jpn.J.Appl.Phys. **28**, L952 (1989).

[13] J.W.Denneman,"Determination of electromagnetic properties of low-pressure electrodeless inductive discharges", J.Phys.D **23** 293 (1990).

[14] G.G.Lister and M.Cox,"Modeling of inductively coupled discharges with internal and external coils", Plasma Sources Sci.Technol. **1**, 67 (1992).

[15] R.B.Piejak, V.A.Godyak and B.M.Alexandrovich,"A simple analysis of an inductive RF discharge", Plasma Sources Sci.Technol. **1**, 179 (1992).

[16] J.R.Hollahan and A.T.Bell: *Techniques and Application of Plasma Chemistry*, (John Wiley and Sons, New York, 1974), p.2.

[17] J.Amorim, H.S.Maciel, and J.P.Sudano, "High-density plasma mode of an inductively coupled radio frequency discharge", J.Vac.Sci.Technol.B **9**, 362 (1991).

[18] H.Nagahama and T.Takamoto, "Experimental studies of inductively coupled r.f.discharge plasma in the low pressure", Shinku **32**, 20 (1989) (in Japanese).

[19] T.Fukumura and T.Takamoto, "Study of High-frequency discharge mechanism by means of equivalent circuit", Denki gakkai ronbunshi A **97**, 243 (1977) (in Japanese).

[20] T.Fukumura and T.Takamoto, "The power absorption of high-frequency plasma in the low pressure", Denki gakkai ronbunshi A **100**, 64 (1980) (in Japanese).

[21] T.Fukumura, H.Nagahama and T.Takamoto, "Effect of electric field on the conductivity of high frequency discharge plasma", Denki gakkai ronbunshi A **103**, 265 (1983) (in Japanese).

[22] Teruo Takamoto, *Kitai denshi kougaku*, (Genbunsya, Kyoto) (in Japanese) (1989).

[23] P.K.Lam, R.M.Wentzcovitch and M.L.Cohen, in *Synthesis and Properties of Boron Nitride* (edited by J.J.Pouch and S.A.Alterovitz, Trans Tech Publications), p.165 (1990).

[24] R.S.Pease, "An X-ray study of boron nitride", Acta Cryst. **5**, 356 (1952).

[25] Y.Matsui, Y.Sekikawa, T.Sato and T.Ishii,"Formations of rhombohedral boron nitride, as revealed by TEM – electron energy loss spectroscopy", J.Mater.Sci. **16**, 1114 (1981).

[26] T.Ishii, T.Sato, Y.Sekikawa and M.Iwata, "Growth of whiskers of hexagonal boron nitride", J.Cryst.Growth **52**, 285 (1981).

[27] F.R.Corrigan and F.P.Bundy, "Direct transitions among the allotropic forms of boron nitride at high pressures and temperatures", J.Chem.Phys. **63**, 3812 (1975).

[28] T.Soma, A.Sawaoka and S.Saito,"Characterization of wurtzite type boron nitride synthesized by shock compression", Mater.Res.Bull. **9**, 755 (1974).

[29] A.Sawaoka, T.Soma and S.Saito, "Structure determination of boron nitride transformed by shock compression", Jpn.J.Appl.Phys. **13**, 891 (1974).

[30] T.Akashi, A.Sawaoka, S.Saito and M.Araki, "Structural changes of boron nitride caused by multiple shock-compression", Jpn.J.Appl.Phys. **15**, 891 (1976).

[31] T.Akashi, H.Pak and A.Sawaoka, "Structural changes of wurtzite-type and zincblende-type boron nitrides by shock treatments", J.Mater.Sci. **21**, 4060 (1986).

[32] T.Sato, T.Ishii and N.Setaka, "Formation of cubic boron nitride from rhombohedral boron nitride by explosive shock compression", J.Am.Cer.Soc. **10**, C-162 (1982).

[33] J.Thomas,JR., N.E.Weston and T.E.O'Connor, "Turbostratic boron nitride, thermal transformation to ordered-layer-lattice boron nitride", J.Am.Chem.Soc. **84**, 4619 (1963).

[34] H.Grigoriew and J.Leciejewicz,"X-ray and electron microscopy study of amorphous boron nitride films", Thin Solid Films **172**, L75 (1989).

[35] W.Schmolla and H.Hartnagel, "Amorphous BN films produced in a double-plasma reactor for semiconductor applications", Solid State Electronics **26**, 931 (1983).

[36] T.Takahashi, H.Itoh and M.Kuroda, "Structure and properties of CVD-BN thick films prepared on carbon steel substrate", J.Cryst.Growth **53**, 418 (1981).

[37] K.Nakamura, "Preparation and properties of a-BN films by molecular flow CVD", J.Electrochem.Soc. **132**, 1757 (1985).

[38] R.H.Wentorf,Jr., "Cubic form of boron nitride", J.Chem.Phys. **26**, 956 (1957).

[39] R.H.Wentorf,Jr., "Synthesis of the cubic form of boron nitride", J.Chem.Phys. **34**, 809 (1961).

[40] L.Kleinman and J.C.Phillips, "Crystal potential and energy bands of semiconductors. II. Self-consistent calculations for cubic boron nitride", Phys.Rev. **117**, 460 (1960).

[41] F.Bassani and M.Yoshimine, "Electronic band structure of group IV elements and of III-V compounds", Phys.Rev. **130**, 20 (1963).

[42] D.R.Wiff and R.Keown, "Energy bands in cubic boron nitride", J.Chem.Phys. **47**, 3113 (1967).

[43] A.Zunger and A.J.Freeman,"*Ab initio* self-consistent study of the electronic structure and properties of cubic boron nitride", Phys.Rev.B **17**,2030 (1978).

[44] R.M.Wentzcovitch, K.J.Chang and M.L.Cohen, "Electronic and structural properties of BN and BP", Phys.Rev.B **34**, 1071 (1986).

[45] R.M.Chrenko, "Ultraviolet and infrared spectra of cubic boron nitride", Solid State Commun. **14**, 511 (1974).

[46] V.A.Fomichev and M.A.Rumsh, "Investigation of X-ray spectra of hexagonal and cubic boron nitride", J.Phys.Chem.Solids **29**, 1015 (1967).

[47] S.Larach and R.E.Shrader, "Multiband luminescence in boron nitride", Phys.Rev. **104**, 68 (1956).

[48] M.Wakatsuki, K.Ichinose and T.Aoki,"Synthesis of polycrystalline cubic boron nitride (BN)",Mat.Res.Bull. **7**, 999 (1972).

[49] G.A.Slack,"Nonmetalic crystals with high thermal conductivity", J.Phys.Chem.Solids **34**, 321 (1973).

[50] P.J.Gielisse, S.S.Mitra, J.N.Plendl, R.D.Griffis, L.C.Mansur, R.Marshall and E.A.Pascoe, "Lattice infrared spectra of boron nitride and boron monophosphide" Phys.Rev. **155**, 1039 (1967).

[51] D.J.Joyner and D.M.Hercules,"Chemical bonding and electronic structure of B_2O_3, H_3BO_3, and BN: an ESCA, Auger, SIMS, and SXS study", J.Chem.Phys. **72**, 1095 (1980).

[52] S.P.S.Arya and A.D'amico, "Preparation, properties and applications of boron nitride thin films", Thin Solid Films **157**, 267 (1988).

[53] R.H.Wentorf,Jr., "Preparation of semiconducting cubic boron nitride", J.Chem.Phys. **36**, 1990 (1962).

[54] O.Mishima, J.Tanaka, S.Yamaoka and O.Fukunaga, "High-temperature cubic boron nitride p-n junction diode made at high pressure", Science **238**, 181 (1987).

[55] O.Mishima, K.Era, J.Tanaka,and S.Yamaoka, "Ultraviolet light-emitting diode of a cubic boron nitride pn junction made at high pressure", Appl.Phys.Lett. **53**, 962 (1988).

[56] M.Hirayama and K.Shono, "CVD-BN for boron diffusion in Si and its application to Si devices", J.Electrochem.Soc. **122**, 1671 (1975).

[57] E.Yamaguchi and M.Minakata, "Study of boron nitride gate insulators onto InP grown by low-temperature chemical vapor deposition", J.Appl.Phys. **55**, 3098 (1984).

[58] S.S.Dana and J.R.Maldonado, "Low pressure CVD boro-hydro-nitride films and their use in x-ray masks", J.Vac.Sci.Technol. B **4**, 235 (1986).

[59] D.Maydan, G.A.Coquin, H.J.Levinstein, A.K.Sinha, and D.N.K.Wang, "Boron nitride mask structure for X-ray lithography", J.Vac.Sci.Technol. **16**, 1959 (1979).

[60] *Synthesis and Properties of Boron Nitride*, edited by J.J.Pouch and S.A.Alterovitz (Trans Tech Publications, Aedormannsdorf, 1990), Vol 54-55.

[61] A.S.Korhonen, "Corrosion of thin hard PVD coatings", Vacuum, **45**, 1031 (1994).

[62] M.Sokolowski, "Deposition of wurtzite type boron nitride layers by reactive pulse plasma crystallization", J.Cryst.Growth **46**, 136 (1979).

[63] S.S.Batsanov, G.E.Blokhina and A.A.Deribas,"Effect of an explosion on a substance Structural changes of boron nitride", Zh.Srukt.Khim. **6**, 227 (1965) (in Russian). (This structure is also described in ref [30,31].)

[64] M.Sokolowski, A.Sokolowska, A.Rusek, Z.Romanowski, B.Gokieli and M.Gajewska, "Properties and growth of β-BN (borazon) layers from a pulsed plasma under reduced pressure.", J.Cryst.Growth **52**, 165 (1981).

[65] C.Weissmantel, K.Bewilogua, D.Dietrich, H-J.Erler, H-J.Hinneberg, S.Klose, W.Norwick and G.Reisse, "Structure and properties of quasi-amorphous films prepared by ion beam techniques", Thin Solid Films **72**, 19 (1980).

[66] C.Weissmantel, "Ion beam deposition of special film structure", J.Vac.Sci.Technol. **18**, 179 (1981).

[67] C.Weissmantel, K.Bewilogua, K.Breuer, D.Deitrich, U.Ebersbach, H.-J.Erler, B.Rau and G.Reisse, "Preparation and properties of hard i-C and i-BN coatings", Thin Solid Films **96**, 31 (1982).

[68] C.Weissmantel, K.Breuer and B.Winde, "Hard films of unusual microstructure", Thin Solid Films **100**, 383 (1983).

[69] B.Rother, H.D.Zscheile, C.Weissmantel, C.Heiser, G.Holzhüter, G.Leonhardt and P.Reich, "Preparation and characterization of ion-plated boron nitride", Thin Solid Films **142**, 83 (1986).

[70] M.Satou and F.Fujimoto, "Formation of cubic BN films by boron evaporation and nitrogen ion beam bombardment", Jpn.J.Appl.Phys. **22**, L171 (1983).

[71] M.Satou, K.Yamaguch, Y.Andoh, Y.Suzuki, K.Matsuda and F.Fujimoto, "Nitride film formation by ion and vapour deposition", Nucl.Instrum.Meth. **B7/8**, 910 (1985).

[72] T.Wada and N.Yamashita, "Formation of cBN films by ion beam assisted deposition", J.Vac.Sci.Technol.A **10**, 515 (1992).

[73] Y.Andoh, K.Ogata, Y.Suzuki, E.Kamijo, M.Satou and F.Fujimoto, "Properties of boron nitride coating films prepared by the ion beam and vapor deposition method (IVD)", Nucl.Instrum.Meth. **B19/20**, 787 (1987).

[74] Y.Andoh, K.Ogata and E.Kamijo, "On the formation of BN films by ion beam and vapor deposition", Nucl.Instrum.Meth. **B33**, 678 (1988).

[75] F.Fujimoto, "Coating film formation by dynamic mixing method", Vacuum **39**, 361 (1989).

[76] F.Fujimoto, "Boron nitride film formation by means of dynamic mixing method", Vacuum **42**, 67 (1991).

[77] K.L.Chopra, V.Agarwal, V.D.Vanker, C.Deshpandey and R.F.Bunshah, "Synthesis of cBN films by activated reactive evaporation of H_3BO_3", Thin Solid Films **126**, 307 (1985).

[78] K.Inagawa, K.Watanabe, I.Tanaka, S.Saitoh and A.Itoh, "Cubic boron nitride film deposition by HCD-ARE method", Proc.9th Symp.on ISIAT'85, Tokyo (1985) p.299.

[79] K.Inagawa, K.Watanabe, K.Saitoh, and A.Itoh, Proc.10th Symp.on ISIAT'86, Tokyo (1986) p.381.

[80] K.Inagawa, K.Watanabe, H.Ohsone, K.Saitoh, and A.Itoh, "Preparation of cBN films by activated reactive evaporation with a gas activation nozzle", J.Vac.Sci.Technol. A **5**, 2696 (1987).

[81] T.Ikeda, Y.Kawate, and Y.Hirai, "Formation of cBN films by arc-like plasma-enhanced ion plating method", J.Vac.Sci.Technol. A **8**,3168(1990)
Sinku, **31**, 968 (1988).

[82] N.Tanabe, T.Hayashi and M.Iwaki,"Deposition of cubic boron nitride thin films by ion-beam-enhanced deposition", Diamond Relat.Mater. **1**, 883 (1992).

[83] N.Tanabe, T.Hayashi and M.Iwaki,"Substrate temperature influence of c-BN thin film formation by IBED", Diamond Relat.Mater. **1**, 151 (1992).

[84] N.Tanabe and M.Iwaki,"Influence of sputtering target material on the formation of cubic BN thin films by ion beam enhanced deposition", Diamond Relat.Mater. **2**, 512 (1993).

[85] N.Tanabe and M.Iwaki,"Effects of Ar ion beam bombardment on the formation of cubic BN in IBED", Nucl.Instrum Meth. **B80/81**, 1349 (1993).

[86] M.Murakawa and S.Watanabe, "The synthesis of cubic BN films using a hot cathode plasma discharge in a parallel magnetic field", Surf.Coat.Technol. **43/44**, 128 (1990).

[87] M.Murakawa and S.Watanabe, "The possibility of coating cubic BN films on various substrate", Surf.Coat.Technol. **43/44**, 145 (1990).

[88] K.H.Seidel, K.Reichelt, W.Schaal and H.Dimigen, "The preparation of cubic boron nitride films by reactive diode sputtering", Thin Solid Films **151**, 243 (1987).

[89] M.Mieno and T.Yoshida, "Preparation of cBN films by rf sputtering", Jpn.J.Appl.Phys. **29**, L1175 (1990).

[90] M.Mieno and T.Yoshida, "Preparation of cubic boron nitride by radio frequency bias sputtering", Surf.Coat.Technol. **52**, 87 (1992).

[91] K.Bewilogua, J.Buth, H.Hübsch and M.Grischke, "Preparation of c-BN containing films by reactive r.f.sputtering", Diamond Relat.Mater. **2**, 1206 (1993).

[92] S.Kidner, C.A.Taylor II and R.Clarke, "Low energy kinetic threshold in the growth of cubic boron nitride films", Appl.Phys.Lett. **64**, 1859 (1994).

[93] G.Kessler, H.-D.Bauer, W.Pompe and H.-J..Scheibe,"Laser pulse vapour deposition of polycrystalline wurtzite-type BN", Thin Solid Films **147**, L45 (1987).

[94] G.L.Doll, J.A.Sell, C.A.Taylor II and R.Clarke, "Growth and characterization of epitaxial cubic boron nitride films on silicon", Phys.Rev.B **43**, 6816 (1991).

[95] S.Komatsu, Y.Moriyoshi, M.Kasamatsu and K.Yamada,"Cubic boron nitride crystallites grown by laser-enhanced plasma chemical vapour deposition", J.Phys.D **24**, 1687 (1991).

[96] T.A.Friedmann, K.F.McCarty, E.J.Klaus, D.Boehme, W.M.Clift, H.A.Johnsen, M.J.Mills and D.K.Ottesen,"Cubic boron nitride formation on Si (100) substrates at room temperature by pulsed laser deposition", Appl.Phys.Lett. **61**, 2406 (1992).

[97] F.Qian, V.Nagabushnam and R.K.Singh,"Pulsed laser deposition of cubic boron nitride films on silicon substrate", Appl.Phys.Lett. **63**, 317 (1993).

[98] S.Mineta and N.Yasunaga,"Cubic BN film formation by laser PVD", seimitsu kougakkaishi **53**, 1532 (1987).

[99] S.Mineta, M.Kolrata, N.Yasunaga and Y.Kikuta,"Preparation of cubic boron nitride film by CO_2 laser physical vapour deposition with simultaneous nitrogen ion supply", Thin Solid Films **189**, 125 (1990).

[100] A.K.Ballal, L.Salamanca-Riba, G.L.Doll, C.A.Taylor II and R.Clarke,"Ion-assisted pulsed laser deposition of cubic BN films on Si (001) substrates", J.Mater.Res. **7**, 1618 (1992).

[101] A.K.Ballal, L.Salamanca-Riba, C.A.Taylor II and G.L.Doll,"Structural characterization of preferentially oriented cubic BN films grown on Si (001) substrates", Thin Solid Films **224**, 46 (1993).

[102] K.Kaneda and K.Shibata,"A comparison of the effects of RF plasma discharge and ion beam supply on the growth of cubic boron nitride films formed by laser physical vapor deposition", Jpn.J.Appl.Phys. **33**, 266 (1994).

[103] T.A.Friedmann, P.B.Mirkarimi, D.L.Medlin, K.F.McCarty, E.J.Klaus, D.R.Boehme, H.A.Johnsen, M.J.Mills and D.K.Ottesen,"Ion-assisted pulsed laser deposition of cubic boron nitride films", J.Appl.Phys. **76**, 3088 (1994).

[104] A.Chayahara,H.Yokoyama,T.Imura and Y.Osaka, "Function of substrate bias potential for formation of cubic boron nitride films in plasma CVD technique", Jpn.J.Appl.Phys. **26**, L1435 (1987).

[105] A.Chayahara, H.Yokoyama, T.Imura and Y.Osaka, "Properties of BN thin films deposited by plasma CVD", Appl.Surf.Sci. **33/34**, 561 (1988).

[106] M.Okamoto, H.Yokoyama and Y.Osaka, "Formation of cubic boron nitride film on Si with boron buffer layers", Jpn.J.Appl.Phys. **29**, 930 (1990).

[107] M.Okamoto, Y.Utsumi and Y.Osaka, "Formation of cubic boron nitride films on diamond by plasma CVD technique", Jpn.J.Appl.Phys. **29**, L1004 (1990).

[108] M.Okamoto, Y.Utsumi and Y.Osaka, "Formation and properties of cubic boron nitride films on tungsten carbide by plasma chemical vapor deposition", Jpn.J.Appl.Phys. **31**, 3455 (1992).

[109] A.Weber, U.Bringmann, R.Nikulski and C.-P.Klages, "Growth of cubic boron nitride and boron-carbon-nitrogen coatings using N-trimethylborazine in an electron cyclotron resonance plasma process", Diamond Relat. Mater. **2**, 201 (1993).

[110] A.Weber, U.Bringmann, R.Nikulski and C.-P.Klages, "Electron cyclotron resonance plasma deposition of cubic boron nitride using N-trimethylborazine", Surf.Coat.Technol. **60**, 493 (1993).

[111] T.Ichiki and T.Yoshida,"Preparation of cubic boron nitride films by low-pressure ICP-CVD", Proc. 11th Int. Symp. Plasma Chem. Loughborough U.K. 1993, p.1022.

[112] T.Ichiki and T.Yoshida,"Preparation of cubic boron nitride films by low pressure inductively coupled plasma enhanced chemical vapor deposition", Appl.Phys.Lett. **64** 851 (1994).

[113] T.Ichiki, T.Momose and T.Yoshida,"Effect of the substrate bias on the formation of cubic boron nitride by inductively coupled plasma enhanced chemical vapor deposition", J.Appl.Phys. **75** 1330 (1994).

[114] T.Ichiki and T.Yoshida,"Growth of cubic boron nitride films by low-pressure inductively coupled plasma enhanced chemical vapor deposition", Proc. 2nd Int.Conf.Reactive Plasma, Yokohama (1994).

[115] T.Ichiki and T.Yoshida, "Growth of cubic boron nitride films by low-pressure inductively coupled plasma enhanced chemical vapor deposition", Jpn.J.Appl.Phys. **33**, 4385 (1994).

[116] T.Ichiki, S.Amagi and T.Yoshida,"Growth process of cubic boron nitride on silicon by low-pressure ICP-CVD", Proc. 7th Symp. Plasma Sci. Mater. p.119 (1994).

[117] M.Kuhr, S.Reinke and W.Kulisch,"Deposition of cubic boron nitride with an inductively coupled plasma (ICP)", to be presented at the Plasma Surface Engineering '94, Garmisch Partenkirchen, Germany (1994).

[118] W.Dworschak, K.Jung and H.Ehrhardt,"Growth of cubic boron nitride coatings in a magnetic field enhanced rf-glow discharge", Diamond Relat.Mater. **3**, 337 (1994).

[119] I.Langmuir and K.T.Compton,"Electrical discharges in gases Part II. Fundamental phenomena in electrical discharges", Rev.Mod.Phys. **3**, 191 (1931).

[120] R.F.Kemp and J.M.Sellen,Jr. "Plasma potential measurements by electron emissive probe", Rev.Sci.Instrum. **37**, 455 (1966).

[121] N.Hershkowitz, B.Nelson, J.Pew, and D.Gates, "Self-emissive probes", Rev.Sci.Instrum. **54**, 29 (1983).

[122] S.Iizuka, P. Michelsen, J. Juul Rasmussen, R. Schrittwieser, R. Hatakeyama, K. Saeki and N. Sato, "A method for measuring fast time evolutions of the plasma potential by means of a simple emissive probe", J.Phys.E **14**, 1291 (1981).

[123] M.A.Makowski and G.A.Emmert, "New method to measure plasma potential with emissive probes", Rev.Sci.Instrum. **54**, 830 (1983).

[124] A schematic diagram of the circuit is seen in Fig.1 in the reference [120], for example.

[125] B.N.Chapman, in Glow Discharge Processes (Wiley, New York, 1980)

[126] C.Charles, R.W.Boswell, A.Bouchoule, C.Laure, and P.Ranson, "Plasma diffusion from a low pressure radio frequency source", J.Vac.Sci.Technol.A **9** (1991) 661.

[127] M.A.Hussein and G.A.Emmert,"Modeling of plasma flow downstream of an electron cyclotron resonance plasma source", J.Vac.Sci.Technol.A **8** (1990) 2913.

[128] M.J.Rand, J.F.Roberts, "Preparation and properties of thin film BN", J.Electrochem.Soc. **115**, 423 (1968).

[129] S.P.Murarka,C.C.Chang,D.N.K.Wang and T.E.Smith, "Effect of growth parameters on the CVD of BN and phosphorus doped BN", J.Electrochem.Soc. **126**, 1951 (1979).

[130] A.C.Adams and C.D.Capio, "The chemical deposition of boron-nitrogen films", J.Electrochem.Soc. **127**, 399 (1980).

[131] S.B.Hyder and T.O.Yep, "Structure and properties of BN films grown by high temperature reactive plasma deposition", J.Electrochem.Soc. **123**, 1721 (1976).

[132] H.Miyamoto, M.Hirose, and Y.Osaka, "Structural and electronic characterization of discharge-produced BN", Jpn.J.Appl.Phys. **22**, L216 (1983).

[133] T.H.Yuzuriha, W.E.Mlynko and D.W.Hess, "Magnetic field effects in the plasma-enhanced chemical vapor deposition of boron nitride", J.Vac.Sci.Technol.A **3**, 2135 (1985).

[134] M.Sano and M.Aoki, "CVD of thin films of BN onto fused silica and sapphire", Thin Solid Films **83**, 247 (1982).

[135] T.Takahashi, H.Itoh and A.Takeuchi, "CVD of hBN thick films on iron", J.Cryst.Growth **47**, 245 (1979).

[136] S.Motojima,Y.Tamura, and K.Sugiyama, "Low temperature deposition of hBN films by CVD", Thin Solid Films **88**, 269 (1982).

[137] O.Gafri, D.Itzhak and A.Inspektor, "BN coating on steel and graphite produced with a low pressure rf plasma", Thin Solid Films **72**, 523 (1980).

[138] T.H.Yuzuriha and D.W.Hess, "Structural and optical properties of plasma deposited BN films", Thin Solid Films **140**, 199 (1986).

[139] W.Schmolla and H.Hartnagel, "Low temperature double-plasma process for BN films on semiconductors", J.Electrochem.Soc. **129**, 2636 (1982).

[140] W.Schmolla and H.Hartnagel, "Properties of BN films produced by a low temperature double-plasma process", Solid State Electronics **15**, 95 (1982).

[141] A.C.Adams, "Characterization of films formed by pyrolysis of borazine", J.Electrochem.Soc. **128**, 1378 (1981).

[142] G.Constant and R.Feurer, "Preparation and characterizaton of thin protective films in silica tubes by thermal decomposition of hexachloro-borazine", J.Less.Common Metals **82**, 113 (1981).

[143] T.Matsuda, N.Uno, and H.Nakae, "Synthesis and structure of chemically vapour-deposited boron nitride", J.Mater.Sci. **21**, 649 (1986).

[144] S.Komatsu, T.Yoshida and K.Akashi,"Deposition of BN films by chemical transport of B in RF H_2+N_2 plasma", Proc. 9th Symp.on ISIAT'85, Tokyo, 421 (1985).

[145] Y.Ichinose, H.Saitoh and T.Ishiguro,"Synthesis of cubic boron nitride film by a new method of rf plasma CVD thermally activated with tungsten filament", Proc. 11th Symp.on ISIAT'87, Tokyo, 469 (1987).

[146] H.Saitoh, T.Hirose, H.Matsui, Y.Hirotsu and Y.Ichinose, "Synthesis of BN films by the plasma CVD with various solids: BH_3NH_3, H_3BO_3 and $NaBH_4$", Surf.Coat.Technol. **39/40**, 265 (1989).

[147] H.Saitoh, Y.Hirotsu and Y.Ichinose,"Conditions for formation of BN film by thermally assisted RF plasma CVD", Nippon Kinzoku Gakkaishi **54**, 186 (1990) (in Japanese).

[148] H.Saitoh, Y.Hirotsu and Y.Ichinose,"Influence of atomic hydrogen on the formation of boron nitride film", Nippon Kinzoku Gakkaishi **54**, 526 (1990) (in Japanese).

[149] H.Saitoh and W.A.Yarbrough,"Preparation and characterization of nanocrystalline cubic boron nitride by microwave plasma-enhanced chemical vapor deposition", Appl.Phys.Lett. **58**, 2228 (1991).

[150] H.Saitoh, H.Morino and Y.Ichinose,"Deposition rate of boron nitride films using plasma jet technique", Jpn.J.Appl.Phys. **32**, L1684 (1993).

[151] H.Saitoh, T.Hirose, T.Ohtsuka and Y.Ichinose,"Nucleation of boron nitride on cubic boron nitride microcrystalline using chemical vapor deposition", Appl.Phys.Lett. **64**, 1638 (1994).

[152] J.Kouvetakis, V.V.Patel, C.W.Miller and D.B.Beach, "Composition and structure of boron nitride films deposited by chemical vapor deposition from borazine", J.Vac.Sci.Technol.A **8**, 3929 (1990).

[153] W.L.Wang, R.B.Ji, J.Y.Gao, K.J.Liao and X.L.Zhang,"Formation of c-BN film on Fe with seeped boron using RF plasma CVD thermally assisted by a tungsten filament", phys.stat.sol.(a) **136**, K89 (1993).

[154] W.L.Wang, K.J.Liao and J.Y.Gao,"Cubic boron nitride films formed by DC plasma CVD", phys.stat.sol.(a) **139**, K25 (1993).

[155] T.Ichiki, M Takamura and T.Yoshida, "Preparation of boron nitride films by low pressure ICP-CVD", Proc. 4th Jpn.Symp.Plasma Chem. 227 (1991).

[156] R.Geick and C.H.Perry, "Normal modes in hexagonal boron nitride", Phys.Rev. **146**, 543 (1966).

[157] B.E.Warren, "X-ray diffraction in random layer lattices", Phys.Rev. **59**, 693 (1941).

[158] T.M.Duncun,R.A.Levy,P.K.Gallagher and M.W.Walsh,Jr, "Structural characterization of BN films", J.Appl.Phys. **64**, (1988) 2990.

[159] W.L.Hsu, "Chemical erosion of graphite by hydrogen impact: A summary of the database relevant to diamod growth", J.Vac.Sci.Technol.A **6**, 1803 (1988).

[160] P.B.Hirsch, A.Howie, R.B.Nicholson, and D.W.Pashley, "Electron Microscopy of Thin Crystals", Butterworths, London (1965).

[161] D.G.Brandon, B.Ralph, S.Ranganathan and M.S.Wald,"A field ion microscope study of atomic configuration at grain boundaries", Acta Met. **12**, 813 (1964).

[162] D.L.Medlin, T.A.Friedmann, P.B.Mirkarimi, P.Rez, M.J.Mills and K.F.McCarty, "Microstructure of cubic boron nitride thin films grown by ion-assisted pulsed laser deposition", J.Appl.Phys. **76**, 295 (1994)

[163] Y.Matsui,"Small particles of cubic boron nitride prepared by electron irradiation of hexagonal boron nitride in a transmission electron microscopy", J.Cryst.Growth **66**, 243 (1984).

[164] R.Trehan, Y.Lifshitz and J.W.Rabalais, "Auger and X-ray electron spectroscopy studies of *h*BN, cBN, and N_2^+ ion irradiation of boron and boron nitride", J.Vac.Sci.Technol.A **8**, 4026 (1990).

[165] G.Hanke, M.Kramer and K.Müller,"Low energy Auger transitions of h-BN and c-BN: an example of the influence of crystallographic structure on the Auger decay", in *Synthesis and Properties of Boron Nitride*, edited by J.J.Pouch and S.A.Alterovitz (Trans Tech, Aedermannsdorf, 1990), Vol.54-55, p.207.

[166] D.R.McKenzie, D.Muller and B.A.Pailthorpe, "Compressive-stress-induced formation of thin-film tetrahedral amorphous carbon", Phys.Rev.Lett. **67**, 773 (1991).

[167] C.Weissmantel, C.Schürer, F.Fröhlich, P.Grau and H.Lehmann, "Mechanical properties of hard carbon films", Thin Solid Films **61**, L5 (1979).

[168] A.Kinbara, S.Baba, N.Matuda and K.Takamisawa,"Mechanical properties of and cracks and wrinkles in vacuum-deposited MgF_2, carbon and boron coatings", Thin Solid Films **84**, 205 (1981).

[169] D.Nir,"Stress relief forms of diamond-like carbon thin films under internal compressive stress", Thin Solid Films **112**, 41 (1984).

[170] G.Gille and B.Rau,"Buckling instability and adhesion of carbon layers", Thin Solid Films **120**, 109 (1984).

[171] D.Nir,"Intrinsic stress in diamond-like carbon films and its dependence on deposition parameters", Thin Solid Films **146**, 27 (1987).

[172] H.Y.Yu, C.Kim and S.C.Sanday,"Buckle formation in vacuum-deposited thin films", Thin Solid Films **196**, 229 (1991).

[173] J.Seth, R.Padiyath and S.V.Babu,"Influence of the deposition gas mixture on the structure and failure modes of diamondlike carbon films", J.Vac.Sci.Technol.A **10**, 284 (1992).

[174] J.A.Thornton and D.W.Hoffman,"Stress-induced effects in thin film", Thin Solid Films **171**, 5 (1989).

[175] F.M.d'Heurle,"Aluminum films deposited by rf sputtering", Metall.Trans. **1**, 725 (1970).

[176] D.W.Hoffman and M.R.Gaerttner,"Modification of evaporated chromium by concurrent ion bombardment", J.Vac.Sci.Technol. **17**, 425 (1980).

[177] H.Windischmann,"Intrinsic stress in sputtered thin films", J.Vac.Sci.Technol.A **9**, 2431 (1991).

[178] K.-H.Müller, "Stress and microstructure of sputter-deposited thin films: Molecular dynamics investigation", J.Appl.Phys. **62**, 1796 (1987).

[179] K.-H.Müller, "Ion-beam-induced epitaxial vapor-phase growth: A molecular-dynamic study", Phys.Rev.B **35**, 7906 (1987).

[180] C.C.Fang, V.Prasad and F.Jones,"Molecular dynamics modeling of microstructure and stresses in sputter-deposited thin films", J.Vac.Sci.Technol. A **11**, 2778 (1993).

[181] C.C.Fang, F.Jones and V.Prasad,"Effect of gas impurity and ion bombardment on stresses in sputter-deposited thin films: A molecular-dynamics approach", J.Appl.Phys. **74**, 4472 (1993).

[182] R.Messier, A.R.Badzian, T.Badzian, K.E.Spear, P.Bachmann, and R.Roy, "From diamond-like carbon to diamond coatings", Thin Solid Films **153**, 1 (1987).

[183] A.Chayahara, H.Yokoyama, T.Imura, Y.Osaka and M.Fujisawa, "Reflectance spectra of BN materials in the vacuum ultraviolet", Jpn.J.Appl.Phys. **27**, 440 (1988) (Short note).

[184] H.Yokoyama, M.Okamoto, T.Hamada, T.Imura, Y.Osaka, A.Chayahara and M.Fujisawa, "Imaginary part of the dielectric function of sintered and microcrystalline cubic boron nitride", Jpn.J.Appl.Phys. **28**, 555 (1989) (Short note).

[185] H.Kohzuki and M.Motoyama,"Characterization of BN powder and BN films by EPMA", J.Japan Inst.Metals **56**, 565 (1992).

[186] H.Kohzuki and M.Motoyama,"Characterization of Ion-plated BN films from X-ray Emission Spectra of boron", J.Japan Inst.Metals **56**, 572 (1992).

[187] D.R.McKenzie, W.G.Sainty and D.C.Green,"The microstructure of boron nitride thin films", in *Synthesis and Properties of Boron Nitride* (edited by J.J.Pouch and S.A.Alterovitz, Trans Tech Publications), p.193 (1990).

[188] D.R.McKenzie, D.J.H.Cockayne, D.A.Muller, M.Murakawa, S.Miyake, S.Watanabe and P.Fallon,"Electron optical characterization of cubic boron nitride thin films prepared by reactive ion plating", J.Appl.Phys. **70**, 3007 (1991).

[189] D.J.Kester and R.Messier, "Phase control of cubic boron nitride thin films", J.Appl.Phys. **72**,504(1992)

[190] H.Yokoyama, M.Okamoto and Y.Osaka, "Effects of a negative self-bias on the growth of cubic boron nitride prepared by plasma chemical vapor depostion", Jpn.J.Appl.Phys. **30**, 344 (1991).

[191] D.M.Mattox,"Particle bombardment effects on thin-film deposition: a review", J.Vac.Sci.Technol.A **7**, 1105 (1989).

[192] F.Seitz and J.S.Koehler, in *Solid State Physics*, Vol.2 (Accademic, New York, 1957), p.30.

[193] J.D.Targove and H.A.Macleod,"Verification of momentum transfer as the dominant densifying mechanism in ion-assisted deposition", Appl.Opt. **27**, 3779 (1988).

[194] C.K.Hwangbo, L.Lingg, J.P.Lehan, H.A.McCleaod, J.L.Makous and S.Y.Kim,"Ion assisted deposition of thermally evaporated Ag and Al films", Appl.Opt. **28**, 2769 (1989).

[195] H.Windischmann,"An intrinsic stress scaling law for polycrystalline thin films prepared by ion beam sputtering", J.Appl.Phys. **62**, 1800 (1987).

[196] R.A.Roy, P.Catania, K.L.Saenger, J.J.Cuomo and R.L.Lossy, "Role of energetic atoms and ions in Ta films grown by different physical vapor deposition methods", J.Vac.Sci.Technol.B **11**, 1921 (1993).

[197] Y.Yamamura, N.Matsunami and N.Itoh,"Theoretical studies on an empirical formula for sputtering yield at normal incidence", Radiat Eff., **71**, 65 (1983).

[198] P.Mezzentzeff, Y.Lifshitz and J.W.Rabalais,"BN formation from bombardment of boron with N_2^+", Nucl.Instr.and Meth.B **44**, 289 (1990).

[199] J.C.Bourgoin and B.Massarani,"Threshold energy for atomic displacement in diamond", Phys.Rev.B **14**, 3690 (1976).

[200] J.F.Prins, T.E.Derry and J.P.F.Sellschop,"Volume expansion of diamond during ion implantation", Phys.Rev.B **34**, 8870 (1986).

[201] W.Wu and S.Fahy,"Molecular-dynamics study of single-atom radiation damage in diamond", Phys.Rev.B **49**, 3030 (1994).

[202] J.P.Biersack and L.G.Haggmark,"A Monte Carlo computer program for the transport of energetic ions in amorphous targets", Nucl.Instr.and Meth. **174**, 257 (1980).

[203] J.P.Biersack,"Computer simulations of sputtering", Nucl.Instr.and Meth.B **27**, 21 (1987).

[204] J.F.Ziegler, J.P.Biersack and U.Littmark, *The Stopping and Ranges of Ions in Matter*, vol.1, ed., Z.F.Ziegler (Pergamon, New York, 1985).

[205] H.P.Lang, H.Haefke, G.Leemann and H.-J.Güntherodt,"Scanning tunneling microscopy study of different growth stages of $YBa_2Cu_3O_{7-\delta}$ thin film", Physica C **194**, 81 (1992).

[206] A.Matsuda and K.Tanaka,"Investigation of the growth kinetics of glow-discharge hydrogenerated amorphous silicon using a radical separation techique", J.Appl.Phys. **60**, 2351 (1986).

[207] P.Grütter, W.Zimmermann-Edling and D.Brodbeck, "Tip artifacts of microfabricated force sensors for atomic force microscopy", Appl.Phys.Lett. **60**, 2741 (1992).

[208] L.Montelius and J.O.Tegenfeldt, "Direct observation of the tip shape in scanning probe microscopy", Appl.Phys.Lett. **62**, 2628 (1993).

[209] K.Watanabe, K.Saitoh, Y.Yuchi, K.Sekino, K.Inagawa and A.Itoh, "Influences of added elements on the interface structure and adhesion of c-BN films by ARE method", Proc.11th Symp. on ISIAT'87 Tokyo, 347 (1987).

[210] K.Inagawa, K.Watanabe, K.Saitoh, Y.Yuchi and A.Itoh, "Structure and properties of c-BN film deposited by activated reactive evaporation with a gas activation nozzle", Surf. Coat. Technol. **39/40**, 253 (1989).

[211] D.J.Kester, K.S.Ailey, R.F.Davis and K.L.More, "Phase evolution in boron nitride thin films", J.Mater.Res. **8**, 1213 (1993).

[212] D.R.McKenzie, W.D.McFall, W.G.Sainty, C.A.Davis and R.E.Collins, "Compressive stress induced formation of cubic boron nitride", Diamond Relat. Mater. **3**, 970 (1993).

[213] D.R.McKenzie, "Generation and applications of compressive stress induced by low energy ion beam bombardment", J.Vac.Sci.Technol.B **11**, 1928 (1993).

[214] H.Kohzuki, T.Ishihara, Y.Okuno and M.Motoyama,"Effect of self-bias voltage on formation of c-BN film.", Funtai oyobi funmatsu yakin, **41**, 57 (1994) (in Japanese).

[215] D.J.Kester, K.S.Ailey, D.J.Lichtenwalner and R.F.Davis, "Growth and characterization of cubic boron nitride thin film", J.Vac.Sci.Technol.A **12**, 3074 (1994).

[216] R.J.Nemanich, J.T.Glass, G.Lucovsky, and R.E.Shroder, "Raman scattering characterization of carbon bonding in diamond and diamondlike thin films", J.Vac.Sci.Technol.A,**6**,1783(1988)

[217] D.J.Vitkavage, R.A.Rudder, G.G.Fountain and R.J.Markunas, "Plasma enhanced chemical vapor depostion of polycrystalline diamond and diamondlike films", J.Vac.Sci.Technol. A **6**, 1812 (1988).

[218] H.Kawarada, K.S.Mar and A.Hiraki,"Large area chemical vapour deposition of diamond particles and films using magneto-microwave plasma", Jpn.J.Appl.Phys. **26**, L1032 (1987).

[219] J.Wei, H.Kawaraka, J.Suzuki and A.Hiraki,"Growth of diamond films at low pressure using magneto-microwave plasma CVD", J.Cryst.Growth **99**, 1201 (1990).

Acknowledgement

本論文は東京大学工学部金属工学科吉田研究室において行われた研究の成果をまとめたものである。指導教官でありました吉田豊信教授には、自由で創造的な研究の機会と環境を与えていただき、また、多岐にわたり大変お世話になりました。ここに深く謝意と敬意を表します。同研究室の寺島和夫助教授、石塚隆一助手、津田統助手、江口敬祐技官の方々のおかげで有意義な研究室生活を送ることができました。どうも有り難うございました。工作室の木村暢生氏、杉田洋一氏には幾度も複雑な装置の試作をお願いし、大変お世話になりました。共通機器室の中村光弘氏には試料の分析やその他、大変お世話になりました。HRTEM 観察につきましては材料学科の市野瀬英喜氏に御協力頂きました。修士、博士課程の5年間をともに過ごした高村禅氏をはじめ、研究室生活を共にした院生、学部生の皆様にも深く感謝致します。特に卒論で直接、研究を指導して頂いた中條和秀氏、共同研究者であった、高村正人氏、百瀬寿弘氏、天城聡氏、佐々木弘次氏には多くの苦労をおかけいたしました。事務室をはじめ、4号館の多くの方々にお世話になりました。また、位置分解光電子分光測定、データ処理につきましては、島津製作所の長曽哲夫氏、大薮又茂両氏に御協力頂きました。本当に皆様有り難うございました。

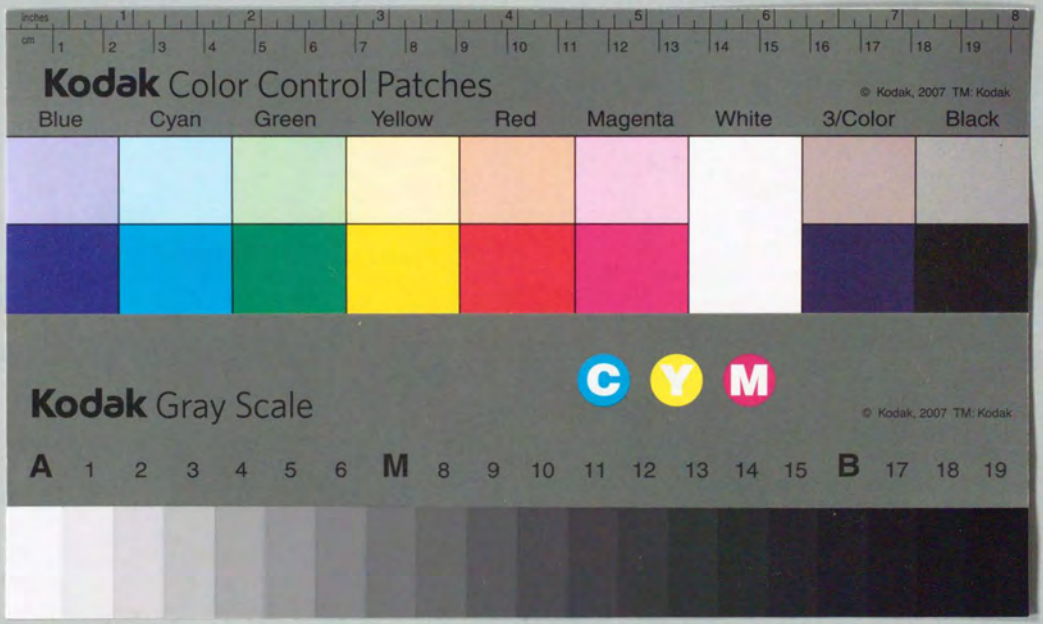
inches
cm
Kodak Color Control Patches
© Kodak, 2007 TM: Kodak
Blue
Cyan
Green
Yellow
Red
Magenta
White
3/Color
Black
C
Y
M
Kodak Gray Scale
© Kodak, 2007 TM: Kodak
A 1 2 3 4 5 6 M 8 9 10 11 12 13 14 15 B 17 18 19